ELECTRICAL AND THERMAL PROPERTIES OF NON-

STOICHIOMETRIC RUTILE AT LOW TEMPERATURES

By

GARY ALLEN BAUM

Bachelor of Science
Wisconsin State University
River Falls, Wisconsin
1961

Master of Science
Oklahoma State University
Stillwater, Oklahoma
1964

Submitted to the Faculty of the Graduate College
of the Oklahoma State University
in partial fulfillment of the requirements
for the degree of
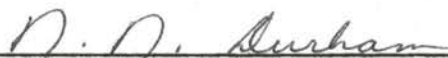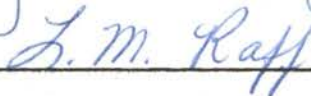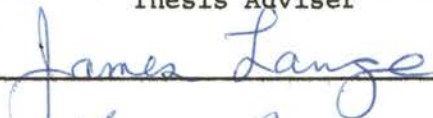DOCTOR OF PHILOSOPHY
August, 1969

ELECTRICAL AND THERMAL PROPERTIES OF NON-

STOICHIOMETRIC RUTILE AT LOW TEMPERATURES

Thesis Approved:

_____
Thesis Adviser

_____

_____

_____
Dean of the Graduate College

729853

ACKNOWLEDGEMENTS

TABLE OF CONTENTS

TABLE OF CONTENTS (Continued)

LIST OF TABLES

LIST OF FIGURES

CHAPTER I

INTRODUCTION

Background Information

Rutile (titanium dioxide) is a transition metal oxide characterized by a high melting point and a pale yellow appearance. On the basis of the electronic configuration of titanium $(3d^2 4s^2)$, simple band theory suggests rutile should be a conductor due to the unfilled d-shells. Stoichiometric rutile is an insulator, however, and it is unclear whether the 3d cation wavefunctions overlap forming a conduction band or are non-interacting. To the extent that conduction is due to 3d electrons one would expect a low mobility characteristic of 3d conduction.

It has been known for many years that nonstoichiometric rutile having an anion deficiency is an n-type semiconductor[1]. Because of the experimental difficulties encountered in making measurements on the high resistivity stoichiometric composition, most studies relate to nonstoichiometric material. This state can be achieved by heating the rutile in a hydrogen atmosphere, a vacuum, or a titanium atmosphere. The result of any one of these methods is an anion-deficient composition which behaves like an n-type semiconductor. The reduction of a sample in this manner provides a system which is comparatively easy to study experimentally, with the physical properties strongly dependent upon the time, temperature and nature of the reduction process.

Many studies have been made of the electrical and optical proper-

1

ties of reduced rutile[2-15], and also on the defect mechanisms involved in the reduction process[8,13,16-30]. An exhaustive review of all work up through 1958 is given by Grant[31]. For the most part the studies lack direct quantitative correlation due to differences in foreign impurity content and unclearly defined reduction techniques. The thermal properties of rutile in the nonstoichiometric state have received considerably less attention. Measurements have been made of the specific heat[32-35], Seebeck coefficient[4,36], and thermal conductivity[36].

Scope of Present Study

It has been the purpose of this study to investigate some of the electrical and thermal properties of rutile single crystals reduced in a high vacuum for various times and temperatures, thus providing systems varying in stoichiometry. The Seebeck effect, electrical conductivity, and thermal conductivity in the temperature range 5 to 300 $^{\circ}$K were of primary interest. The objectives were twofold. First, by studying these properties as a function of the reduction state, one hopes to be able to elucidate the nature of the transport processes at low temperatures and to evaluate the appropriate parameters. Secondly, it is of importance to relate these parameters to the still unexplained defect mechanism of vacuum-reduced rutile in an effort to provide some insight into the nature of the defect.

To these ends, all reduction parameters have been carefully recorded and additional measurements of weight loss upon reduction and Hall coefficients were also made on some of the samples. In addition, all samples have been cut from a single large boule of rutile which contained a low concentration of foreign impurities.

A model has been developed in terms of a two-defect mechanism which qualitatively explains the behavior of the electrical properties in vacuum-reduced rutile. Analysis of the thermal results in terms of existing theories should extend the understanding of the scattering processes involved in the transport mechanisms associated with compound semiconductors.

CHAPTER II

PREVIOUS WORK AND THEORETICAL BACKGROUND

Electrical Properties of Rutile

The rutile structure is tetragonal, with a = 4.594 $\overset{o}{A}$ and c = 2.959
$\overset{o}{A}$. Titanium ions occupy positions 0,0,0 and ½,½,½ and oxygens are lo-
cated at ± x,x,0 and ± ½ + x, ½ - x, ½ with x = 0.306[37]. Rutile is pre-
dicted to have a 40% ionic character[31].

The majority of experimental investigations on rutile began after
it was first prepared synthetically by a Verneuil technique in the early
1950's. Cronemeyer[2] measured some electrical and optical properties of
rutile single crystals and correlated the high temperature conductivity
(E_g = 3.05 eV) with the optical absorption threshold at low temperatures
(3.03 eV). These results implied an energy gap in rutile of about 3.04
eV. Cronemeyer also investigated hydrogen-reduced rutile and concluded
that the resultant defect was an oxygen vacancy. Breckenridge and
Hosler[3] studied hydrogen-reduced ceramic and crystalline materials.
They investigated the electrical properties from room temperature to
liquid nitrogen temperatures and, in general, found very low values for
the mobility, indicating a large effective mass for the electron. The
temperature dependence of the Hall coefficient implied that there
existed two types of donor centers. These were postulated to be oxygen
vacancies and oxygen vacancies associated with a titanium ion on a

4

normal titanium site. The small room temperature value of the mobility (≤ 1 cm^2/volt-sec) suggested conduction might be taking place in a 3d conduction band.

Because rutile has a strong ionic character, the question arises as to whether it is possible to use simple band theory in the same fashion as it is applied to predominantly covalent semiconductors. Frederikse[6] investigated the possibility of polaron conduction in rutile. From his conductivity, Hall, and thermoelectric power data he concluded conduction was by free electrons in a 3d band above 5 $^{\circ}$K, but below 5 $^{\circ}$K that conduction took place by polarons in a polaron band. Hasiguti, et.al.[9] postulated that conduction below 20 $^{\circ}$K was a result of impurity band conduction. Becker and Hosler[12] have shown that the conduction process in rutile is compatible with a multiple band conduction mechanism, although no hypothesis as to the origin of these bands is given.

Defect Nature

Until about 1961 it was generally accepted that the predominant defect in reduced rutile was an oxygen vacancy. The reduction process itself appears completely reversible, e.g., the weight loss resulting from the reduction process is equal to the weight gain upon reoxidation[4]. In 1961 Chester[17] performed an electron spin resonance study on hydrogen- and vacuum-reduced rutile and noted two significant features. First, there appeared to be a difference in the defect nature resulting from the different reduction processes and secondly, in the vacuum-reduced specimens he observed a signal which he postulated, among other things, might be due to a titanium interstitial defect.

The first of these was clarified by von Hippel, et. al.[8], who

demonstrated that hydrogen can enter the lattice and act as a donor. The hydrogen combines with oxygen ions within the crystal creating an OH^- concentration. This effect is probably significant in hydrogen-reduced material and previous works should be re-examined in light of this. In addition, since the Verneuil technique employs an oxyhydrogen flame, it is reasonable to assume that synthetic rutile has hydrogen incorporated into it during the growth process. This has recently been studied, along with the effect of the hydrogen upon oxygen diffusion rates, by Hill[27].

There has been considerable effort to establish the nature of the defect in reduced rutile. One technique employed is to study the oxygen pressure dependence of the electrical conductivity. According to the theory of reversible defects[38], a defect equilibrium is given by the law of mass action. (Appendix A includes a discussion and derivation of the law of mass action in terms of concentrations.) The creation of an oxygen vacancy defect may be represented by the following equations,

$$\text{Stoichiometric Crystal (S.C.)} \rightleftarrows O_v^{2+} + 2e^- + \tfrac{1}{2}O_2(g)$$

$$\text{S.C.} \rightleftarrows (O_v^{2+}e^-) + e^- + \tfrac{1}{2}O_2(g)$$

$$\text{S.C.} \rightleftarrows (O_v^{2+}2e^-) + \tfrac{1}{2}O_2(g).$$
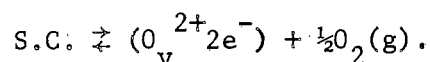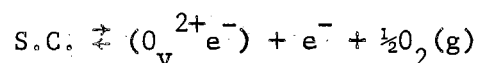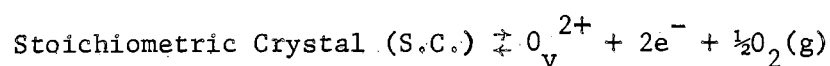
Application of the law of mass action yields

$$[O_v^{2+}] \, n^2 P_{O_2}^{\frac{1}{2}} = K_1 \ \text{(constant)}$$

$$[O_v^{1+}] \, n \, P_{O_2}^{\frac{1}{2}} = K_2$$

$$[O_v^{\ o}] \ P_{O_2}^{\frac{1}{2}} = K_3 .$$

In these equations the square bracket represents a concentration, $n = [e^-]$ is the concentration of electrons, and P_{O_2} is the partial pressure of oxygen measured in atmospheres. Since the electrical conductivity is proportional to n ($\sigma = ne\mu$) one deduces[16]

$$\sigma = constant \ P_{O_2}^{-1/6}$$

$$\sigma = constant \ P_{O_2}^{-1/4}$$

$$\sigma = constant \ (independent \ of \ P_{O_2})$$

for oxygen vacancies with none, one, or two trapped electrons, respectively. Thus a study of σ versus oxygen partial pressure should yield information regarding the nature of the defect. If however, as Chester implies, there exists the possibility of a cation interstitial, the problem is more complicated. Consider the creation of a titanium interstitial, with a valence of m+, to be given by the reaction

$$TiO_2 \ \rightleftarrows \ Ti_i^{m+} + me^- + O_2(g) .$$
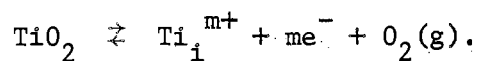
The law of mass action then gives

$$[Ti_i^{m+}] \ n^m \ P_{O_2} = K_4 ,$$

and the resultant conductivity is

$$\sigma = constant \ P_{O_2}^{-\frac{1}{m+1}} .$$

Thus if titanium 3+ interstitials (Ti_i^{3+}) were formed during the reduction process, $\sigma \propto P_{O_2}^{-\frac{1}{4}}$, the same value predicted for oxygen vacancies with one trapped electron. On the other hand Ti_i^{4+} gives $\sigma \propto P_{O_2}^{-1/5}$, the same value as for the case of singly and doubly ionized oxygen vacancies appearing simultaneously[19]. Calling $\sigma \propto P_{O_2}^{-\frac{1}{x}}$, the value of x reported in the literature ranges from 4 to 6[26]. In general then, it is difficult to establish the defect nature conclusively using this approach.

Hurlen[16] pointed out several arguments in favor of the titanium interstitial model. If there are N normal Ti sites then there are 2N octahedral interstitial sites (at ½, 0, ½) and 2N tetrahedral sites. The tetrahedral sites may be disregarded because titanium is not known to occur with coordination number four. The octahedral sites might favor the creation of an interstitial defect in that it is physically larger than the normal titanium site (10.91 vs. 9.89 $\overset{o}{A}^3$). Figure 1 compares the normal O_6 octahedron site with the interstitial O_6 octahedron.

Hurlen's second argument is that continual removal of oxygen should result in an orderly progression toward the next oxide, Ti_2O_3. If this were not so, a drastic structural change must occur when a fourth of the oxygen is removed if oxygen vacancies are the only defect.

Results of investigations of dielectric relaxations in reduced rutile at low temperatures by Dominick and MacCrone[39,40] are interpreted in terms of an O_v associated with a trivalent substitutional impurity,
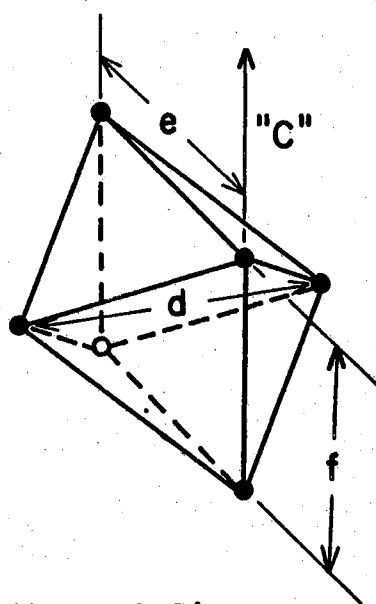
Normal Site
O_6 octahedron

$d = 3.959 \text{ Å}$
$e = 2.526 \text{ Å}$
$f = 2.959 \text{ Å}$
Volume $= 9.89 \text{ Å}^3$
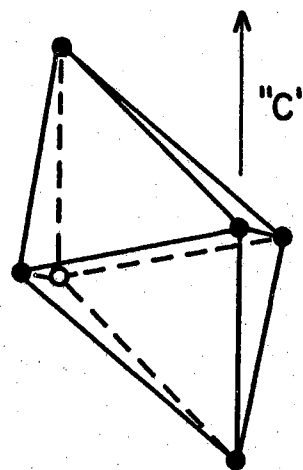
Interstitial Site
O_6 octahedron

$d = 3.326 \text{ Å}$
$e = 3.326 \text{ Å}$
$f = 2.959 \text{ Å}$
Volume $= 10.91 \text{ Å}^3$

Figure 1. Comparison of the Normal and Interstitial O_6-
Octahedron Sites

and an interstitial Ti^{3+} ion associated with two trivalent substitution-al impurities. Recent studies using optical absorption techniques[21], electrical conductivity techniques[13], and electron spin resonance methods[28] lend additional evidence to an interstitial type defect.

Thermal Properties

The thermal properties of rutile have been studied less extensively than the electrical or defect properties. Studies of the specific heat in stoichiometric rutile by Keesom and Pearlman[32] indicate the specific heat capacity is proportional to T^3, as expected, at very low tempera-tures ($< 4\ ^\circ K$). A value of 758 $^\circ K$ was obtained for the corresponding Debye temperature. In the temperature range from 10 to 20 $^\circ K$ the Debye temperature decreased from 650 to 460 $^\circ K$. Measurements taken on reduced rutile by Keesom and Pearlman[33] and later by Keesom and Sandin[34] are in-terpreted on the basis of a localized donor state feeding a narrow im-purity band. Recently, however, Sandin and Keesom[35] have decided that the conduction process below 20 $^\circ K$ takes place in a polaron band.

The thermal conductivity of "pure" rutile has been measured by Berman, et. al.[41], at low temperatures and by Kingery, et. al.[42], and Yoshida[43] at high temperatures. The most recent investigation has been performed by Thurber and Mante[36] who studied pure rutile in both the "a" and "c" directions. In addition they investigated one pair of vacuum-reduced samples and a hydrogen-reduced "a" direction sample. In general, the pure samples displayed a typical insulator behavior. A maximum occurred near 15 $^\circ K$ with $\kappa \alpha T^3$ at lower temperatures and κ vary-ing exponentially with temperature in the range 25 to 100 $^\circ K$. Thurber and Mante also measured the Seebeck effect on the reduced samples at low

temperatures and observed a large phonon drag effect. The thermoelectric power of reduced rutile has frequently been measured at high temperatures (e.g. References 4 and 6) but the author is unaware of any other low temperature (< 80 $^{\circ}$K) measurements of this effect in rutile.

Theory of the Electronic Thermoelectric Power of Semiconductors

Simply stated, the Seebeck effect is the generation of a thermoelectric voltage in a circuit of two conductors, the junctions of which are at different temperatures[44]. Because thermal emf's are additive, it is meaningful to talk of an absolute thermoelectric power of a substance. In the case of a metal-semiconductor-metal system the thermoelectric effects of the metal are so small compared to the semiconductor, they may be neglected. Thus the measured thermoelectric power is assumed to be a characteristic of the semiconductor.

The electronic contribution to the thermoelectric power has been derived by many authors (e.g. Tauc[44]) and will not be done here. Derived from the Lorentz-Sommerfeld theory of conduction in metals, the electronic contribution for a nondegenerate n-type semiconductor is given as

$$Q = (E_f - \Delta E_t)/eT.$$

Here e is the electronic charge, Q is the thermoelectric power, and T is the absolute temperature. E_f is the Fermi level measured from the bottom of the conduction band. When the Fermi level lies below the conduction band this term is negative. ΔE_t is the average energy of the transported electrons relative to the band edge, or more simply it is a kinetic energy transport term. The magnitude of ΔE_t is of the order of

kT and is thus usually smaller than E_f.

The utility of this expression depends upon the ability to determine E_f and ΔE_t. Consider first the Fermi level, E_f. Evaluation of this quantity from measurements of Hall coefficients necessitates an assumption regarding the effective mass of the carriers. This in turn requires a knowledge of the electronic energy band structure of the semiconductor in question. To date, the exact energy band structures have not been established conclusively for any oxide semiconductor.

Three energy band models often discussed in the literature are shown in Figure 2. These give the schematic forms of the locus in k-space of a given single value of energy near the band edge. The heavy dots represent the extremums. The first of these models (A) represents the single valley-many sheeted case, where the band edge is a triply degenerate state with wave vector k = 0, split slightly by spin orbit coupling. The second case (B) is that of a band edge consisting of a number of states with different wave vectors, $k_\nu \neq 0$, and related symmetrically with one another. This is an example of a many valley-single sheeted case. The locus of constant energy points in this model consists of identical ellipsoids centered around the points k_ν. The model most often assumed in the literature is that depicted in C, the single valley-single sheeted case.

On the basis of these three models it becomes apparent that each model requires a different effective mass, since they involve different types of averages over the parameters describing the multivalued non-spherical energy surfaces. For example, the "density of states effective mass", m*, in terms of the conventional model, C, is defined by
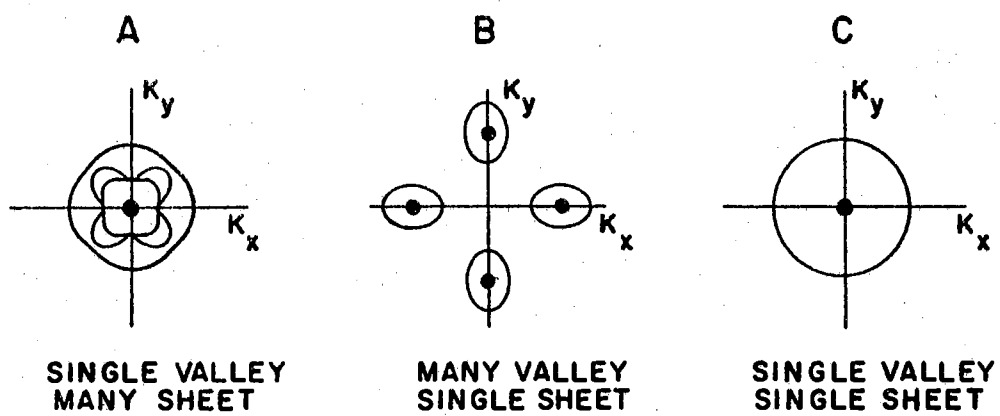
Figure 2. Three Simple Energy Band Schemes Often Used in the Literature

$$N(E) = (\frac{4\pi}{h^3})(2m^*)^{3/2}(E - E_c)^{1/2}.$$

Here $N(E)dE$ is the number of levels per unit volume within the range E to $E + dE$ and E_c is the energy of the edge of the conduction band (for an n-type semiconductor). If, however, each surface of constant E was a single ellipsoid, the m^* in the above equation is a geometric mean of the three principle effective masses, m_i^*. Thus, in the case of model B, $N(E)$ is N_v times as large as for a single ellipsoid and hence m^* is $N_v^{2/3}$ times the geometric mean of the three principle effective masses. The point to be made is that the above expression is applicable to the various models only as long as the proper effective mass is employed. In the case of model A an additional restriction is required, however, in that the spin-orbit splitting must be $<<$ kT or $>>$ kT or else m^* may vary considerably over the thermal range if defined as above.

From basic semiconductor statistics the density of charge carriers, n, is given as[45]

$$n = \int_0^\infty N(E)f(E)dE$$

where $f(E)$ is the Fermi function,

$$f(E) = [\exp (E - E_f)/kT + 1]^{-1}.$$

Upon performing the integration,

$$n = N_c \exp (E_f/kT)$$

for $E_f < -2kT$, and where

$$N_c = 2\left(\frac{2\pi\ m^*\ kT}{h^2}\right)^{3/2}.$$

One can now evaluate E_f/kT and thus find an expression for the electronic component of the thermoelectric power. Hence

$$\frac{E_f}{kT} = -\ln\left[\frac{2(2\pi\ m_e\ kT)^{3/2}}{h^3 n}\ \left(\frac{m^*}{m_e}\right)^{3/2}\right]$$

and

$$Q_{el} = \frac{-k}{e}\left[\ln\frac{C}{n} + \frac{3}{2}\ln\frac{m^*}{m} + \frac{3}{2}\ln T + \frac{\Delta E_t}{kT}\right]$$

where

$$C = \frac{2}{h^3}(2\pi\ m_e\ k)^{3/2}$$

and m_e is the mass of a free electron. This is the usual expression found in the literature for the electronic component of Q[44,46].

It is still necessary, however, to determine the value of $\Delta E_t/kT$. This has been done by several authors (Herring[46] for example) and their results will be given here. Assuming that the processes responsible for scattering the electrons can be described by a relaxation time τ_e, and that $\tau_e \alpha |E - E_c|^r$, one obtains $\Delta E_t/kT = 5/2 + r$. For the case of acoustical mode lattice scattering $r = -\frac{1}{2}$ while for Conwell-Weiskopf ionized impurity scattering[47], $r = 3/2$. These represent the two extreme values of r and yield $\Delta E_t/kT$ equal to 2 and 4, respectively. Actually mixtures of various scattering types may yield different values less than 2. Since the scattering mechanisms may vary with temperature, the value $\Delta E_t/kT$ might be expected to do so also, and thus introduce an

error into Q_{el}. In general, however, the kinetic energy transport term

contributes only a small fraction of the total electronic thermoelec-

tric power in semiconductors.

A further consideration, often neglected in treating experimental

results, is that of the effect of various impurity concentrations. As

Herring[46] points out, present day theories are generally applicable to

low concentrations of impurities or to high concentrations of impuri-

ties and carriers. In the former case, the motion of charge carriers

can be described by band theory, treating the carriers as entities

moving in regions of a perfectly crystalline material. In the latter

case one treats the carriers as a degenerate Fermi gas and the impuri-

ties as sources of scattering. It is in the region between these two

extremes that problems are encountered. As the number of impurities

increases, scattering by impurities becomes more important, and conduc-

tion may even occur in an "impurity" band in addition to the normal

conduction process. Present theories cannot treat these effects satis-

factorily, if at all. For example, one cannot expect the effective

mass previously defined to be applicable to a carrier in an impurity

band. Thus, it appears that the parameters normally used in semicon-

ductor statistics may require new definitions in these intermediate

ranges of impurity concentration.

Phonon Contribution to the Thermoelectric Power

Measurements on Ge in the early 1950's showed a very large in-

crease in the thermoelectric power at low temperatures. Frederikse[48]

and Herring[46] independently explained this phenomenon on the basis of a

lattice contribution to the thermoelectric power. Qualitatively one can

see how this effect might arise in a crystalline solid. Consider an n-type semiconductor whose ends are at temperatures T_1 and T_2, where $T_2 > T_1$. Neglecting any phonon effects, there is a net flow of electrons from the hot end to the cold end. That is, there are more electrons moving from hot to cold than from cold to hot. If one now considers phonons present, there is also a net flow of phonons from the hot end to the cold end. This is just what occurs in the thermal conduction process due to phonons. In the presence of a thermal gradient the phonon distributions are not isotropic, and the waves travel preferentially from hot to cold.

Because of this, scattering of charge carriers by phonons is not random, but acts in such a manner as to "push" or "drag" the carriers more often toward the cold end than the hot end. The result is that zero current in the semiconductor occurs only when the cold end acquires enough excess carriers such that the electrostatic field created by them counterbalances the effects of both this phonon contribution and the normal diffusion of carriers from hot to cold. This preferential scattering of electrons by phonons has come to be known as the "phonon drag effect". At ordinary temperatures this effect is small due to phonon-phonon scattering processes which tend to restore the lattice vibrations to randomness.

A brief outline of Frederikse's development of the phonon drag effect will now be given to help clarify the nature of this phenomenon. Consider a semiconductor under the influence of a temperature gradient and an external electric field, F, (both in the x direction). Equilibrium is established through the interaction of phonons and electrons by

the scattering mechanisms:

phonon-phonon
phonon-electron
phonon-impurity
phonon-sample boundary
electron-impurity
electron-phonon.

At equilibrium the phonon and electron distribution functions are respectively given by

$$N_o = (e^z - 1)^{-1}$$

$$f_o = \exp (\eta - \varepsilon)$$

where $z = \frac{\hbar\omega}{kT}$, $\hbar\omega$ = phonon energy, $\varepsilon = E/kT$, and $\eta = E_f/kT$. When external forces are present, these distributions differ from their equilibrium values and are customarily written (see for example Drabble and Goldsmid[50]),

$$N = N_o + N_1 = N_o + b(\vec{q}) \frac{q_x}{k_B T} \frac{\partial N_o}{\partial z}$$

$$f = f_o + f_1 = f_o + c(\vec{k}) \frac{k_x}{k_B T} \frac{\partial f_o}{\partial \varepsilon}$$

with $\vec{q}$ = phonon wave vector and $\vec{k}$ = electron wave vector. The Boltzmann equations give the steady state conditions:

$$\left(\frac{\partial N}{\partial t}\right)_{collision} = -\left(\frac{\partial N}{\partial t}\right)_{drift}$$

$$\left(\frac{\partial f}{\partial t}\right)_{collision} = -\left(\frac{\partial f}{\partial t}\right)_{drift}.$$

If the solutions for N and f can be obtained, it is thus possible to evaluate the heat current density, W, and the electric current density,

J, from

$$W = \frac{1}{4\pi^3} \int V_x E f d^3 k,$$

$$J = \frac{-e}{4\pi^3} \int V_x f d^3 k$$

The thermoelectric power (and electrical and thermal conductivities) can then be determined[49].

Frederikse neglects scattering of phonons by electrons and impurities and considers phonon-phonon processes to be described by a mean free path $l_{ph}(q)$. Scattering of electrons by phonons and electrons by ionized impurities are both treated with mean free paths l_{ep} and l_{ei} respectively. The complex manipulations will be omitted here, but with these approximations and the Boltzmann equations it is possible to evaluate the parameters $b(\vec{q})$ and $c(\vec{k})$ and therefore N and f.

The resultant expressions for the electrical and heat current densities are then:

$$J = -K_1 \{e^2 F + eT \, grad_x \, (\frac{E_F}{T})\} - e \, (\frac{K_2}{T} + K^{(1)}) \, grad_x \, T$$

$$W = K_2 \{eF + T \, grad_x \, (E_F/T)\} + (\frac{K_3}{T} + K^{(2)}) \, grad_x \, T$$

where

$$K_i = C \int E^i \, l_e \, \frac{\partial f}{\partial E} \, dE$$

$$K^{(j)} = C \int E^j \, \frac{l_e}{l_{ep}} \, \frac{\hbar s}{T} \, (\frac{2mE}{\hbar^2})^{\frac{1}{2}} \, l_{ph} \, \frac{\partial f}{\partial E} \, dE$$

$$C = \frac{16\pi m}{3h^3}$$

$$s = \text{Velocity of Sound}$$

and where $(\ell_e)^{-1} = (\ell_{ep})^{-1} + (\ell_{ei})^{-1}$ for the case that $N_1 = 0$ $(b(q)=0)$.

Writing J in terms of $\text{grad}_x E_f$ one has, for $F = 0$,

$$J = -K_1 e \text{ grad}_x E_F - \{e(\frac{K_2}{T} + K^{(1)}) - eK_1 \frac{E_F}{T}\} \text{ grad}_x T.$$

This can be compared directly with the phenomenological expression for J as given by Drabble and Goldsmid[49]:

$$J = \frac{\sigma}{e} \text{ grad } E_F - \sigma Q \text{ grad } T.$$

Q is the thermoelectric power and σ is the electrical conductivity. By comparing coefficients the value of Q is found to be:

$$Q = -\frac{1}{e} (\frac{K_2}{K_1 T} - \frac{E_F}{T} + \frac{K^{(1)}}{K_1}).$$

The term K_2/K_1 is just the quantity ΔE_t discussed in the preceding section and in fact the first two terms on the right hand side are simply the electronic component of the thermoelectric power. The additional term, $-K^{(1)}/eK_1$ is thus the phonon contribution to the thermoelectric power arising when the lattice is not in equilibrium $(N \neq N_o)$.

If lattice scattering is the dominant mechanism, $\ell_e \simeq \ell_{ep}$ and $K^{(1)}/K_1$ is proportional to ℓ_{ph}/ℓ_{ep}, whereas if $\ell_e \simeq \ell_{ei}$, $K^{(1)}/K_1$ α

ℓ_{ph}/ℓ_{ei}. The important feature is thus the ratio of the phonon mean

free path to the electron mean free path. The evaluation of ℓ_{ph}, how-

ever, is a very complex problem. The treatment of phonon interactions

has received much attention in regard to thermal conductivity studies,

and some of these interactions will be discussed in the next section.

Herring[46] approached the lattice effect on the thermoelectric

power through the energy transport by waves in the direction of motion

of the carriers, that is by considering the absolute Peltier coefficient

π. The thermoelectric power is related to π through the Kelvin rela-

tion, $Q = \pi/T$. Herring obtained for the phonon drag component

$$Q_{ph} = -(fs^2\tau/\mu T).$$

In this expression f is the fraction of the momentum lost by electrons

which is delivered to the lattice, s is the sound velocity, τ a phonon

relaxation time, and μ is the electron mobility. This result is ana-

logous to Frederikse's since μ contains an electron relaxation time.

In order for an electron-phonon interaction to occur, the wave vectors

of the two must be comparable. Thus τ is interpreted to be an average

relaxation time for long wavelength phonons (small $\vec{q}$) and may vary con-

siderably from the relaxation time for phonons of high $\vec{q}$ considered in

thermal conductivity studies.

To obtain an estimate of the temperature dependence of Q_{ph}, Her-

ring assumed $\mu \alpha T^{-3/2}$ (acoustical phonon scattering). In addition, for

$T \ll \Theta_D$, he assumed $\tau^{-1} \alpha T^4 q$ for transverse phonon modes and $\tau^{-1} \alpha T^3 q^2$ for

longitudinal modes. These relaxation times yield $Q_{ph} \alpha T^{-3.5}$ for longi-

tudinal modes and $Q_{ph} \alpha T^{-4}$ for transverse modes. At very low temperatures, the predominant scattering of phonons is due to the boundaries of the sample, as given by Casimir[50] and is temperature independent. In this case $Q_{ph} \alpha T^{+\frac{1}{2}}$ (boundary scattering).

Herring's derivation was for a cubic system, and an anisotropy in Q_{ph} would be expected for a tetragonal crystal such as rutile. Gashim-zade[51] has extended the results to the tetragonal system and predicts $Q_{ph} \alpha T^{-3.5} \ln T$ in the "c" direction and $Q_{ph} \alpha T^{-3.5}$ in an "a" direction. It should also be pointed out that if the number of carriers is high, they may constitute an important source of phonon scattering. This would decrease τ and therefore Q_{ph}.

Lattice Thermal Conductivity

The electronic thermal conductivity of an extrinsic semiconductor is derived from phenomological theory[49] as

$$\kappa_{el} = \sigma TL = \sigma T \left(\frac{k}{e}\right)^2 (r + 5/2)$$

Here σ is the electrical conductivity, L the Lorentz number, and r a constant dependent upon the type of scattering mechanism as defined earlier. To obtain an estimate of the magnitude of κ_{el} for rutile, consider $\sigma = 10^2$ (ohm-cm)$^{-1}$ and $T = 50$ $^{\circ}K$. These values would correspond to highly reduced rutile. Using the maximum value of r as 3/2 (ionized impurity scattering) one calculates $\kappa_{el} \simeq 1.5 \times 10^{-4}$ watt/cm $- ^{\circ}K$. This number is at least three orders of magnitude smaller than measured values of κ for rutile. Hence the electronic contribution to κ in this

material is negligible and the lattice thermal conductivity is the dominant mechanism.

A lack of knowledge of vibration spectra and of anharmonic forces in crystals, however, precludes an exact calculation of the lattice thermal conductivity. In 1959 Callaway[52] developed a phenomenological model which has been successful in describing the thermal conductivity of several materials.

A brief description of Callaway's model will be given here. He assumes all phonon scattering processes can be described by frequency and temperature dependent relaxation times. In addition, the crystal is assumed elastically isotropic and no distinction is made between longitudinal and transverse phonons. The phonon scattering processes considered include normal three-phonon processes which conserve total crystal momentum, and umklapp processes, impurity scattering and boundary scattering, which are all momentum-destroying processes. The momentum-destroying processes tend to return the phonon system to an equilibrium Bose-Einstein distribution.

Specifically, the relaxation time for boundary scattering, τ_B, is independent of temperature and described by L/c. c is the sound velocity and L is a length depending upon the sample dimensions. According to Holland[53] $L = 1.12 \, (L_1 L_2)^{\frac{1}{2}}$ where $L_1 L_2$ is the sample cross section. The relaxation time for impurity or isotope scattering is assumed to have the form given by Klemens[54], $\tau_i = (A\omega^4)^{-1}$ where A is a constant proportional to the number of impurities per unit volume and ω is the angular frequency. This will be discussed in more detail in Chapter V. Normal processes and umklapp processes are described re-

spectively by

$$\tau_N = (B_2 \omega^2 T^3)^{-1}$$

$$\tau_u = (Be^{-\theta/\underline{a}T} \omega^2 T^3)^{-1} = (B_1 \omega^2 T^3)^{-1}.$$

In the last expression θ is the Debye temperature and $\underline{a}$ is a constant characteristic of the vibrational spectrum of the material. The combined relaxation time is then $\tau^{-1} = \tau_B^{-1} + \tau_i^{-1} + \tau_N^{-1} + \tau_u^{-1}$.

Callaway obtained an approximate solution to the Boltzmann equation in terms of this relaxation time. At lower temperatures he found the normal processes may be neglected, and in this case the thermal conductivity may be expressed as

$$\kappa = \frac{k}{2\pi^2 c} \left(\frac{kT}{h}\right)^3 \int_0^{\theta/T} \tau_T(x,T) \frac{x^4 e^x}{(e^x - 1)^2} \, dx$$

where $x \equiv \frac{\hbar\omega}{kT}$. τ_T is the relaxation time just given, but without the normal processes term.

CHAPTER III

EXPERIMENTAL DETAILS

Introduction

Experimental measurements were taken only on single crystals. A 200 carat rutile single crystal was purchased from the National Lead Company. This boule was grown by a Verneuil flame fusion technique and had a pale yellowish appearance. A qualitative spectrochemical analysis performed by the Jarrell-Ash Company revealed foreign impurities of less than one ppm for Al, Si, Fe, Ni, and Ag, and less than 10 ppm of Cu. The axis of the cylindrically shaped boule was approximately in the "c" direction. An x-ray diffraction pattern made in this laboratory revealed the "c" direction was about 8° off the boule axis.

All specimens used in this study were cut from the boule with the use of a diamond saw and string saw. In some instances a lapping machine was used to remove irregularities left by the cutting operations. Typical dimensions of samples whose length was parallel to the "c" direction (PA series) were 1.8 x 2.3 x 18 mm^3, while samples whose length was perpendicular to the "c" direction (PE series) were 1.8 x 2.3 x 14 mm^3. The difference in length was due to the initial diameter of the starting boule. Samples having any visible flaws were not used in the measurements.

Reduction Procedure

Dimensions of all specimens were recorded and placed in separately marked vials. Before the vacuum reduction process, samples were cleaned with acid, organic solvents and distilled water and placed into a quartz capsule (pig). The specimen and pig were then weighed separately or together on a Mettler M5 microbalance with a sensitivity of ± 2 micrograms. The reproducibility on this balance, however, was about ± 5 micrograms. After weighing, the sample and pig were placed into a quartz tube and attached to the high vacuum system (Figure 3). The vacuum system itself consisted of a glass diffusion pump backed by a Welch Model 1405 roughing pump. A cold trap using either dry ice – acetone or LN_2 was located between the specimen and the diffusion pump. The quartz tube was then evacuated to a pressure of 10^{-5} to 10^{-6} torr. Pressures were measured with a Veeco RG-75 ionization guage together with an RG-31A controller. A Hoskins FH303A tube furnace was used to heat the sample. After the furnace had reached the desired operating temperature, it was inserted over the quartz tube so that the specimen was located at the midpoint of the furnace. A Pt:Pt-10% Rh thermocouple, positioned as shown in Figure 3, monitored the temperature. This thermocouple was referenced to room temperature, and the emf was measured with a Leeds and Northrup K-3 potentiometer. Readings of pressure, temperature and time were recorded periodically throughout the day. Line voltage fluctuations between morning and evening hours resulted in temperature fluctuations of 20 to 25 ^{o}C. For this reason the reduction temperatures listed for the various samples are necessarily average values.

After the desired time had elapsed the furnace was withdrawn from
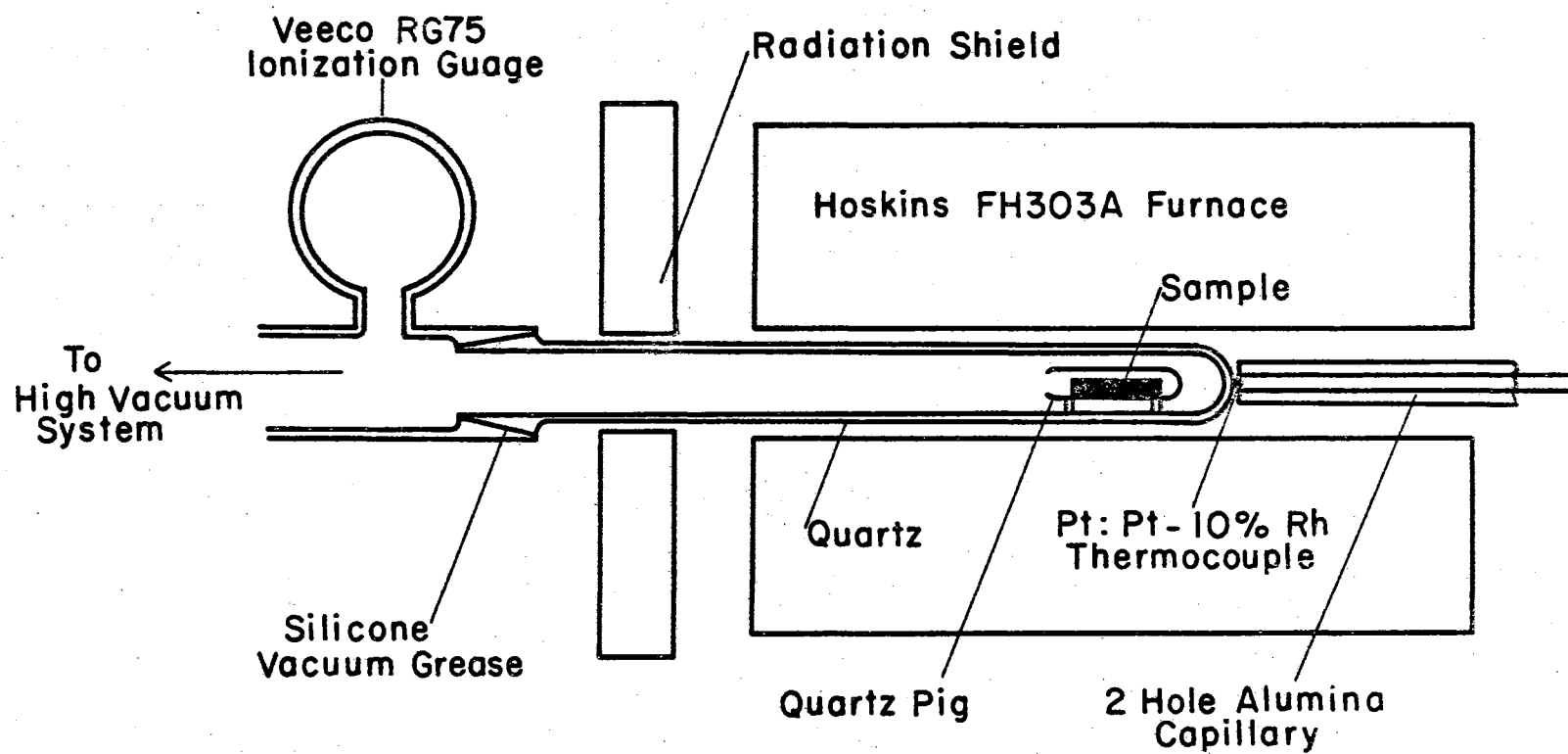
Figure 3. Vacuum Reduction System

the quartz tube and the sample allowed to cool. The thermocouple was

left in place to determine the cooling rate. Typically the temperature

fell to less than 100 ^{o}C in 2 or 3 minutes, resulting in fairly rapid

quenching of the sample. When room temperature had been achieved the

quartz rod was removed from the vacuum system and the sample and pig

reweighed to determine any weight loss. Because weight losses were

always small, extreme caution had to be exercised in handling the speci-

mens, to prevent any dirt or moisture (from breath) from contacting them

and introducing errors. Even with reasonable precautions it is felt the

weight loss measurements are probably not very accurate although there

is reasonable consistency as will be shown in Chapter IV.

Method of Attaching Leads to Samples

A necessary requirement in performing dependable measurements is a

reliable means of affixing leads to the sample. Poor contacts result in

spurious data. The following method was developed by trial and error

and usually resulted in good contacts. For resistivity or Hall measure-

ments 0.010 inch slits were cut into the sample with a string saw to

approximately the same depth. In some cases an ultrasonic drill was

used to drill 0.010 inch diameter holes into the sample. A 0.040 inch

diameter solder tip was filed to a knife edge and tinned with indium or

indium-10% silver solder. Indium contacts were then applied to the

clean samples by abrading the inside edges of the slits (or holes) with

the knife edge. Apparently the surface of reduced rutile reoxidizes

rapidly, and it is necessary to penetrate this oxidized layer to pro-

vide good contact. When applied in this manner the indium readily ad-

hered to the rutile, whereas it would not without the abrading. Similar

contacts were made on the ends of the specimens.

Any dirt or solder flux on the solder tip resulted in poor contacts, so it was necessary to keep the tip clean and use it only for making contacts. These contacts seemed to deteriorate with age so before each new type of measurement the old contacts were removed (by scraping and acid) and new ones attached.

Room Temperature to LN_2 Sample Holder

Measurements of resistivity and thermoelectric power from room temperature to liquid nitrogen temperatures were made using the apparatus depicted in Figures 4 and 5. Essentially, the main requirements are a sample holder with a high leakage resistance, a sure way of clamping the sample, and a means of varying the temperature. In the sample holder shown in Figure 4, the sample is clamped between two brass plugs which act as heat sinks. The bottom plug is spring loaded to securely clamp the sample in place, and is also insulated electrically (and thermally) from other components with a teflon sleeve. Calibrated copper-constantan thermocouples are soldered with indium to the sample ends of these plugs. As previously noted, the ends of the sample are also tinned with indium, thus providing a good thermal contact between the thermocouples and the specimen. For four-probe resistivity measurements the potential probes from the sample are soldered to the terminal strip adjacent to the specimen. Number 40 copper wires were used for these leads. The copper leads of the thermocouples were used as current leads during resistivity measurements and as Seebeck voltage leads for thermoelectric power measurements. Ambient temperature changes were accomplished by allowing the entire apparatus to warm up from (or cool
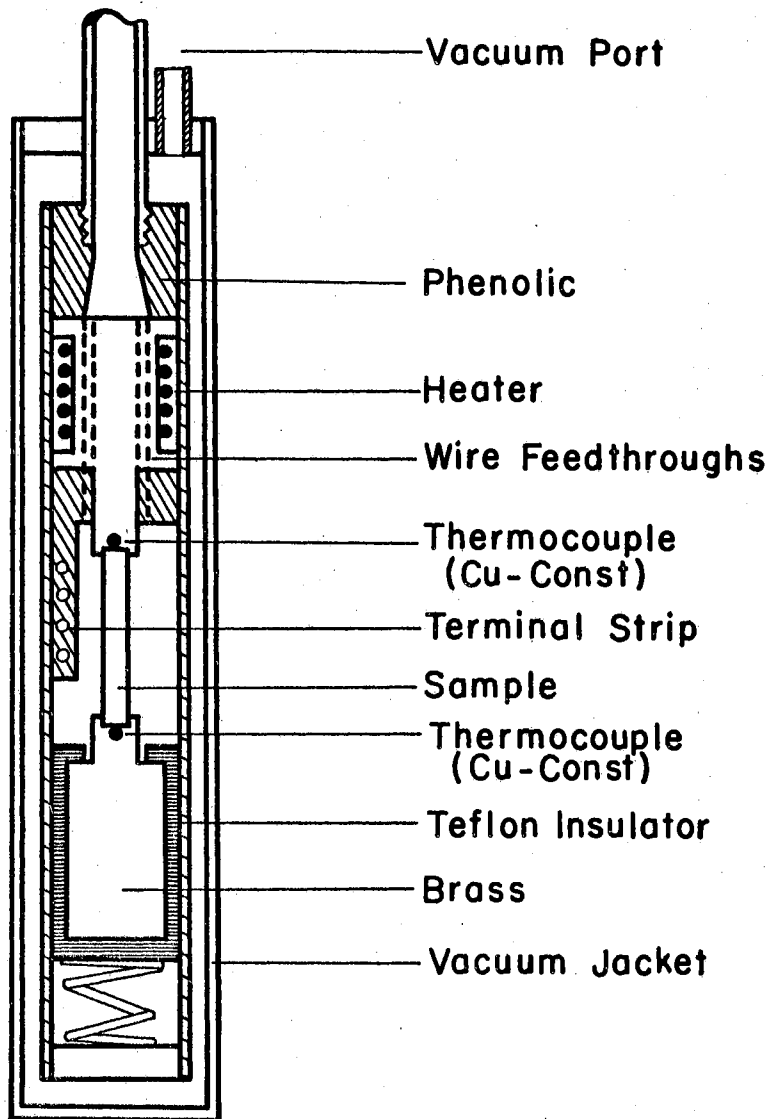
Figure 4. Liquid Nitrogen to Room Temperature Sample Holder
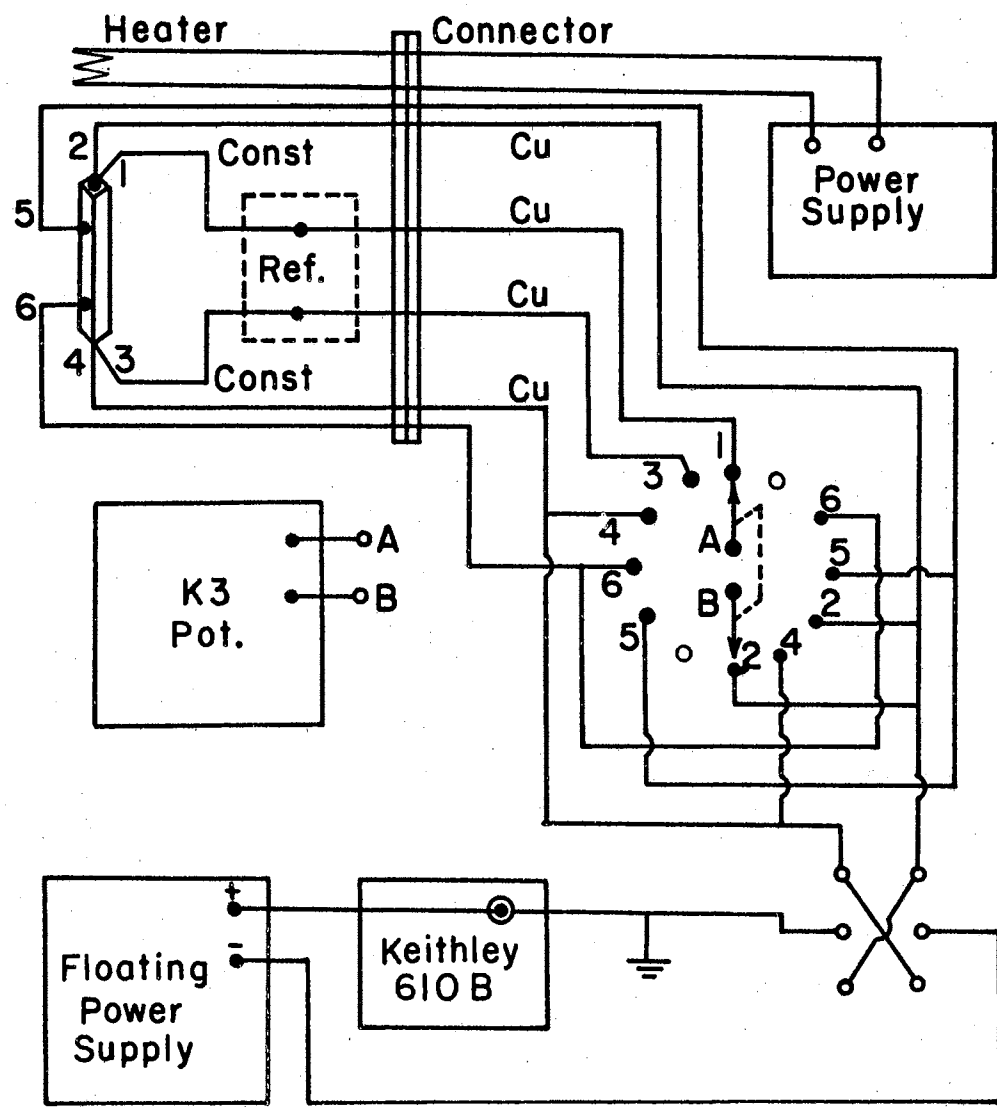
Figure 5. Schematic Diagram of Electrical Circuitry for Resistivity and Thermoelectric Power Measurements

down to) liquid nitrogen temperature. The warming rate and the temperature gradient across the sample could be altered by use of the heater.

The lower thermocouple and wires to the terminal strip were well insulated electrically from ground. All leads passed out through the center tube. A vacuum seal was made on the upper end of this tube (not shown) by use of Torr Seal epoxy.

During thermoelectric power measurements the upper end of the sample was always at ground potential (Figure 5). Denoting the temperature of the upper end of the sample as T_u, the lower end as T_1, and the Seebeck voltage as V_s, data was taken in the order: T_u, T_1, V_s, T_1, T_u. On every other reading this procedure was reversed, that is: T_1, T_u, V_s, T_u, T_1. The reason for this is that the measurement of the thermo-electric power is dynamic in the sense that the temperature is changing. Usually this temperature change was slow and the change in one of the thermocouple outputs, say T_u, during a reading was negligibly small.

During resistivity measurements, the sample ground was alternately changed from one end to the other, depending on the direction of current flow. In these measurements the Keithley 610B electrometer case was used as ground. Temperature measurements were made with zero current in the specimen since this could generate undesirable effects.

Low Temperature Thermoelectric Power
and Thermal Conductivity Apparatus

The apparatus used to measure the low temperature thermoelectric power and thermal conductivity is shown in Figures 6 and 7. In this temperature range the temperature differential across the sample must

¼" x .020" S.S.

⅜" x .020" S.S.

To High Vacuum System

To Vacuum System

Teflon Guide

Heat Leak

Indalloy #8 Solder

Inner Can
(Vertical motion)

Vacuum Port

Heat Leak

Outer Can
(Fixed)

Thermal Tempering
of Leads

Phenolic

Ambient Heater

Phenolic
Lead
Standoffs

Sample Clamp

Thermocouple
Au + 2.1 at.%Co: Normal Ag

Brass Foil

Sample

Indium Solder

Pure TiO$_2$ Sliver

Teflon

Gradient Heater
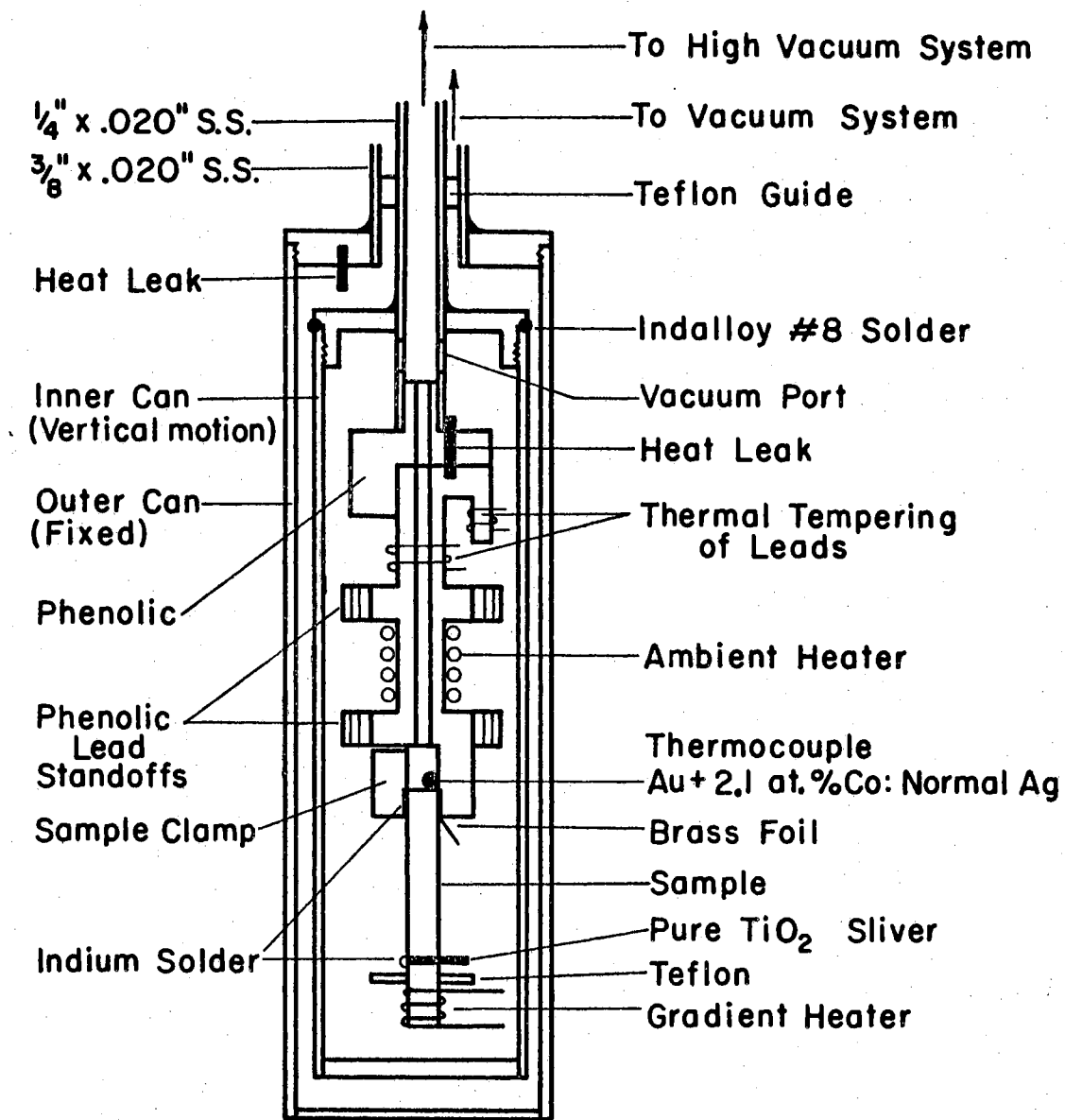
Figure 6. Low Temperature Thermoelectric Power and Thermal Conduc-
tivity Sample Holder
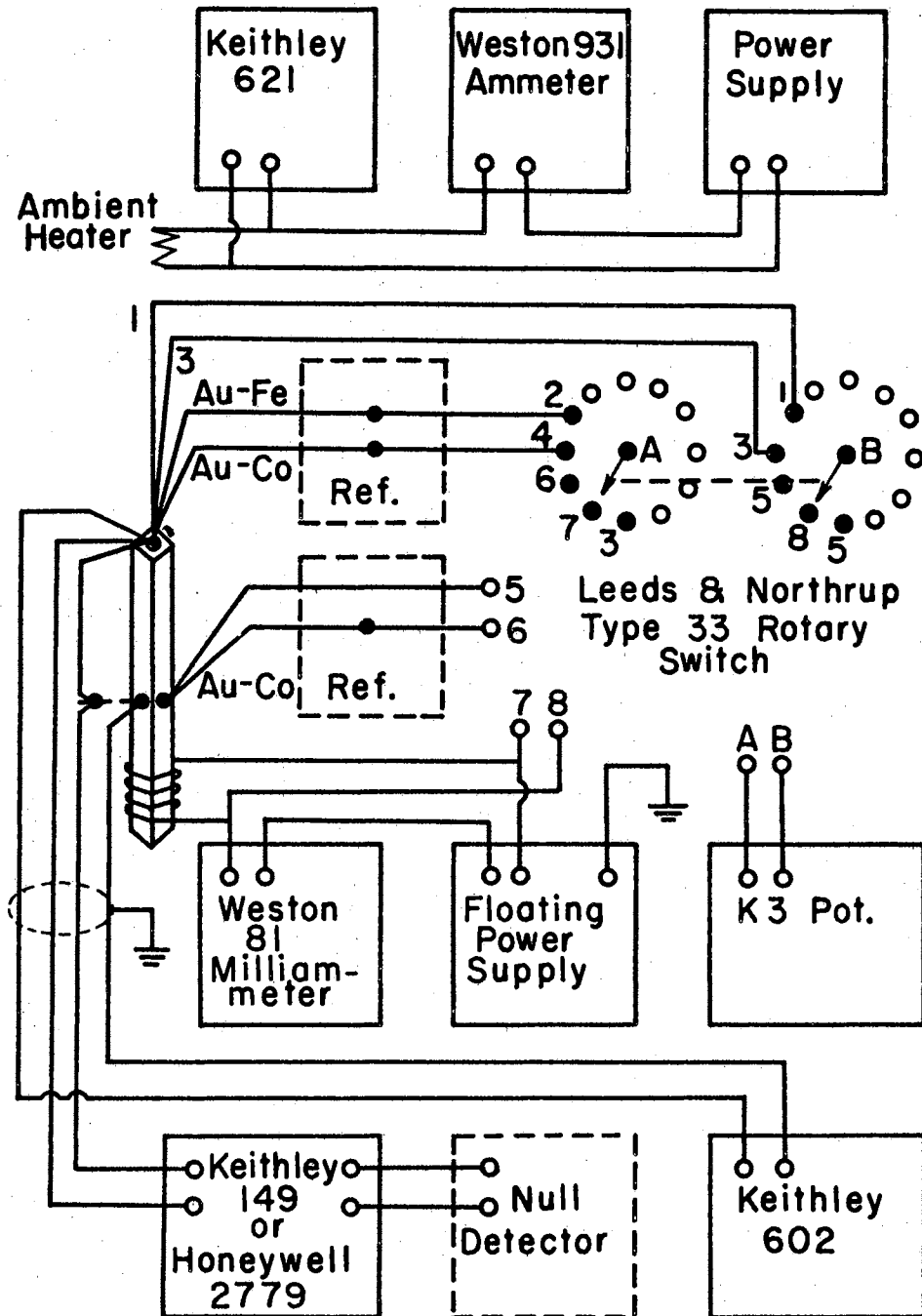
Figure 7. Schematic Diagram of Electrical Circuitry for Low
Temperature Thermoelectric Power and Thermal
Conductivity Measurements

necessarily be small and hence a measurement technique using two ther-

mocouples is not satisfactory. Thus the apparatus depicted here uses

a differential thermocouple in a modified Goldsmid-type[49] thermal con-

ductivity sample holder. Because it is desirable to maintain thermal

equilibrium a two-can type system is used. The ambient temperature of

the sample can be controlled by the ambient heater wound around the heat

sink to which the sample is clamped, and also by the pressure surround-

ing the inner can. The inner can itself is connected to a high vacuum

system. Additional temperature control is achieved by allowing verti-

cal movement of the inner can. Thus with the inner can completely

down, good thermal contact is made between it and the outer can and

hence the coolant (liquid helium). In the maximum up position, a brass

pin provided a controlled heat leak between the inner and outer cans.

In the center position, as shown in Figure 6, the heat flow between the

cans was by conduction through the gas separating them. With this

arrangement it was possible to increase the temperature of the sample

up to about 30 ^{o}K and then cool it back down to liquid helium tempera-

tures.

A temperature gradient across the sample was achieved by winding

a heater directly on it, using constantan wire of 0.14 mm diameter.

Constantan was used because of its low temperature coefficient of re-

sistance. In any measurement at low temperatures it is important that

all leads are thermally tempered. This was achieved by tight wrapping

of the wires around the heat sink. These wires then passed through the

phenolic standoffs (see Figure 6) and on to the sample.

The sample itself is clamped directly to the heat sink. Good

thermal contact is maintained at this point by tinning all mating sur-

faces with indium or an indium alloy. Between the specimen and the clamp a piece of brass foil was inserted. Soldered to this foil with indium was the thermocouple used to measure sample temperature, one end of the differential thermocouple, and a Seebeck voltage lead. The use of the foil provides for easier mounting of the sample since it does away with another contact on the sample, but probably lessens accuracy.

The temperature of the upper end of the specimen was measured with a Au + 2.1 at. % Co versus normal silver thermocouple. A Au + 0.02 at. % Fe versus normal silver thermocouple was also provided since this system has a slightly higher thermoelectric power than gold-cobalt at very low temperatures, but this thermocouple was never calibrated.

On the low resistivity samples it was necessary to provide a means of electrically insulating the lower end of the differential thermo- couple from the sample while still providing good thermal contact. Three separate techniques were used and these are shown in Figure 8. The first of these (A) used a brass clamp. Contact to the sample was made through indium applied to the specimen and to the inside knife edges of the clamp. Soldered on the back of the clamp was a piece of pure rutile (unreduced). The differential thermocouple was then sol- dered to the opposite side of this. At low temperatures pure rutile is a very good electrical insulator and heat conductor. The main dif- ficulty with this clamp arose from the different coefficients of expan- sion of rutile and brass. Thus the cooling process sometimes resulted in the clamp pulling away from the sample and causing poor thermal con- tact between them.

The second method (B) eliminated this problem in that the nylon screws contracted more than the rutile and caused the clamp to become
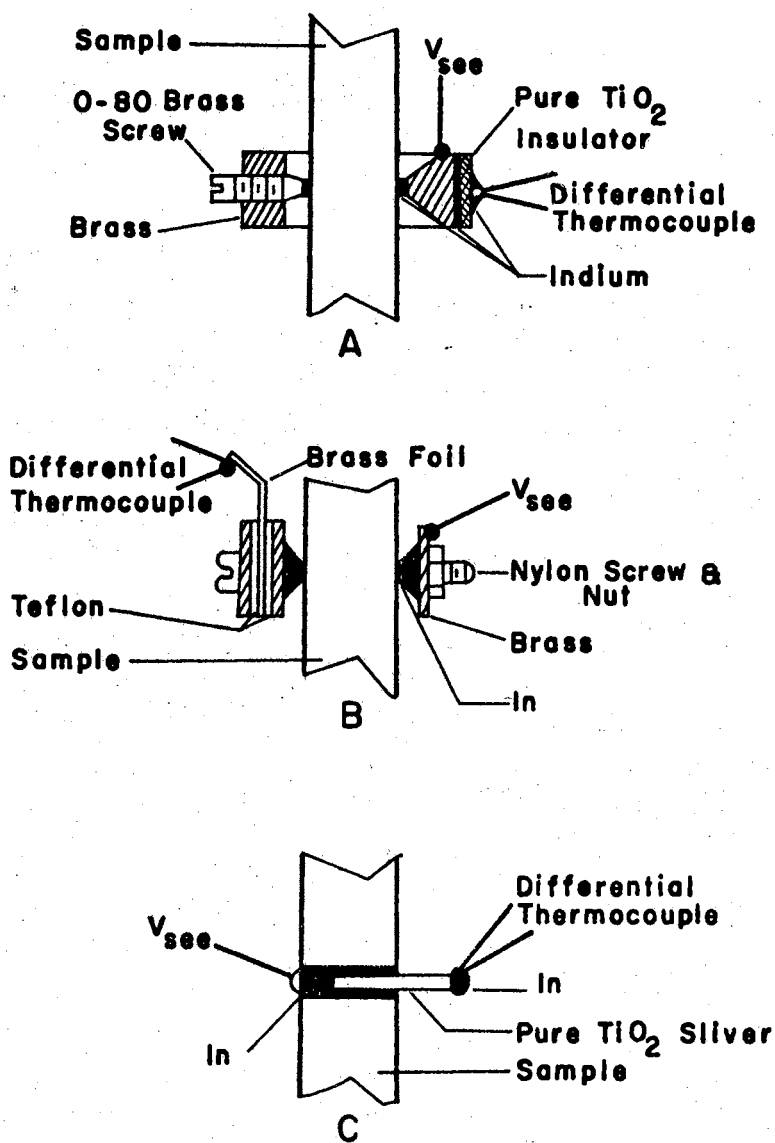
Figure 8. Three Techniques for Attaching Contacts to the Specimen

tighter at low temperatures. Teflon tape was used between the foil and the clamp and this sometimes caused poor thermal contacts, however. The last method shown in Figure 8 (C) involved soldering a small sliver of pure rutile directly to the sample and then soldering the differential thermocouple to the opposite end. This technique gave the most reproducible results and was most commonly used in this study.

The differential thermocouple output was read with either a Honeywell 2779 potentiometer or with a Keithley 149 microvoltmeter. The thermocouple numbered 5-6 in Figure 7 was used to determine the feasibility of employing a two-thermocouple type of measurement at low temperatures. This method proved to be unreliable and this thermocouple was no longer used. A battery-operated Keithley 602 electrometer was used to measure the Seebeck voltage on the high resistance samples (input resistance $\approx 10^{14}$ ohms). On low resistance samples the Seebeck voltage could be measured either with the Keithley 602 or with the K-3 potentiometer across leads 3 and 5. The K-3 was also used to measure the gradient-heater applied voltage.

Measurements procedures and sources of error in this and the preceding apparatus are discussed in Chapter IV.

Resistivity and Hall Effect Apparatus

Resistivity measurements on the high resistance samples were made with the circuit depicted in Figure 9. Hall measurements were also made with this apparatus. The sample holder itself (not shown) consisted of a copper plate to which thin glass slides were attached with General Electric 7031 varnish. Two specimens were then fastened in the same manner to the glass slides (one on each side of the copper plate).
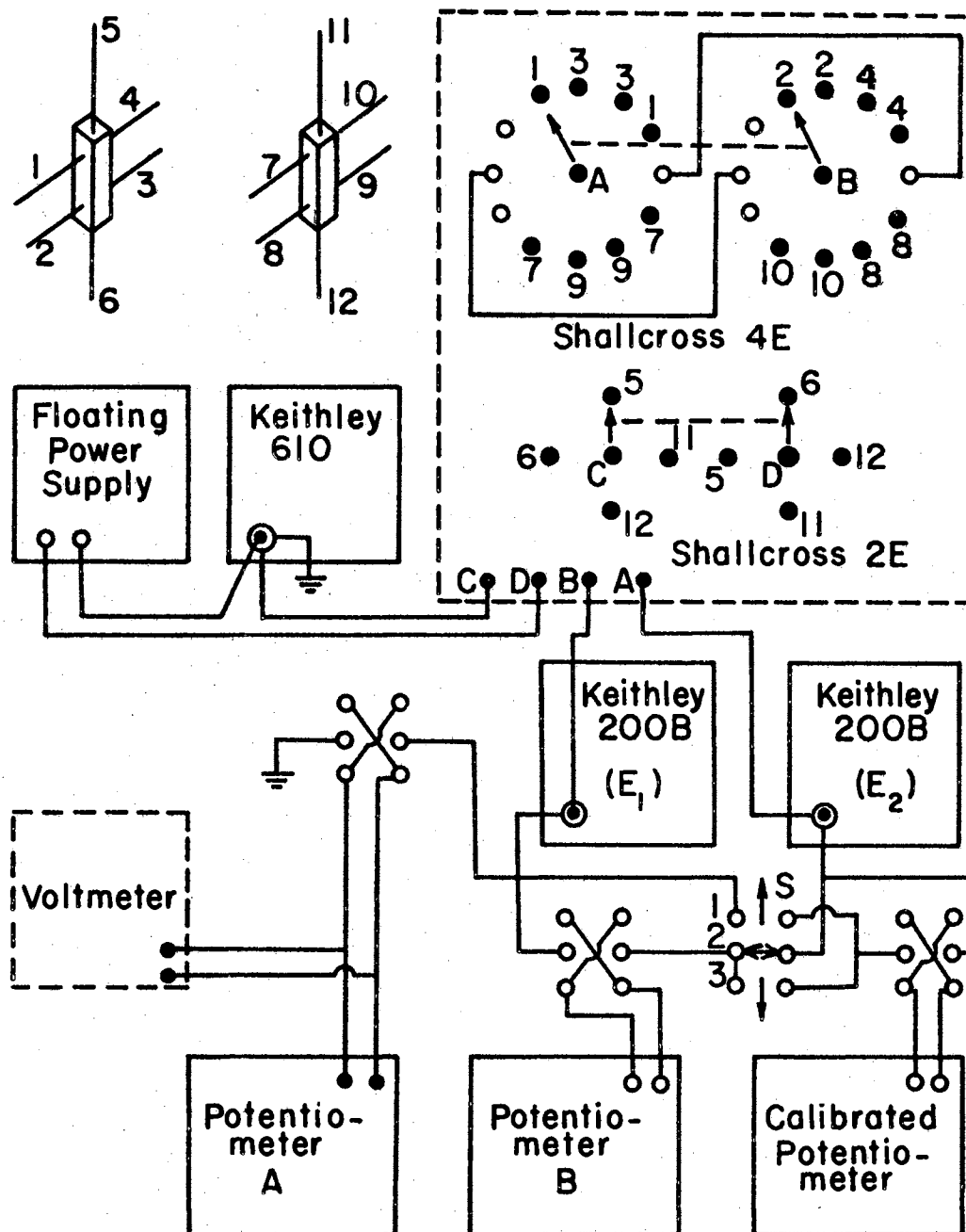
Figure 9. Schematic Diagram of Electrical Circuitry for Low Temperature Resistivity and Hall Effect Measurements

A Au + 2.1 at. % Co versus normal silver thermocouple was imbedded with-
in the copper plate and a phenolic terminal strip attached to the side
received the Hall and resistivity leads from the samples. Leads were
attached to the samples in the manner depicted at the top left of Fig-
ure 9.

The potentiometers shown in Figure 9 were constructed in this lab-
oratory using precision components and are similar in design to those
of Fischer, Greig, and Mooser[55]. Appendix B contains the circuit
diagrams and parts lists for the three potentiometers.

Essentially the Keithley 200B electrometers act as impedance
matching devices (input resistance $\approx 10^{14}$ ohms). For resistivity meas-
urements only potentiometer A and the calibrated potentiometer are
needed. Suppose, for example, that the Shallcross 4E switch is set to
connect resistivity leads 1 and 2 to the electrometers E_1 and E_2. The
current flowing through the sample is measured with the Keithley 610
electrometer. E_1 is then brought to zero by adjustment of potentiometer
A. With switch S in position 1, electrometer E_2 is then balanced using
the calibrated potentiometer, which gives a direct reading of the volt-
age drop across the potential leads.

Potentiometer B is only used during Hall measurements and facili-
tates the elimination of errors which might arise from misalignment of
the Hall probes. In these measurements the Shallcross 4E switch is
used to connect a pair of Hall probes (say 1 and 4) to the electrometers.
A current is then passed through the sample and the magnetic field
applied. With switch S in position 2, E_1 and E_2 are adjusted to zero
using potentiometers A and B respectively. The magnetic field is then
reversed and E_1 again brought to zero using potentiometer A, leaving

potentiometer B unchanged. With switch S in position 3, E_2 is next

balanced with the calibrated potentiometer, which reads out twice the

Hall voltage. This procedure eliminates misalignment errors but cannot

correct for errors arising from thermal gradients in the sample. These

necessitate repeating the measurements with reversed current flow. The

current flow is reversed in the sample by use of the Shallcross 2 series

switch located in the switching box. In addition, each potentiometer

has polarity reversing switches as shown in Figure 9.

This apparatus worked well except that it required isothermal con-

ditions for accurate Hall data, a requirement sometimes difficult to

fulfill. At the time Hall measurements were made a magnet providing

large fields was not available, and most data was thus taken using a

permanent magnet with a field strength of 1.12 gauss, a gap of about 3

inches, and with flat 2" diameter pole pieces.

CHAPTER IV

EXPERIMENTAL RESULTS

Reduction Parameters

This chapter is divided into several main sections, including sample reduction parameters, electrical measurement results, and lastly the thermoelectric power and thermal conductivity results. The reduction of the sample was performed in the apparatus described earlier. During preliminary studies it was found that the reduction process at < 700 °C in a vacuum was very slow. For this reason samples were reduced at three higher temperatures, namely, 850 °C, 950 °C, and 1050 °C, the latter temperature being the maximum operating temperature of the furnace. At these temperatures treatments varied as to the length of time of the process. These treatment times were 3 hrs, 9 hrs, 72 hrs, and 185 hrs, with some other samples reduced different lengths of time.

The color of the specimens changes during the reduction process to a shade of blue. The degree of coloration depends on the state of reduction. Heavily reduced samples (e.g. PA 12) are very dark blue and are opaque. Table I lists the samples in order of increasing blueness as determined visually, together with the reduction parameters and sample dimensions. As mentioned earlier, temperature variations occurred in samples treated for > 24 hrs due to in-house line voltage fluctuations. The numbers given, then, are averaged values, weighted

42

TABLE I

SAMPLE DIMENSIONS AND REDUCTION PARAMETERS

Sample[+]	Dimensions (cm)			Reduction Process			TiO_{2-X}
	W	T	L	Temp (^{o}C)	Pressure (Torr)	Time (Hrs)	X
PA 5	0.234	0.173	1.754	852	3.4×10^{-4}	18	*
PA 4	0.237	0.194	1.795	850	4.0×10^{-4}	42	*
PA 7	0.243	0.182	1.787	846	6.8×10^{-6}	72	*
PA 11	0.234	0.183	1.804	948	4.0×10^{-6}	9	3.2×10^{-5}
PA 8	0.239	0.188	1.798	842	5.8×10^{-6}	185	*
PA 2	0.239	0.186	1.792	827	1.6×10^{-5}	116.5	*
PA 10	0.238	0.188	1.790	950	3.4×10^{-6}	72	2.0×10^{-4}
PA 1	0.256	0.235	1.753	1078	2.0×10^{-5}	3	2.4×10^{-4}
PA 6	0.237	0.183	1.800	1066	1.9×10^{-5}	9	5.2×10^{-4}
	[a]0.126	0.183	1.800				
PA 3	0.235	0.161	1.807	1045	6.9×10^{-6}	72	1.6×10^{-3}
PA 9	0.235	0.118	1.769	1168	2.8×10^{-5}	3	4.0×10^{-4}
PA 12	0.235	0.178	1.790	1047	3.8×10^{-6}	185.5	-----
PE 12	0.236	0.179	1.424	1039	2.3×10^{-6}	181.3	-----
PA 13	0.232	0.188	1.803	1047	2.3×10^{-6}	352	-----

[+]PA specimens are those having L parallel to the "c" axis, PE specimens have $L \perp C$.
*Results in error due to weight loss in quartz capsule.
[a]After cutting to decrease cross-section from 0.0433 to 0.023 cm^2.

with time whenever possible. The pressure data shows that better vac-
uums were obtained when long reduction times were used. This is a re-
sult of outgassing with the vacuum system. Converting these numbers
to a partial pressure of oxygen, $P_{O_2} \approx 10^{-9}$ atm. Time was measured

from the moment the furnace was placed over the quartz tube, even
though it took about 10 minutes for the system temperature to recover
to within 10% of the desired value. Conceivably this could affect sam-
ples treated for short times ($\leq$ 3 hrs), but is negligible in specimens
treated for long times (> 24 hrs).

The number x listed in Table I is determined from the weight loss
measurements and is an indication of the amount of deviation from stoi-
chiometry resulting from the various treatments. Assuming the material
is originally stoichiometric and that only oxygens are removed in the
reduction process, x is evaluated as follows.

If W is the sample weight, then the number of TiO_2 molecules, N_T,
is given by $N_T = WL/A(TiO_2)$, where L is Avagadro's number and $A(TiO_2)$
is the molecular weight of rutile (= 79.8998 gm). Now if only oxygen
atoms are liberated in the treatment, and the weight loss is ΔW, then
the number of oxygens removed, N_0, is $N_0 = \Delta WL/A(0)$, where $A(0)$ is the
atomic weight of oxygen (= 15.9994 gm). In the starting material there
were $2N_T$ atoms of oxygen, whereas after the treatment there are $2N_T - $
N_0 atoms of oxygen remaining. Denoting the composition of the nonstoi-
chiometric material as TiO_{2-x}, the value of x is then given by

$$x = \frac{N_0}{N_T} = \frac{\Delta W}{W} \frac{\text{Molecular wt. of } TiO_2}{\text{Atomic wt. of } 0}$$

or $x = 4.994 \frac{\Delta W}{W}$.

For the samples listed in Table I that are marked with an aster-
isk, the weight loss was not accurately determined. This resulted from
an unmeasured weight loss in the quartz pig which was weighed together
with the sample. Thus, the weight losses for these samples actually
represented a total weight loss for the specimen and the quartz capsule.
The other values are estimated to be accurate to within ± 50%, the main
source of error existing within the microbalance.

Because the samples are quenched quite rapidly from the treatment
temperature back to room temperature, it is assumed in later discus-
sions that the atomic defects are "frozen" into the specimens. Thus
the defect concentration after quenching is assumed to be the same as
the initial high temperature concentration of defects. At room temper-
ature these "frozen-in" defects actually represent a non-equilibrium
situation, and changes in concentration with time might be anticipated.
Resistivity measurements on some of the samples over a period of one
and one half years do not indicate any change, however, at least with-
in the experimental error of the room temperature resistivity measure-
ments (< ± 5%).

Electrical Measurement Results

The electrical resistivity results for some of the samples are
shown in Figures 10 and 11. All measurements above liquid nitrogen
temperatures were made using a four-probe technique as described ear-
lier. All four-probe measurements were carried out at a measured pres-
sure of approximately 10^{-3} torr. In the LN_2 to room temperature appar-
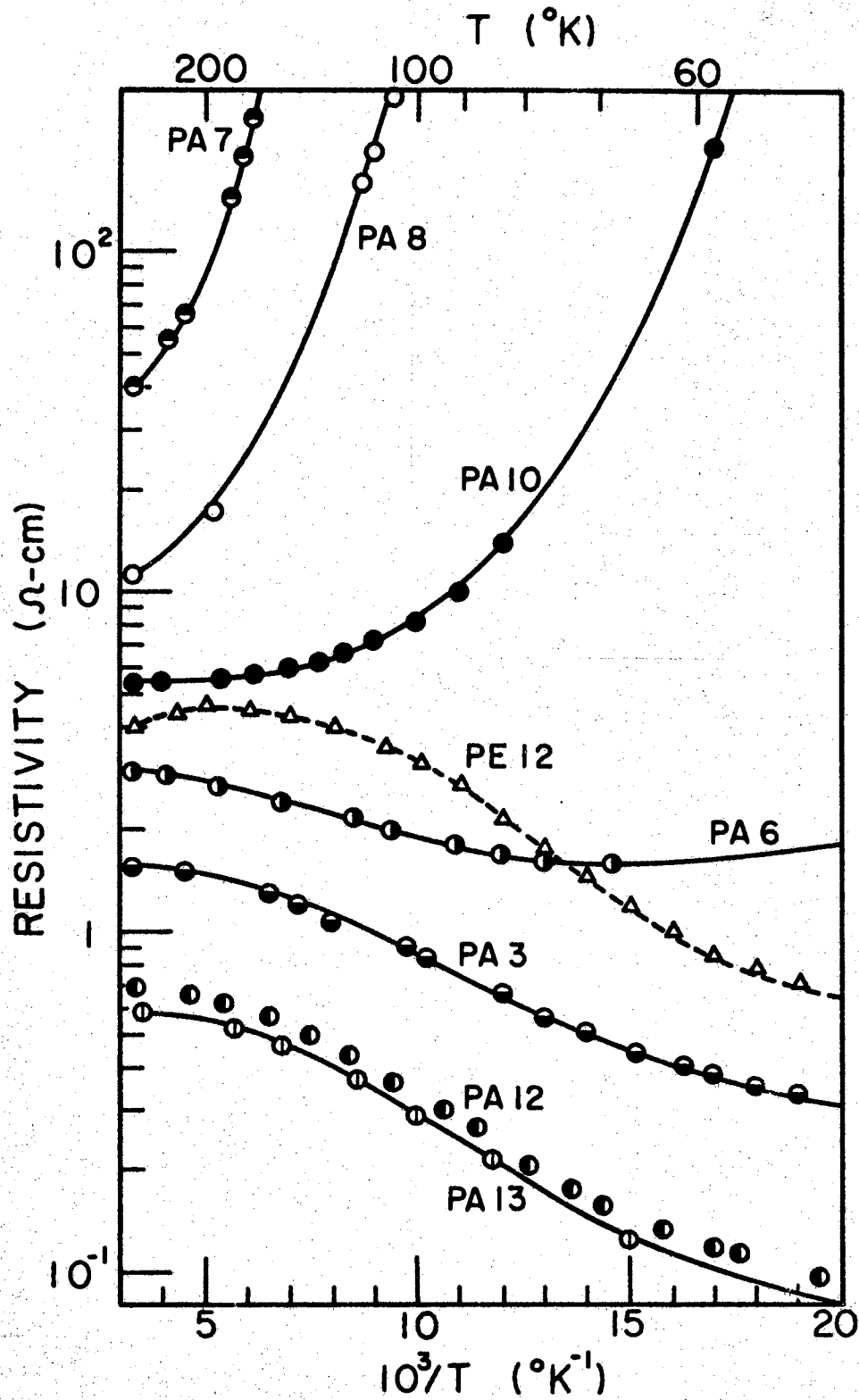
Figure 10. Resistivities of Samples from 50 °K to Room Temperature
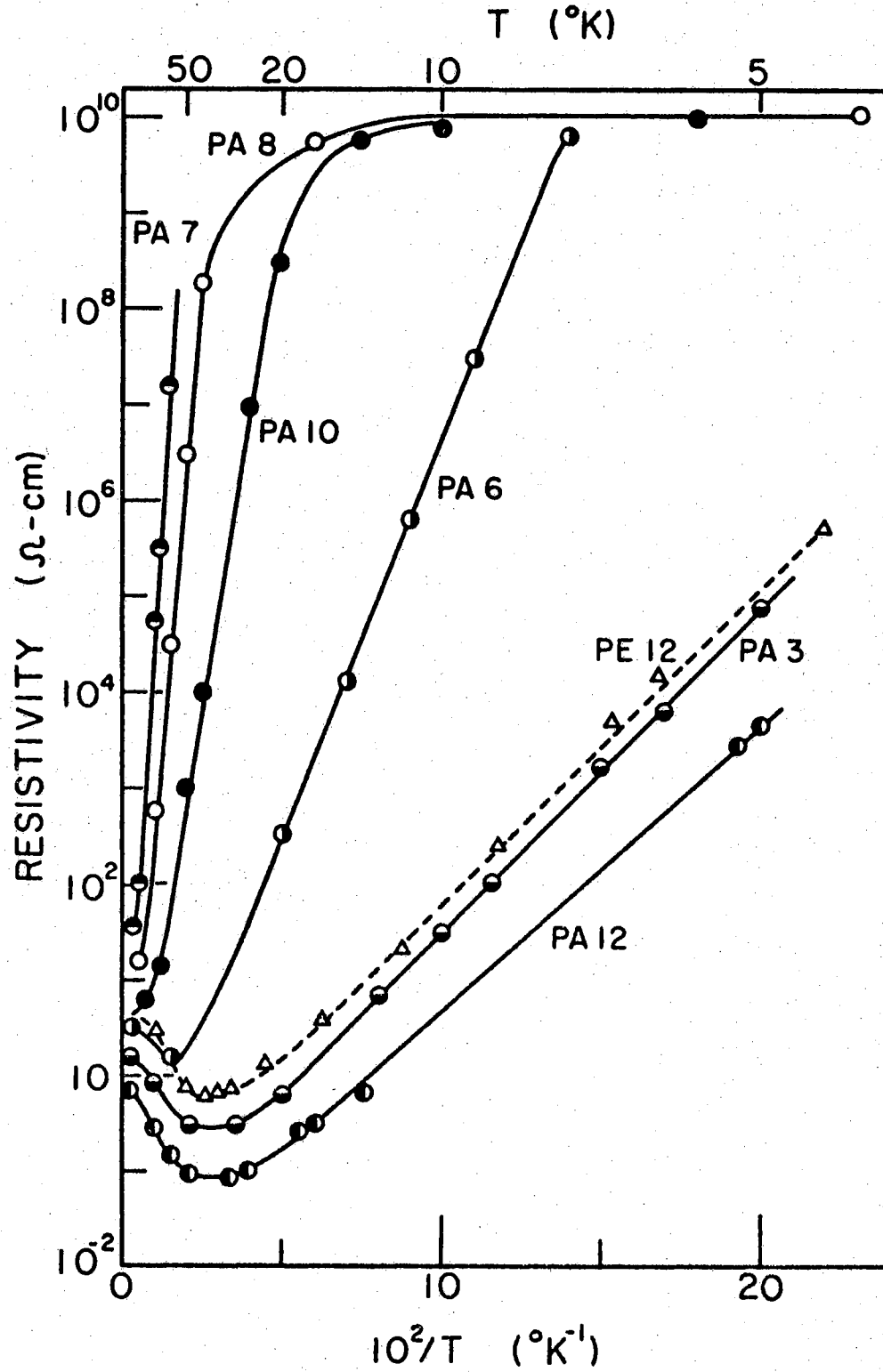
Figure 11. Resistivities of Samples from Liquid Helium to Room Temperatures

atus, measurements could not be made under isothermal conditions since a temperature gradient always existed across the sample. To correct for this error, data were taken first with the current flowing in one direction and then the current was reversed through the sample and data were again taken. The actual value of the resistivity was taken to be the average of these two values. When taken in this fashion the data were independent of the size of the thermal gradient in the sample and were very reproducible. The error in these measurements is estimated to be $< \pm$ 5%, the largest source of error arising from the inability to accurately determine the distance between the potential probes, L.

At temperatures below LN_2, measurements were made using either four-probe (PA 7, PA 8, PE 12, PA 3, and PA 12) or two-probe (PA 10, PA 6) techniques. In the latter case the data were taken while measuring the thermoelectric power, except no temperature gradient existed within the sample. Two-probe measurement results were reproducible at low temperatures when the resistivity was high, but at higher temperatures when the resistivity was $< 10^3$ ohm-cm, contact resistances gave erroneous results. In the low resistance samples the contact resistance ranged from 25 to 50 times the sample resistance near LN_2 temperatures.

The remaining low temperature resistivity data were taken with the four-probe apparatus discussed at the end of the last chapter. In this system it was again possible to reverse the current direction in the sample. Because the sample temperature was changing during these measurements (about 1 $^{\circ}$K/minute) the results could be in some error, especially in the regions of rapid resistivity change. Finally, the nearly-zero slope portions of the resistivity curves for samples PA 8

and PA 10 are probably somewhat more in error since the measured sample resistances in these cases ($\sim 10^{12}$ ohms) are nearing the electrometer input resistance ($\sim 10^{14}$ ohms). Even more important may be the fact that an accurate sample holder leakage resistance is not known, but probably it is of the same order as the specimen resistance. However, comparable results (PA 8 and PA 10) were obtained in two different sample holders.

Figure 11 illustrates a very pronounced change in the resistivity with the reduction process. In particular it is informative to look at samples treated at about the same pressure and for the same length of time, but heated at different temperatures. For example, samples PA 7, PA 10 and PA 3 were treated 72 hours at 4 to 7 x 10^{-6} torr, but at temperatures of 846, 950, and 1045 $^\circ$C, respectively. Figure 11 or 12 shows the striking difference in behavior between these samples. The resistivities of PA 7 and PA 10 are monotonically increasing with decreasing temperature whereas for PA 3 the resistivity actually decreases gradually to a minimum near 35 $^\circ$K and then increases exponentially with inverse T.

To ascertain whether this behavior might in part be attributable to a lack of equilibration of the defects in the lower treatment temperature samples, specimens PA 8 and PA 12 were treated for 185 hours at temperatures of 842 and 1047 $^\circ$C respectively. These two samples, however, still display the marked difference in behavior. The room temperature resistivity of sample PA 12 was a factor of 2.3 less than that of PA 3. To determine if the defect concentration produced by the reduction process had equilibrated, sample PA 13 was treated for 352 hours (14.5 days) under approximately the same conditions as PA 12.

The room temperature resistivity of this sample decreased by 13% from the 185 hour sample. Using the resistivity as an indicator of the reduction state, it appears that much longer times are necessary to achieve thermodynamic equilibrium than has been previously thought[12].

Because rutile has a tetragonal structure, one would expect an anisotropy in the resistivities for samples cut with the length parallel to an "a" direction and a "c" direction. Figure 12 shows the ratio ρ_a/ρ_c for samples PE 12 and PA 12, two samples treated under the same conditions. Curves of this type have meaning if both samples have identical defect concentrations. Unfortunately this is probably never the case even for samples treated simultaneously, since the diffusion constant for oxygen in rutile is known to differ in the "a" and "c" directions[56]. Of interest, however, is the maximum in ρ_a/ρ_c occurring near 100 °K and the trend toward a constant value at lower temperatures.

To determine some other pertinent parameters concerning the conduction process in these samples, Hall measurements were performed on samples PA 3 and PA 6. Experimental determination of the Hall voltage, V_H, allows calculation of the Hall coefficient, R_H, according to the expression

$$R_H = 10^{-8} V_H T/BI,$$

where T is the sample thickness in cm, I the sample current in amperes, and B the applied magnetic field in gauss. For a tetragonal crystal there are three (different) Hall coefficients, depending on the orientation of I and B with respect to the crystal "a" and "c" directions. If L||c||I then B||a, but if L||a||I then B can be parallel to "a" or
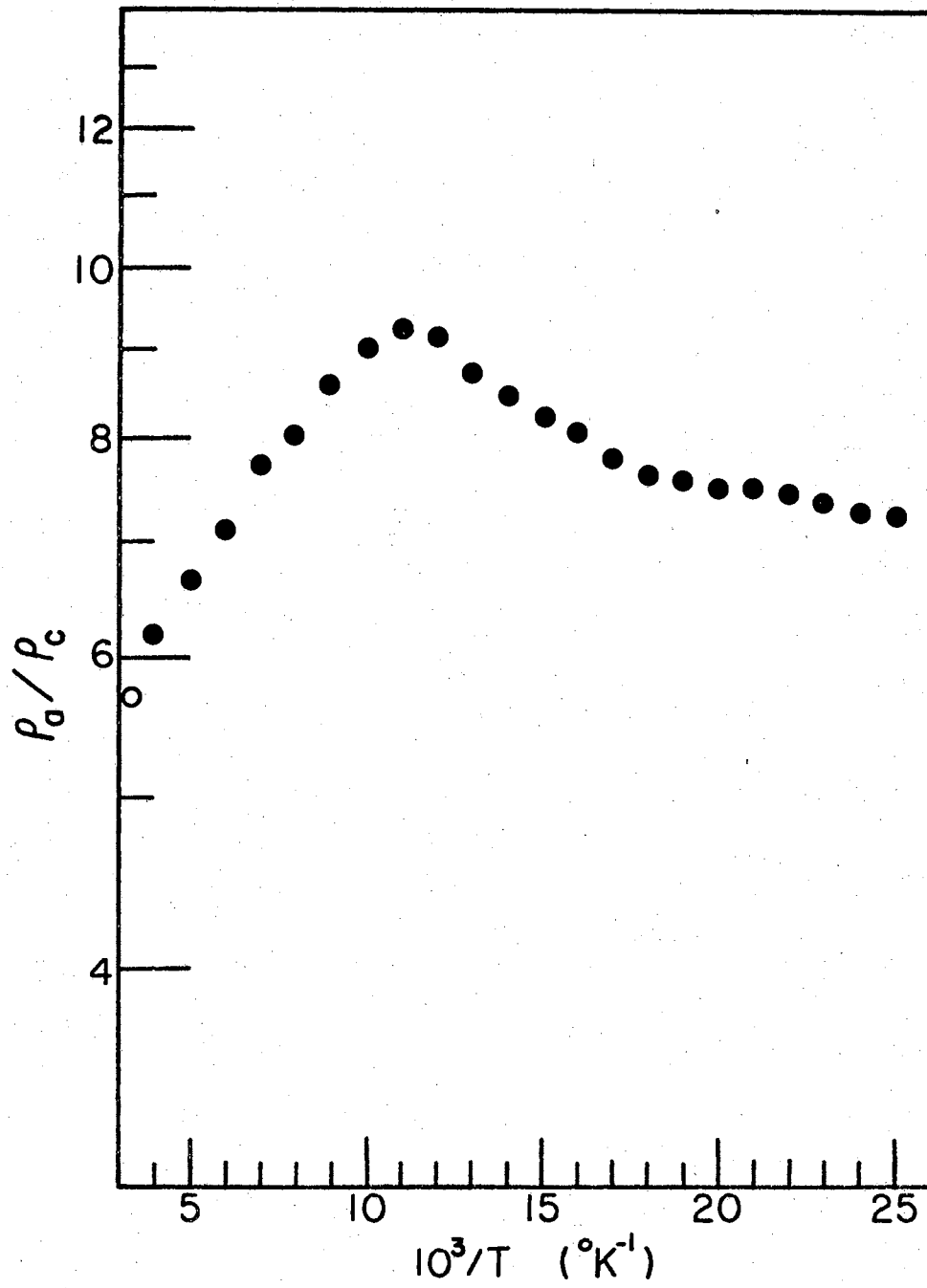
Figure 12. Resistivity Anisotropy as a Function of Temperature

parallel to "c". In this work only L||c (PA series) samples were studied, hence B||a. From measured values of R_H, the charge carrier concentration, n, can be calculated from

$$n = - (3\pi/8e) \ G(E_f)/R_H,$$

where $G(E_f)$ is a function of the Fermi level and varies from $8/3\pi$ for a degenerate material (say a metal) to 1 for nondegenerate specimens. Reduced rutile has never been observed to be degenerate. Measurements of the Hall coefficient and resistivity enable one to determine the Hall mobility since $\sigma = 1/\rho = ne\mu_H$.

Results of measurements on sample PA 3 are shown in Figures 13 and 14. These results are similar to those obtained by Becker and Hosler[12] on vacuum-reduced samples. The carrier concentration results in this temperature range can be fitted by two Boltzmann terms suggesting two sources of conduction electrons. The mobility results reveal that the room temperature value is ≤ 1 cm^2/volt-sec, a value small compared to semiconductors such as germanium or silicon. The temperature dependence of the mobility in the range 50 to 100 ^{o}K is proportional to $T^{-2.5}$, a dependence unexplained by simple existing theories. For example, acoustical phonon scattering yields $\mu\alpha T^{-1.5}$ whereas ionized impurity scattering gives $\mu\alpha T^{+1.5}$.

Thermoelectric Power

Measurements of the Seebeck effect were made using the two different systems described earlier. All data being taken at a measured pressure of approximately 10^{-3} torr. The absolute value of Q is deter-
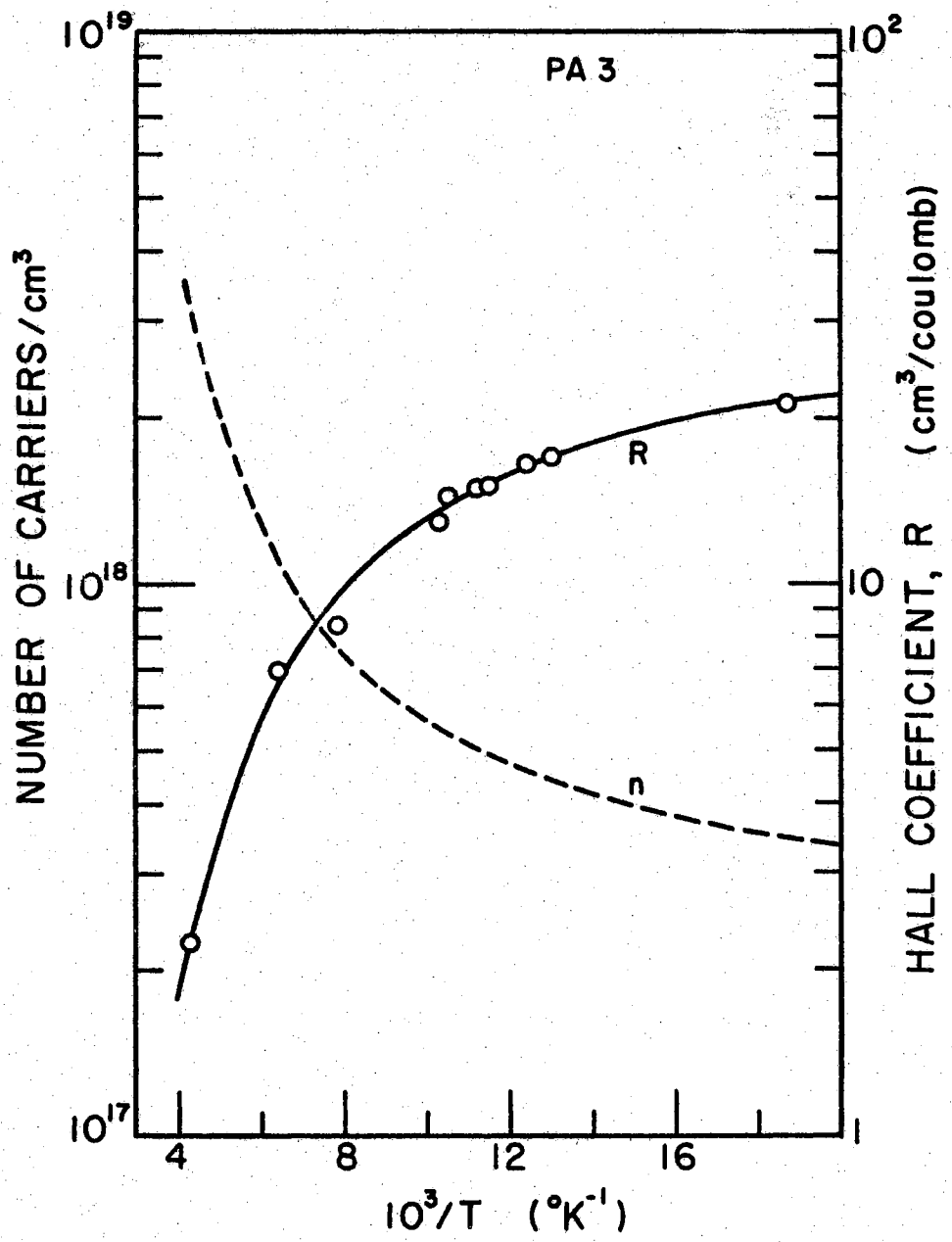
Figure 13. Hall Coefficient and Carrier Concentration for
Specimen PA 3
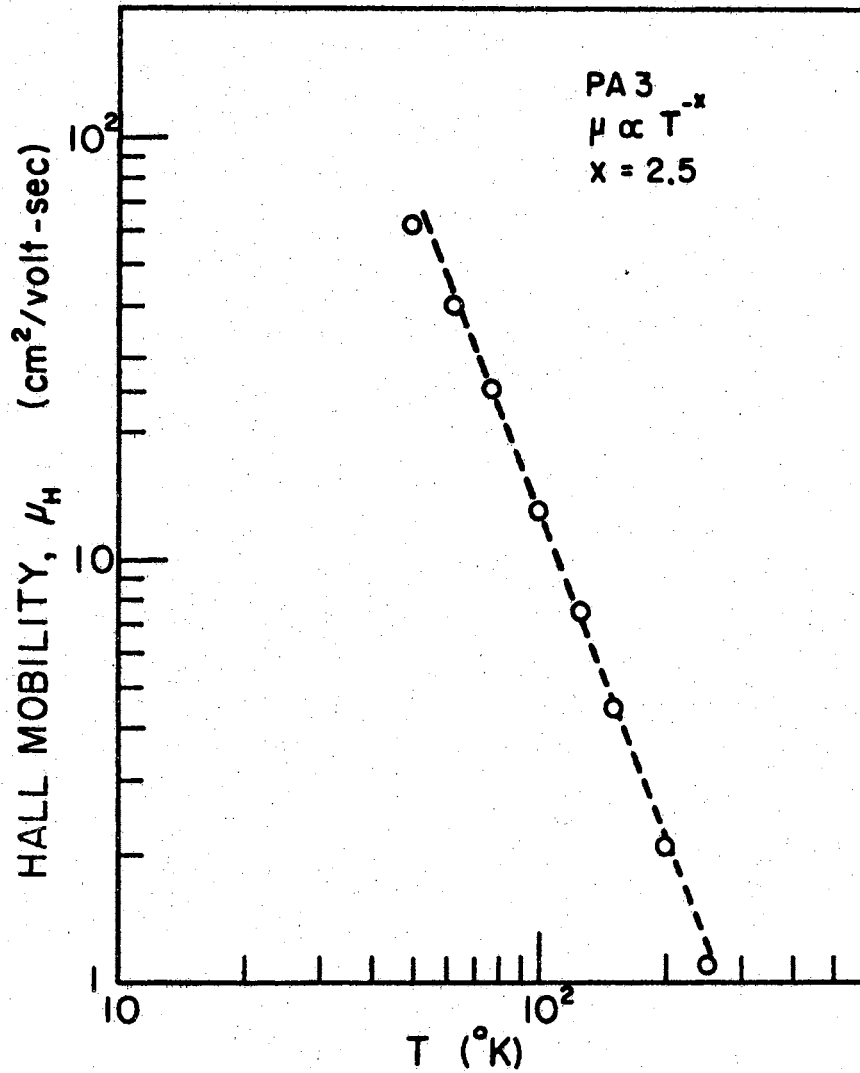
Figure 14. Hall Mobility of Specimen PA 3 Above Liquid
Nitrogen Temperatures

mined from the expression

$$Q = \lim_{\Delta T \to 0} \frac{\Delta V_s}{\Delta T}$$

where ΔV_s is the Seebeck voltage developed across the specimen. At

high temperatures the magnitude of ΔT ranged from 2 to 20 $^\circ$K with lit-

tle effect on the value of Q. Comparison of data taken with the sample

cooling and warming indicates any error resulting from the dynamic

nature of the measurement is small. Above liquid nitrogen temperatures

the data were reproducible to within ± 5%. The two copper-constantan

thermocouples had nearly equal thermoelectric powers over the entire

temperature range and so the Seebeck coefficient could be calculated

from

$$Q = V_s \, \alpha(T)_{Cu-Const.} / (V_1 - V_u),$$

where V_1 is the average value of the lower thermocouple emf, V_u is the

average value of the upper thermocouple emf, and $\alpha_{Cu-Const}$ is the ther-

moelectric power of the copper-constantan system. Using conventional

sign notation for the thermoelectric power, the value of Q was always

negative indicating conduction was by electrons.

Measurements at low temperatures were more difficult due to the

problems in clamping the differential thermocouple to the specimen as

previously noted. Typical values of ΔT in this apparatus were 0.2 to

0.8 $^\circ$K at 10 $^\circ$K and 0.4 to 1.5 $^\circ$K at 20 $^\circ$K. Attaching the differential

thermocouple thermally to the sample with the "pure" rutile sliver gave

the best results.

At low temperatures, with zero gradient-heater input, the differ-

ential thermocouple displayed an emf of about 1.8 μV nearly independent of temperature. It was determined that this value was due to inhomogenities in the wires, and possibly to contact potentials in the exterior circuit. Contact potentials were estimated to be less than ± 0.5 μV, however. In addition to this correction, heat conduction through the system to the sample tended to create a gradient across the sample with the upper end the warmer. The magnitude of this effect ranged from zero to about 1 μV. To correct for these errors the differential thermocouple output was determined as a function of temperature, with zero gradient-heater input, during each run. The necessary corrections were then made in the thermocouple output when the gradient-heater was on and a temperature gradient existed across the sample. These corrections varied little from run to run and, in fact, a large deviation from the normal values usually indicated a poor thermal contact between the differential thermocouple and the sample. The importance of the correction can be seen in the following example. At 20 °K, a one-degree temperature gradient corresponds to 20 μV, and if the correction were 2 μV, failure to take it into account would result in a 10% error. (The correction at 20 °K was never this big, however.) At 5 °K the situation is worse, because a smaller gradient is required, say 0.25 °K, which corresponds to about 4 μV. Thus at 5 °K failure to make the 2 μV correction (typical) causes a 100% error. Obviously the larger the thermal gradient can be, the less effect the correction has.

The temperature of the midpoint of the sample was found by subtracting half the differential thermocouple output from the emf of the thermocouple attached to the upper end of the specimen. Taking all factors into account, including the observed scatter in the experimental

points, it is felt that the values of Q measured below 10 $^{\circ}$K are accurate to ± 20%, while above this temperature, accuracy is probably better than ± 10%. Thermal equilibrium of the specimen could not be achieved in the range from 25 to about 60 $^{\circ}$K, and because of this the measurements are dynamic in nature. The excellent agreement of the data taken in the two different thermoelectric power systems, however, suggest any error arising from this effect is small. The gradual warming of the specimens can be expected to introduce a larger error in thermal conductivity measurements as will be mentioned in the next section.

The liquid nitrogen to room temperature results are shown in Figure 15. Near 100 $^{\circ}$K a rapid increase in the magnitude of Q is observed which is attributed to phonon drag effects. Figures 16, 17, and 18 present the actual data points for three of the samples. Smoothed curves for these samples are also shown on Figure 19, together with a smoothed curve for sample PA 13 and data points for samples PA 8 and PA 10. Accurate data points at the lowest temperatures could not be obtained for these latter two samples due to their very large resistivity. Reference back to Figure 11 shows that they reach their maximum resistivity near the temperatures where the thermoelectric power curves terminate.

In general, the Q results show a large increase in magnitude with decreasing temperature, eventually reaching a maximum and then decreasing. Also, the magnitude of Q shows an inverse relationship to the degree of reduction of the specimen, that is, upon the concentration of defects. The temperature of the maximum in the curves also shifts to higher temperatures with the more highly reduced samples. To ascertain
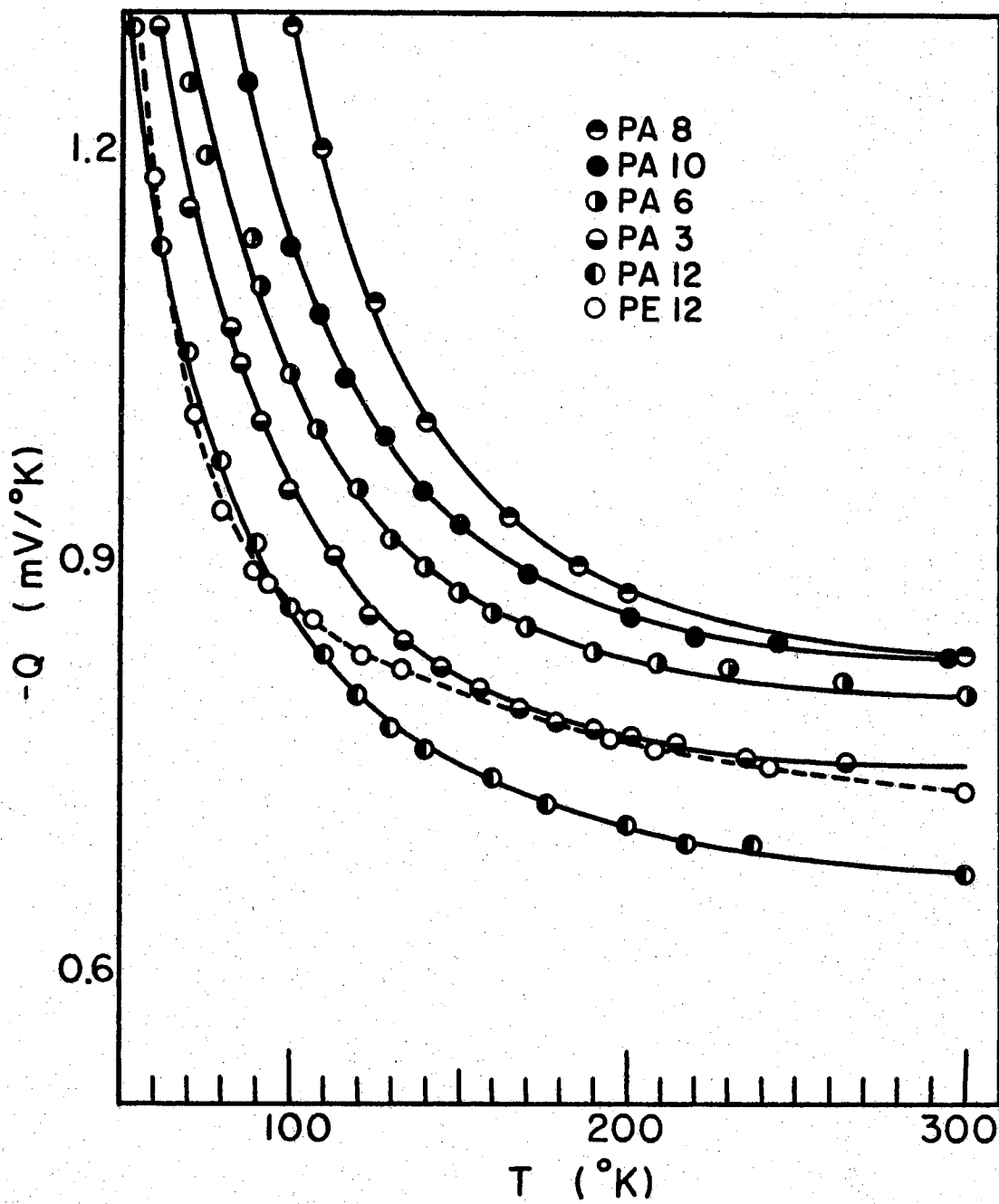
Figure 15. Thermoelectric Powers of Samples from 50 °K to Room Temperature
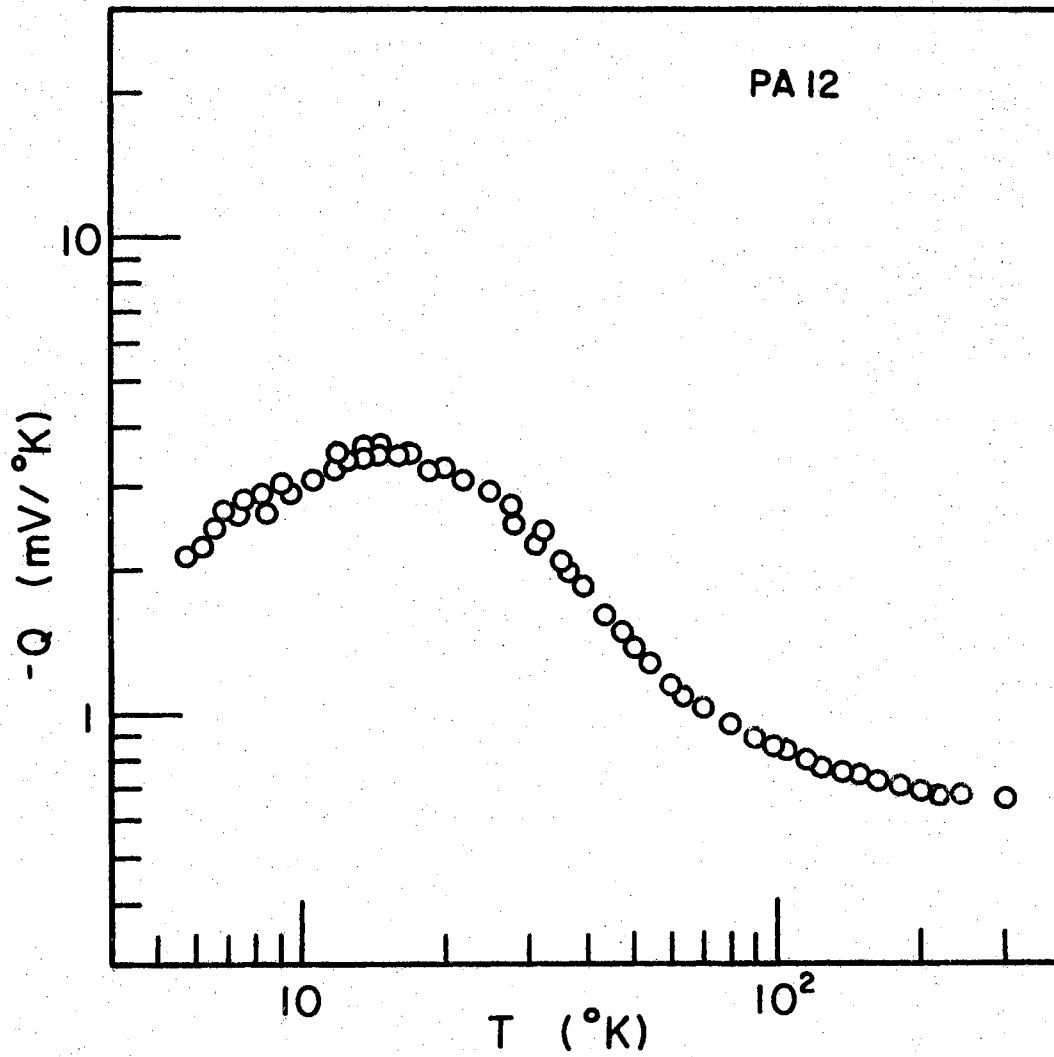
Figure 16. Thermoelectric Power of Specimen PA 12
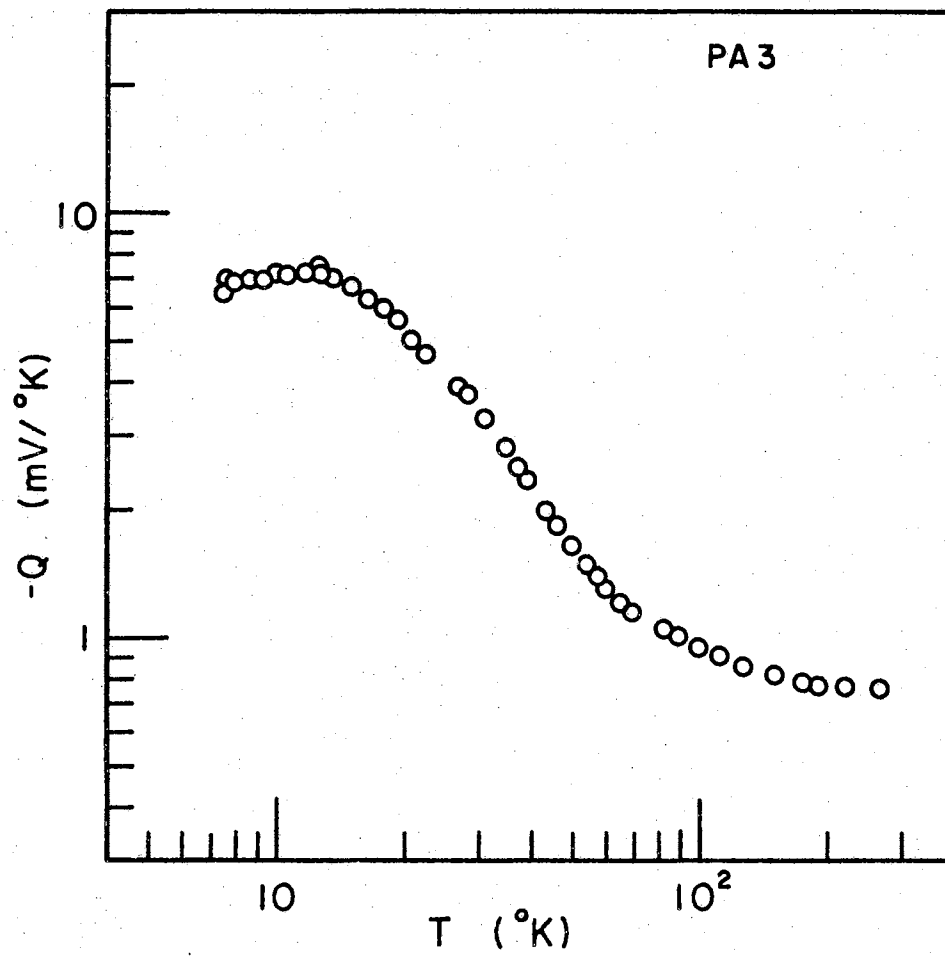
Figure 17.   Thermoelectric Power of Specimen PA 3
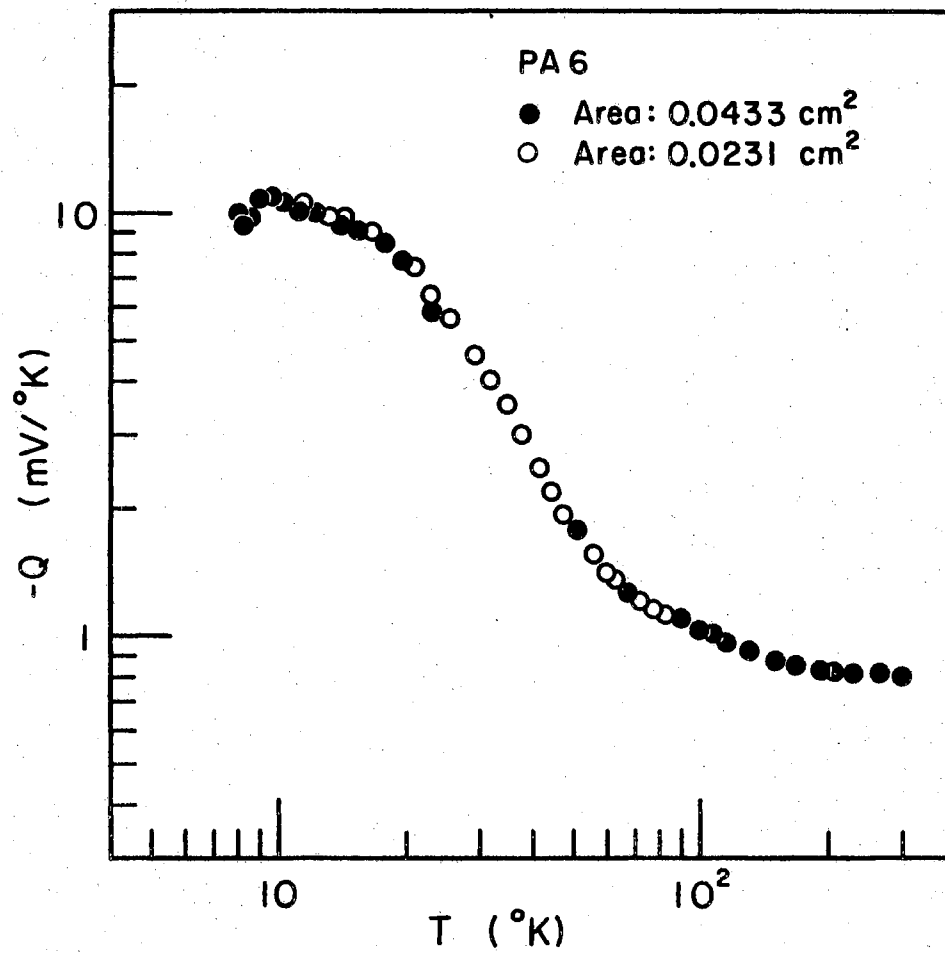
Figure 18. Thermoelectric Power of Specimen PA 6
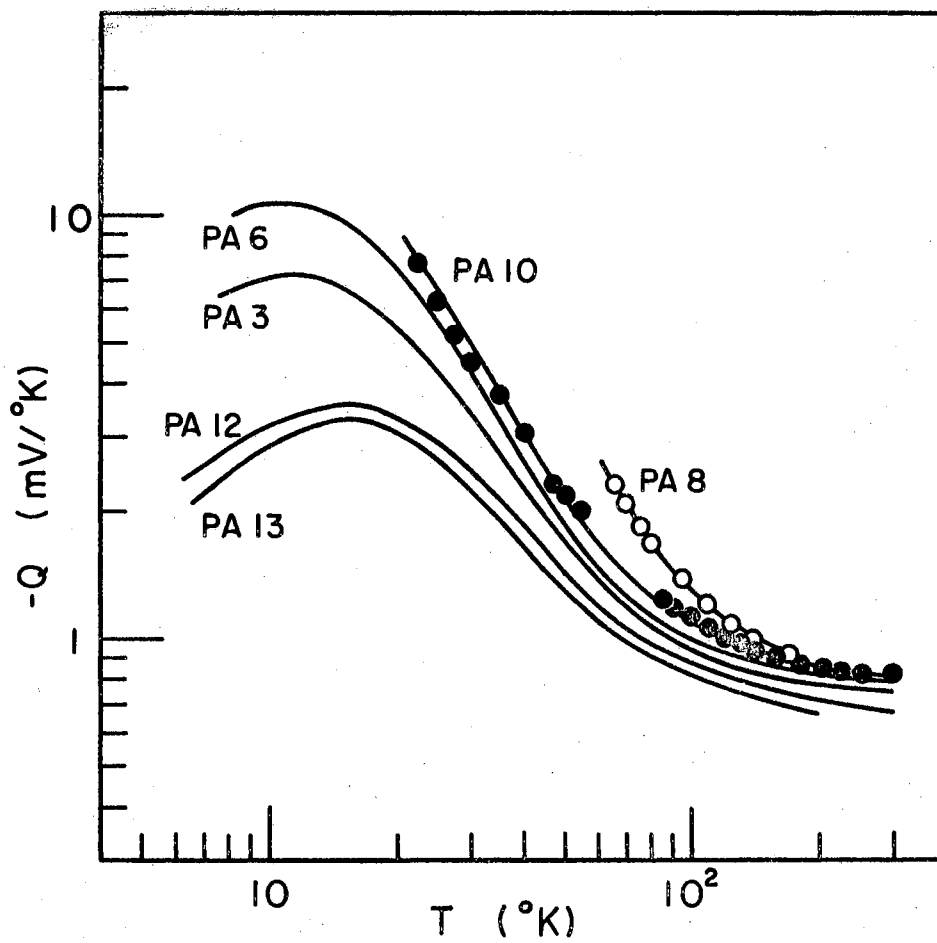
Figure 19. Thermoelectric Powers of Six Samples in
Different States of Nonstoichiometry

what effect boundary scattering has in these samples at low temperatures, sample PA 6 was cut approximately in half, decreasing the cross-sectional area from 0.0433 cm^2 to 0.0231 cm^2. As shown in Figure 18 there was no discernable difference in the measured values of Q.

In Chapter II a method was discussed whereby one could calculate a carrier effective mass if the number of carriers and the electronic component of the thermoelectric power were known. Using this procedure and assuming acoustical mode lattice scattering so that ΔE_T = 2kT, and further assuming that the measured thermoelectric power is purely electronic at 200 ^{o}K, a value of $m^* = 29 m_e$ is obtained for sample PA 3. This is a "density-of-states effective mass" as discussed earlier. If this value of effective mass is assumed to be independent of temperature it can be used together with carrier density data to evaluate the electronic component, Q_{el}, as a function of temperature. This has been done for several samples and the results for PA 3 are presented in Figure 20. The low temperature portion of the solid curve labeled $Q_{electronic}$ was calculated by using a value of n obtained by extrapolation of the Hall data to 35 ^{o}K. The dotted region below this temperature was found in the same manner but the extrapolation may be less valid since other workers[12] have found an increase in the Hall coefficient occurs near the minimum in the resistivity. The resistivity minimum occurs at about 35 ^{o}K for sample PA 3, and so below this temperature the magnitude of Q_{el} probably decreases much more rapidly than shown in Figure 20.

Figure 21 depicts the phonon contribution to the thermoelectronic power for three of the samples as found by subtracting the calculated
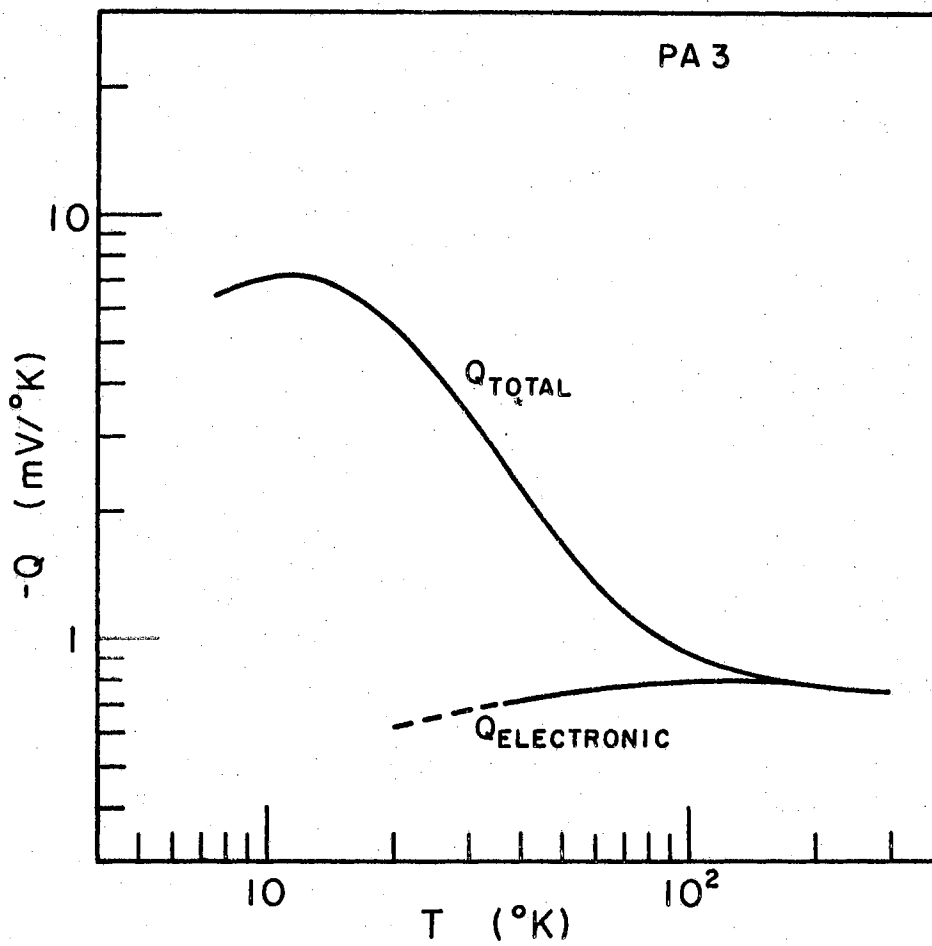
Figure 20. Total Thermoelectric Power and Electronic
Component of the Thermoelectric Power
for Specimen PA 3
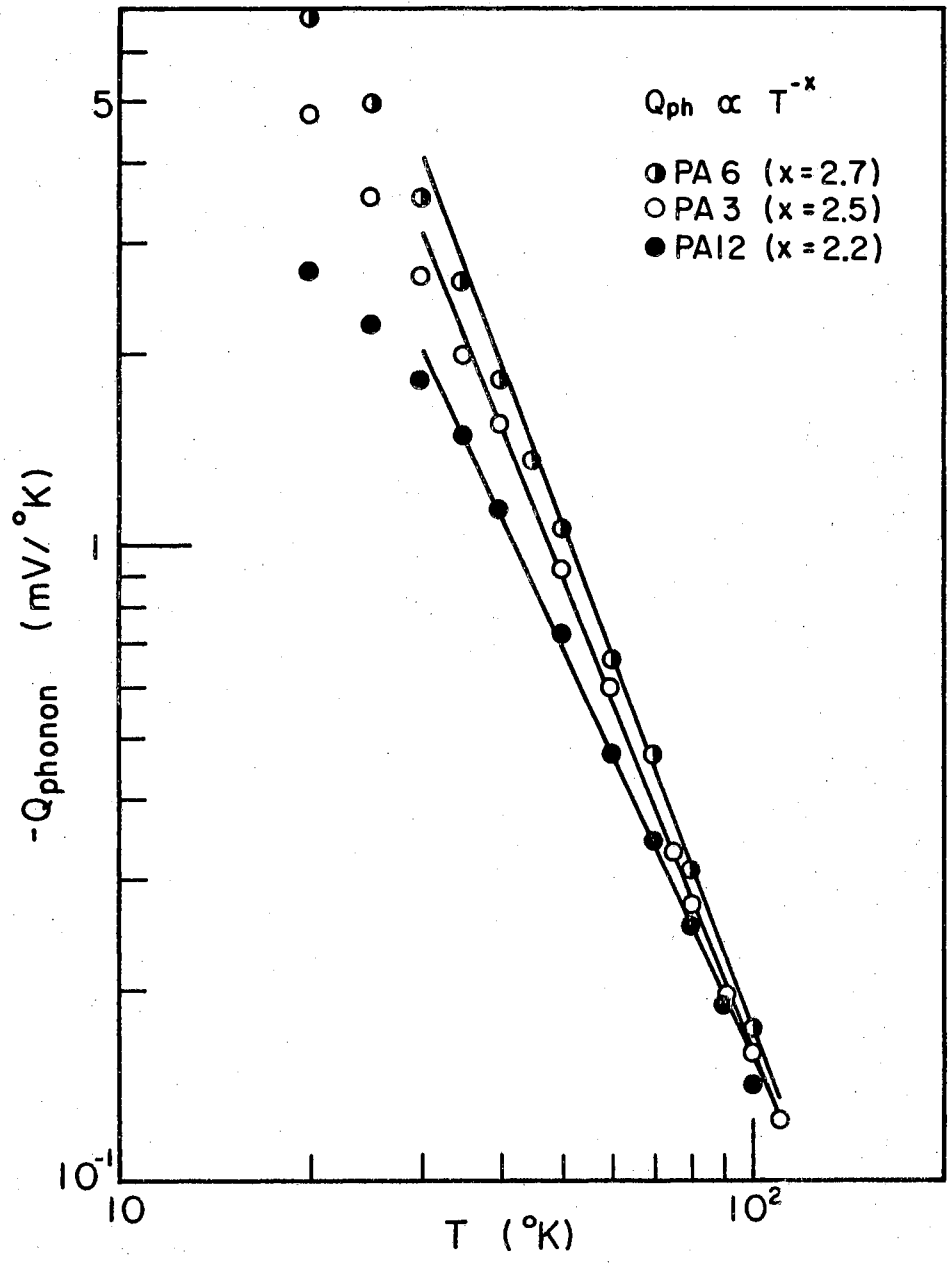
Figure 21. Phonon Contribution to the Thermoelectronic
Power for Three Specimens

electronic components from the measured values. Hall coefficient data
was not obtained for PA 12, so in this case n was determined by compar-
ison of resistivities with sample PA 3. The approximation of n versus
T obtained in this manner is probably quite satisfactory for determina-
tion of Q_{el}, since the calculated value of Q_{el} is relatively insensi-
tive to small changes in n.

Above 100 $^\circ$K the curves in Figure 21 are the differences between
nearly equal numbers. Deviations from the solid lines at low tempera-
tures apparently arise from the error in determining Q_{el} at these tem-
peratures. Assuming $Q_{ph} \propto T^{-x}$ the values of x for each solid curve are
given on the figure. As expected, the value of x varies inversely with
the reduction state. All values of x are less than the theoretical
value of 3.5 predicted by Herring.

Measurements of the Seebeck coefficient for PE 12 are shown on
Figure 22, and PA 12 results are also reproduced for comparison. The
large anisotropy in total Q for the "a" and "c" directions is better
depicted in Figure 23, where a rapid increase in the ratio Q_c/Q_a is ob-
served between 10 and 40 $^\circ$K. Above 40 $^\circ$K the ratio is nearly one. As
mentioned earlier, Gashimzade[51] predicts for the phonon contributions
in a tetragonal crystal, $Q_c \propto T^{-3.5} \ln T$ and $Q_a \propto T^{-3.5}$ which gives for
the ratio, $Q_c/Q_a \propto \ln T$. The dotted line in Figure 23 is a plot of $\ln t$
versus T which has been arbitrarily fitted to the measured ratio at 40
$^\circ$K. The ratio of total Q's can be expected to deviate significantly
from a $\ln T$ relationship at the higher temperatures where Q_{el} becomes
prominent.
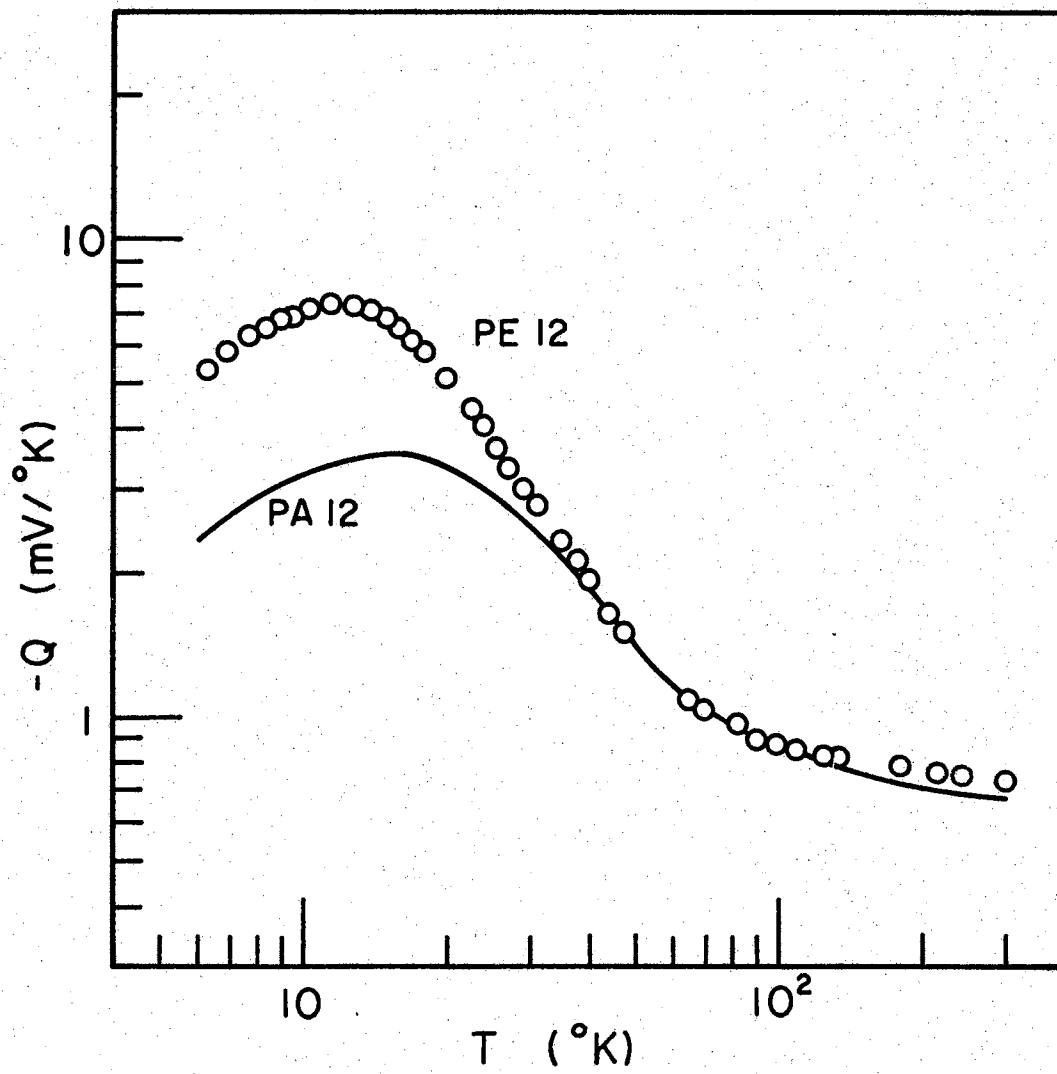
Figure 22. Comparison of the Thermoelectric Powers of Specimens PA 12 and PE 12.
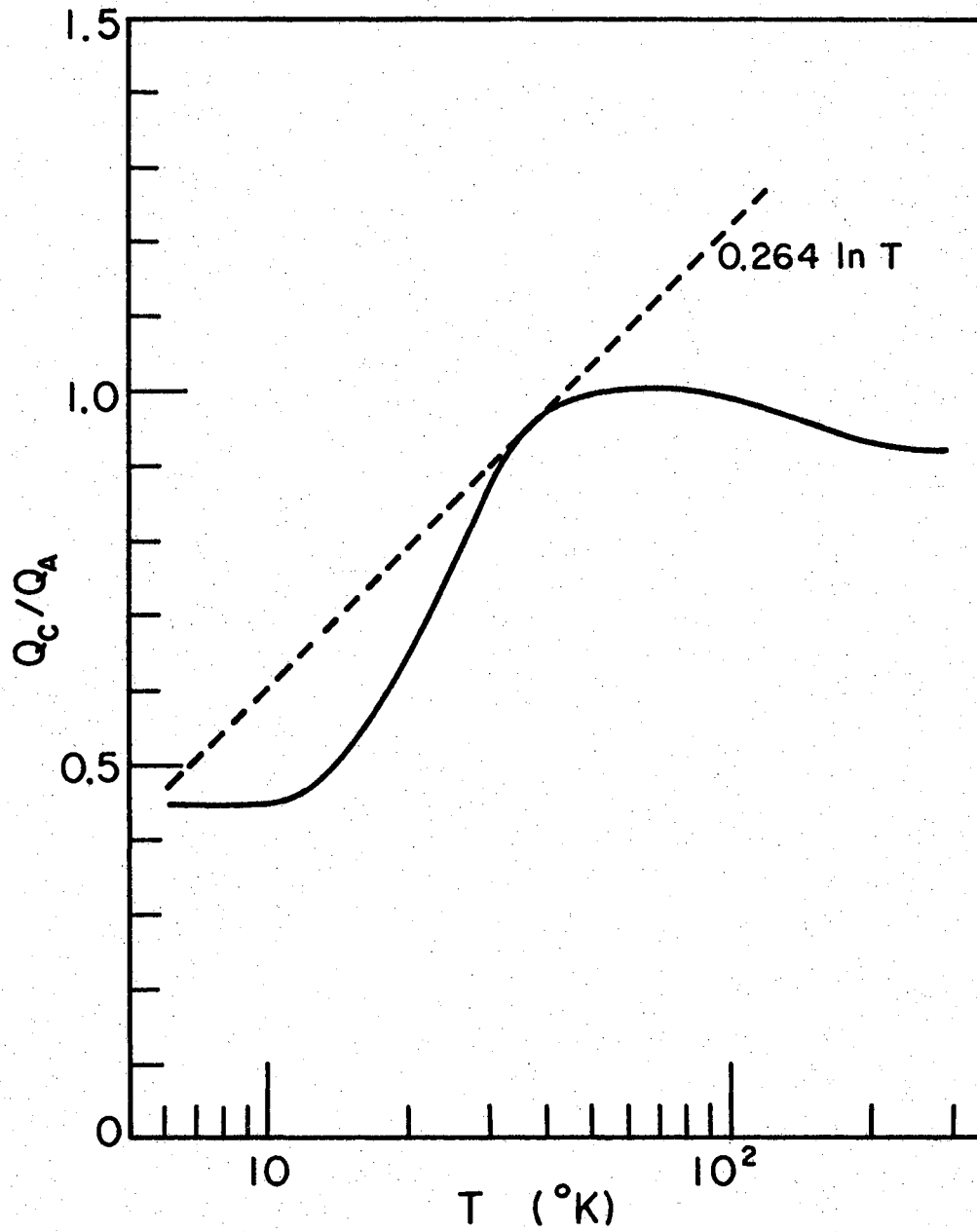
Figure 23. Thermoelectric Power Anisotropy as a Function of Temperature for Vacuum Reduced Rutile

Thermal Conductivity Data

If the power input into the gradient-heater is accurately known the thermal conductivity of the specimen can be determined simultaneously with the thermoelectric power. The thermal conductivity, κ, can be found from the equation

$$\kappa = IVL\alpha/AV_{tc},$$

where I and V are the gradient-heater current (amps) and applied voltage (volts) respectively, L is the distance across which the temperature gradient is measured, A the cross sectional area of the specimen, V_{tc} the corrected differential thermocouple output, and α the thermoelectric power for the Au + 2.1 at. % Co versus normal silver system.

Besides the errors previously mentioned, additional sources of error exist here. Least of these is again the problem of accurately determining L. More important is the determination of the energy flowing through the sample per unit time (IV). The assumption made is that all the energy fed into the heater in turn flows through the sample. This however is probably never the case becuase of radiation and conduction losses from the heater. At low temperatures (< 100 ^{o}K) radiation losses calculated from a T^4 law are completely negligible, whereas heat loss by conduction through the surrounding medium can be appreciable. Obviously the better the vacuum surrounding the sample the smaller the heat losses will be. Since the measured pressure was always around 10^{-3} to 10^{-4} torr, a possibility for significant error is present. Liquid helium, however, is an excellent cryopump and in the absence of helium leaks, the actual pressure within the inner can

is probably less than that measured externally at a sizeable distance from the specimen. In addition, since all specimens were measured at nearly the same pressures, and gradient-heater power levels were nearly the same for all specimens, one would expect good consistency from sample to sample. Thus, even though the absolute magnitudes of κ may be open to question, the data are assumed indicative of the dependence of the thermal conductivity upon reduction treatment. Although not discussed here, measurements of κ for several samples (PA 3 and PA 12) were made in the temperature range 80 to 300 $^{\circ}$K using a Goldsmid-type apparatus and these results agreed well with the data presented here and with other published values near room temperature.

As noted previously it was difficult to achieve thermal equilibrium of the sample in the temperature range 25 to 60 $^{\circ}$K and thus it was difficult to obtain reliable thermal conductivity data in this range.

Figure 24 shows the results for the $L||c$ sample PA 12 and the $L||a$ sample PE 12. Both samples had the same cross-sectional area and leads were attached as nearly as possible to the same value of L. The anisotropy ratio K_c/K_a is shown in Figure 25 together with the ratio obtained by Thurber and Mante[36] for unreduced rutile. These authors estimate their error in the ratio to be ± 0.1 and the data presented here are probably comparable in error. In view of this, the agreement over a large portion of the temperature range measured is gratifying. Of particular interest is the nature of this curve as compared to the ratio Q_c/Q_a (Figure 23). Both have constant values below 10 $^{\circ}$K, increase rapidly from 10 to about 35 $^{\circ}$K, and are relatively constant once again above this temperature.
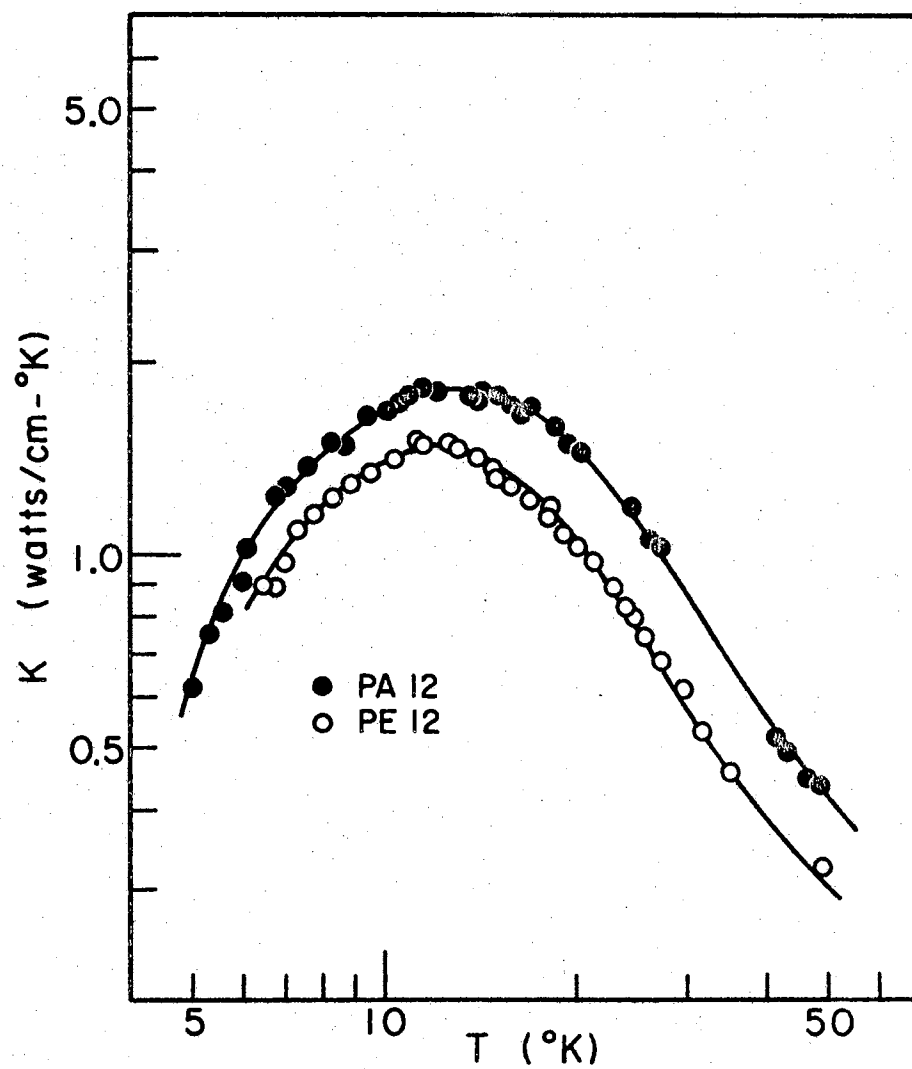
Figure 24.   Thermal Conductivities of Specimens PA 12 and
PE 12
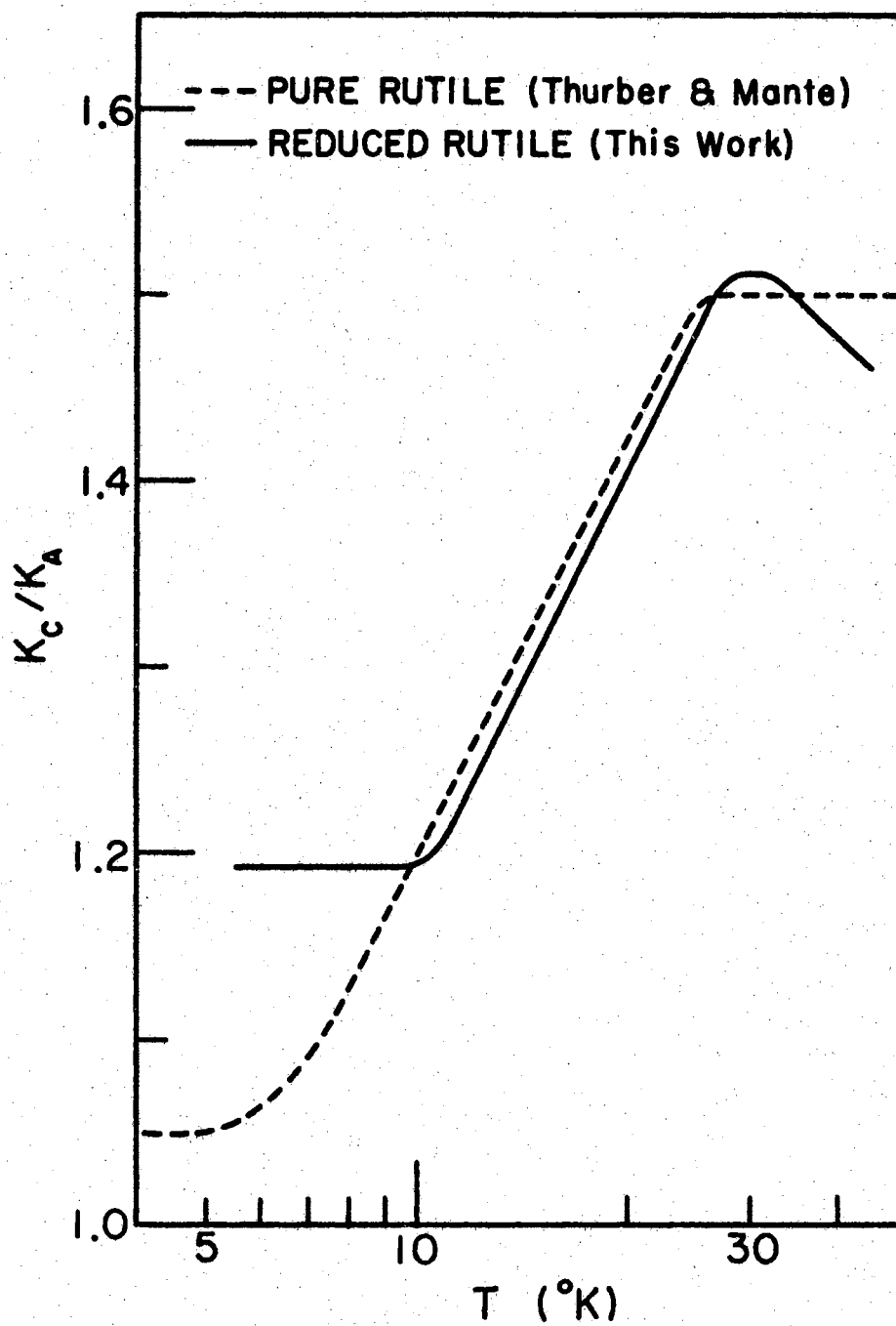
Figure 25. Thermal Conductivity Anisotropy as a Function of Temperature for Vacuum Reduced Rutile

Figure 26 gives the κ data for all the $L||c$ samples measured. Just as in the thermoelectric power results, the magnitude of κ decreases with the degree of reduction. At low temperatures, κ is nearly proportional to T^2 which suggests that scattering of phonons in this temperature range is not solely due to the sample boundaries, since a T^3 dependence is predicted for this effect. The decrease in magnitude of κ with increasing defect concentrations implies impurity scattering may be another important scattering mechanism. For all samples the temperature of the maximum is about 12.5 $^{\circ}$K. As in the case of the thermoelectric power results, the partly-closed circles for PA 6 represent the initial cross-sectional area of 0.0433 cm^2 while the open circles are data taken after reducing the area to 0.0231 cm^2. Again no size effect is noted. The observance of no apparent size effect in both κ and Q results implies that approximately the same group of phonons is influential in both phenomena.

Some of the pertinent parameters are summarized for each sample in Table II.
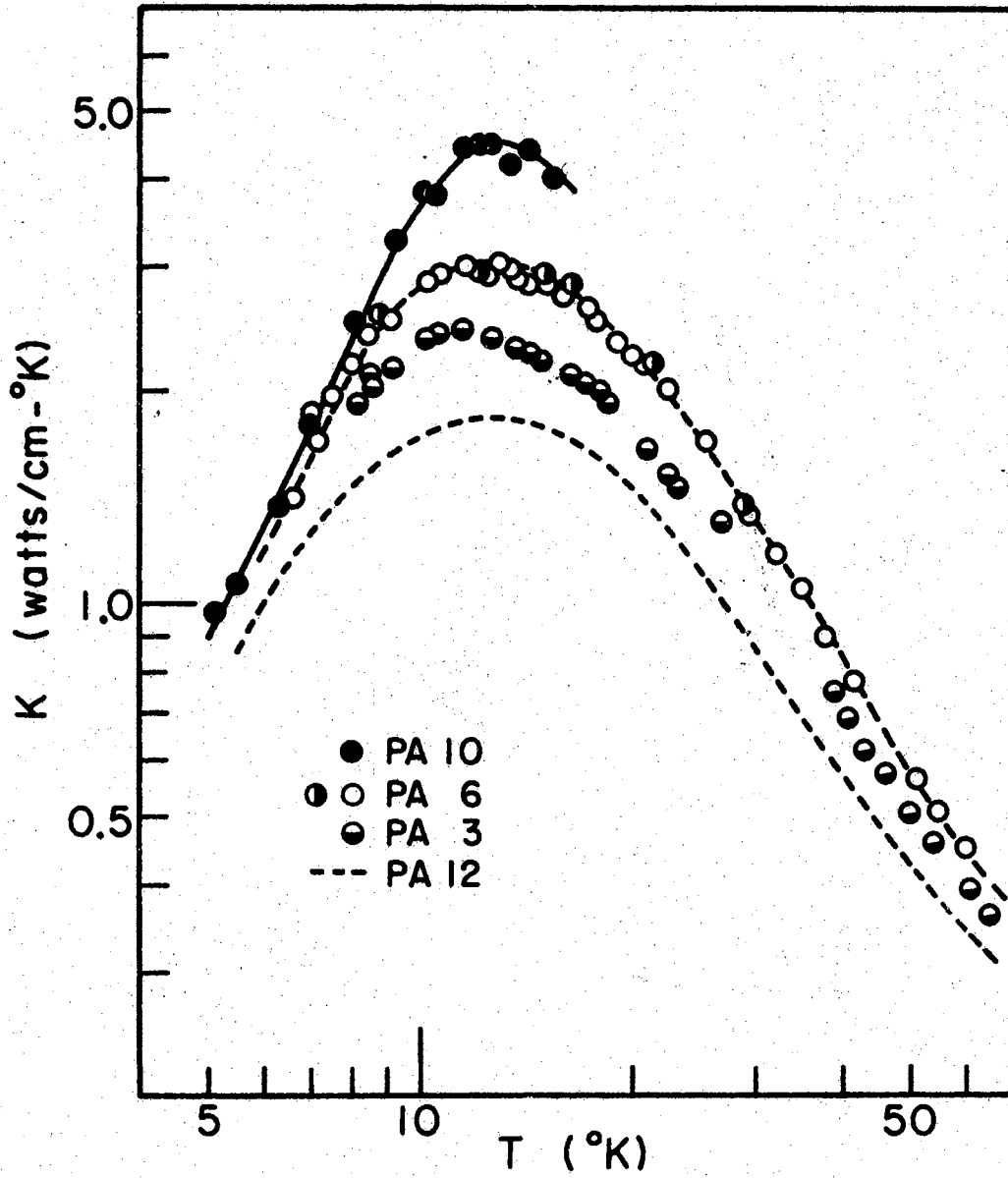
Figure 26. Thermal Conductivities of Four Specimens in
Different States of Nonstoichiometry

TABLE II

SUMMARY OF LOW TEMPERATURE RESULTS AND INTRINSIC ANALYSIS

Sample	ρ(ohm-cm) (300°K)	ρ(ohm-cm) (77°K)	$-E_d$(eV)[a] (100°K)	$-E_d$(eV)[a] (50°K)	(10°K)	m^*/m [c] (200°K)	$-Q$ mV/°K (200°K)	x[d]	$-Q_{max}$ (mV/°K) mag.	$-Q_{max}$ (mV/°K) T_{max}	K_{max} (watt/cm-°K) mag.	K_{max} (watt/cm-°K) T_{max}
PA 7	40	2×10^6	0.114	0.088	----	--	----	---	--	----	----	----
PA 8	12	1×10^4	0.086	0.065	----	--	0.88	---	--	----	----	----
PA 10	5.4	24	------	0.053	----	--	0.86	---	--	----	~4.5	12.5
PA 6	3	1.55	------	------	0.016	24	0.83	2.7	~11	10	3.0	12.5
PA 3	1.55	0.57	0.05[b]	------	0.012	29	0.79	2.5	7.2	12	2.5	11.5
PA 12	0.68	0.20	------	------	0.010	38	0.70	2.2	3.6	15	1.8	13
PE 12	4.0	1.7	------	------	0.012	--	0.765	---	7.2	12	1.5	12
PA 13	0.59	0.17	------	------	------	--	0.67	---	3.3	15	~1.8	13

a: E_d is the slope of ln ρ versus 1/T at the temperature indicated (except b).

b: This E_d is the slope of ln R_H versus 1/T at 200°K.

c: Calculated as discussed in text, with ΔE_t = 2kT.

d: x is the exponent of T in $Q_{phonon} \propto T^{-x}$.

CHAPTER V

DISCUSSION AND CONCLUSIONS

Defect Model

A review of the literature reveals surprisingly little attempt to correlate the low temperature electrical properties of rutile specimens with progressively increasing vacuum-reduction states. Many investigators have reduced rutile in a vacuum, but only to obtain "reduced" rutile, and not to ascertain what graded effect the reduction parameters have upon the physical properties. In this study, using samples cut from a single boule, and thus containing identical impurity concentrations, a systematic approach has been used in that several of the properties of the crystals have been investigated for increasing reduction states. This chapter thus attempts to interpret the results presented in Chapter IV in light of the progressive reduction state.

Of particular concern is the behavior of the resistivity curves as they relate to different reduction temperatures. An explanation of the marked difference in behavior between PA 8 and PA 12, for example, is hard to reconcile with a simple increase in defect concentration. From the spectrochemical analysis of the material used in this study, the total foreign impurity concentration is estimated to be about 3×10^{17} cm^{-3}. The majority of these impurities (Fe, Al, and Ni) have normal valences of less than four. Electron spin measurements on rutile doped with foreign impurities indicate that they exist at substitutional

76

lattice sites where they would be expected to act like acceptors. On

this basis, the specimens discussed are assumed to have an acceptor con-

centration, N_a, of about 3×10^{17} cm^{-3}.

Suppose, for the moment, that the only defect resulting from the

reduction process was a monovalent donor. Let N_d represent the concen-

tration of these defects. The maximum number of extrinsic electrons

that could participate in a conduction process is $N_d - N_a$, since N_a of

the donors are compensated by the acceptors. If the sample is then

cooled, electrons become retrapped on the donors and the Fermi level,

E_f, approaches the donor level energy, E_d. Thus the number of carriers,

n, decreases exponentially with 1/T. This dependence could readily ex-

plain the behavior found for samples PA 7 or PA 8, but not that found

for PA 3 or PA 12. If the only difference resulting from higher reduc-

tion temperatures is an increase in the defect concentration (N_d), then

the result is an increase in n (= $N_d - N_a$), but the temperature depend-

ence of n remains the same. This is clearly not compatible with the

results shown in Figure 13 where n for PA 3 is seen to break away from

a single slope below 150 $^{\circ}$K.

Oxygen vacancies, of course, are expected to be divalent donors

since an oxygen atom leaving the crystal leaves two electrons which in

turn can become bound to the region in the crystal which energetically

favors a minus two charge (i.e. the vacancy). The case of a divalent

donor merits closer consideration because, qualitatively, it displays

a similar behavior to the n versus 1/T results found here. Consider

the following example of a divalent donor center with ionization ener-

gies E_{d1} and E_{d2}, with E_{d1} and E_{d2} separated by several kT. Further

suppose the level with energy E_{d1} lies closest to the conduction band

(see Figure 27A). Since these two levels are not independent, $N_{d1} = N_{d2}$

$= N_d$, the concentration of defects. If both levels were completely

ionized, and $N_a = 0$, the carrier concentration would be $2N_d$. If, how-

ever, $N_a > N_d$, the upper level will be completely compensated by accep-

tors, and will remain empty at all temperatures. In this case the Fermi

level will always be many kT below E_{d1}. Conduction electrons can only

arise from the lower level of energy E_{d2}. This is, in essence, similar

to the previous example of the monovalent donor center, with $N_a = 0$, in

that n varies exponentially with 1/T, as conduction electrons are re-

trapped in the lower donor level ($E_f \approx E_d$) upon cooling.

If $N_a << N_d$, conduction electrons can arise from both levels at

sufficiently high temperatures, since the upper level is no longer com-

pletely compensated, and n = $2N_d - N_a \approx 2N_d$. During the cooling process

the lower level fills up first until the Fermi level moves above this

energy, and in this case n = $N_d - N_a \approx N_d$ and remains at this value un-

til the Fermi level approaches E_{d1}. The upper level is then deionized

and as T → 0 °K, n = 0. Clearly, two distinct regions in carrier den-

sity are observed, n ≈ 2Nd when both levels are completely ionized, and

n ≈ N_d when only the upper level is completely ionized. The ratio of

these two carrier concentrations is two, and simple calculations show,

that for $N_a < N_d$, by various amounts, this ratio is always ≥ 2. This

(A)

(B)
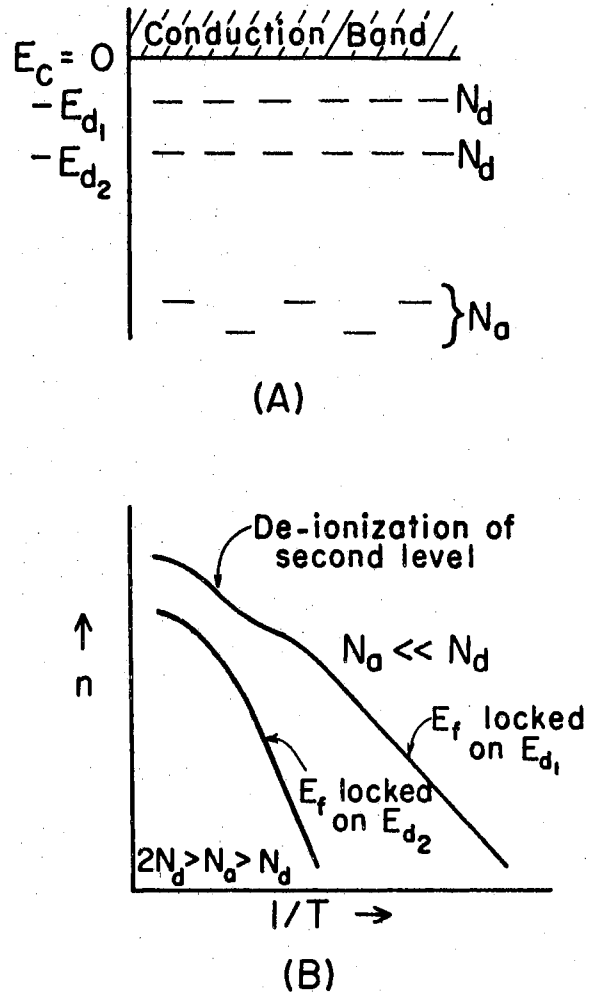
Figure 27. Energy Band Scheme and Carrier Density
as a Function of Temperature for a
Simple Divalent Donor Model

problem of a divalent donor center with activation energies separated

by at least a few kT, and with $N_a = 0$, has been solved by Champness[57].

The details of his calculations need not be given here because the sali-

ent features above indicate that this might be an appropriate model for

rutile. Figure 27B qualitatively illustrates the nature of n versus

$1/T$ for the two cases $2N_d > N_a > N_d$ and $N_a << N_d$.

The high temperature portion of the $N_a << N_d$ curve is similar in

behavior to the results shown in Figure 13 for sample PA 3. Hall data

on a high temperature (1000 ^oC) vacuum-reduced sample taken by Becker

and Hosler[12] shows a behavior similar to the $N_a << N_d$ curve over the

entire temperature range. The resistivity data on, say, PA 7 or PA 8,

however, looks like a single activation energy is involved in these

higher resistance samples. Again substantiation is provided by Becker

and Hosler's data on an 800 ^oC sample. This is the behavior of the

$2N_d > N_a > N_d$ curve in Figure 27B. Qualitatively, then, it appears a

divalent oxygen vacancy defect is compatible with the results of this

and other studies.

Several difficulties arise in the adoption of such a simple model,

however. First of all, inspection of the results obtained for samples

reduced in a vacuum at $T > 1000$ ^oC in this study, as well as for those

reported in the literature, reveals carrier density ratios corresponding

to the de-ionized level cases that never approach the ratio of two,

which would be expected if $N_a << N_d$ as discussed earlier. In fact, at

room temperature complete ionization of all levels apparently does not

occur since a constant n has not been observed in this temperature

range, even in data taken up to 500 ^oC[4]. In spite of this, in the tem-

perature region where n is temperature independent (about 30 to 80 ^{o}K),
the carrier concentration is one to two orders of magnitude smaller than
its room temperature value. Obviously, such a ratio fits the model only
if $N_d \approx N_a$.

Secondly, a slight change in the slope of the resistivity curves
is observed even for samples PA 7 and PA 8, although these cannot be
seen in Figure 11 because of the compact scale (see Table II). This
again agrees with a slight change in the slope of R_H in Becker and
Hosler's 800 ^{o}C sample. This change suggests that there are two sources
of electrons even in the high resistivity samples.

Lastly, and most important, as pointed out in Chapter II, recent
studies support the creation of a titanium interstitial defect during
the reduction process. Thus, it appears that any model developed to
explain the electrical properties of rutile in terms of defects should
include titanium interstitials.

Considerations of these aspects have led the author to suggest a
model wherein both oxygen vacancies and titanium interstials are created
simultaneously, with the interstitials most important in the high re-
duction-temperature samples and the vacancies dominant for the lower
treatment-temperature specimens. The feasibility of this model gained
strength when Kofstad[26] argued that at low temperatures and high partial
pressures of oxygen the principal defect was an oxygen vacancy, but that
high temperatures and low oxygen partial pressures led to the creation
of titanium interstitials. Kofstad's arguments were based on the de-
viation from stoichiometry of reduced ceramic and crystalline material,
as reported in the literature. The recent ESR data of Kingsbury, et.
al.[28], is also of special interest. They concluded from their measure-

ments that below about 8 $^{\circ}$K an electron is trapped on a Ti^{4+} intersti-
tial ion resulting in a Ti_i^{3+}.

Suppose then, one postulates the formation of tri- and tetrava-
lent interstitial titanium ions (as did Blumenthal, et. al.[13]), in
addition to divalent oxygen vacancies. The reaction equations are:

$$TiO_2 \rightleftharpoons Ti_i^{3+} + 3e^- + O_2(q)$$

$$Ti_i^{3+} \rightleftharpoons Ti_i^{4+} + e^-$$

$$S.C. \rightleftharpoons O_v^{2+} + 2e^- + \frac{1}{2} O_2(g).$$
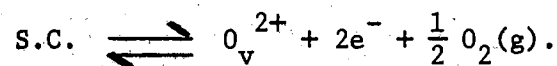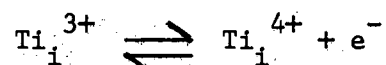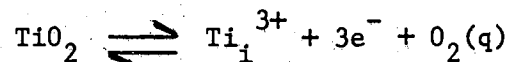
Application of the mass action law yields

$$[Ti_i^{3+}] n^3 P_{O_2} = K_1$$

$$[Ti_i^{4+}] n = K_i [Ti_i^{3+}]$$

$$[O_v^{2+}] n^2 P_{O_2}^{\frac{1}{2}} = K_2.$$

In terms of this model the electroneutrality condition is given by

$$n = 2[O_v^{2+}] + 3[Ti_i^{3+}] + 4[Ti_i^{4+}],$$

where N_a is assumed equal to zero. Combining these last four expres-
sions one obtains for the carrier concentration:

$$n^3 = 2(K_2 P_{O_2}^{-\frac{1}{2}}) + \frac{K_1 P_{O_2}^{-1}}{n} (3 + \frac{4K_i}{n}).$$

This expression can be evaluated for n if the values of the rate con-

stants K_i, K_1, and K_2 are known. From Appendix A the general form of the rate constants is

$$K = C \exp (-\Delta H/kT).$$

Blumenthal, et. al.[13], have estimated from their electrical conductivity studies that $\Delta H_i = 1.4$ eV and $\Delta H_1 = 9.1$ eV. Kofstad[25] determined ΔH_2 by thermogravimetric techniques and used the above mass action equations to calculate the deviation from stoichiometry, x[26]. He found the best agreement between his calculated value of x and existing data with:

$$K_i = 9.5 \times 10^{24} \exp (-1.4/kT) \ (cm^{-3})$$

$$K_1 = 9.5 \times 10^{99} \exp (-9.1/kT) \ (cm^{-12}-atm)$$

$$K_2 = 1.3 \times 10^{70} \exp (-4.6/kT) \ (cm^{-9}-atm^{\frac{1}{2}}).$$

Using these values, and assuming $P_{O_2} = 10^{-9}$ atm (which is in the range of the present study), the previous expression can be solved numerically for n. The value of n versus 1/T found in this manner is shown in Figure 28 as the solid line. The dotted lines give the contribution to n from each type of defect (O_v) and (Ti_i). If the estimated acceptor density of 3×10^{17} cm^{-3} is plotted on this same graph, one notices that for a sample heated at 850 °C, $n(Ti_i) < N_a < n(O_v)$, whereas at 1050 °C, $N_a < n(Ti_i) < n(O_v)$. Thus the increasing importance of the titanium interstitial ions can be seen, since in this 200 °C temperature range, $n(Ti_i)$ increases by well over 2 orders of magnitude whereas
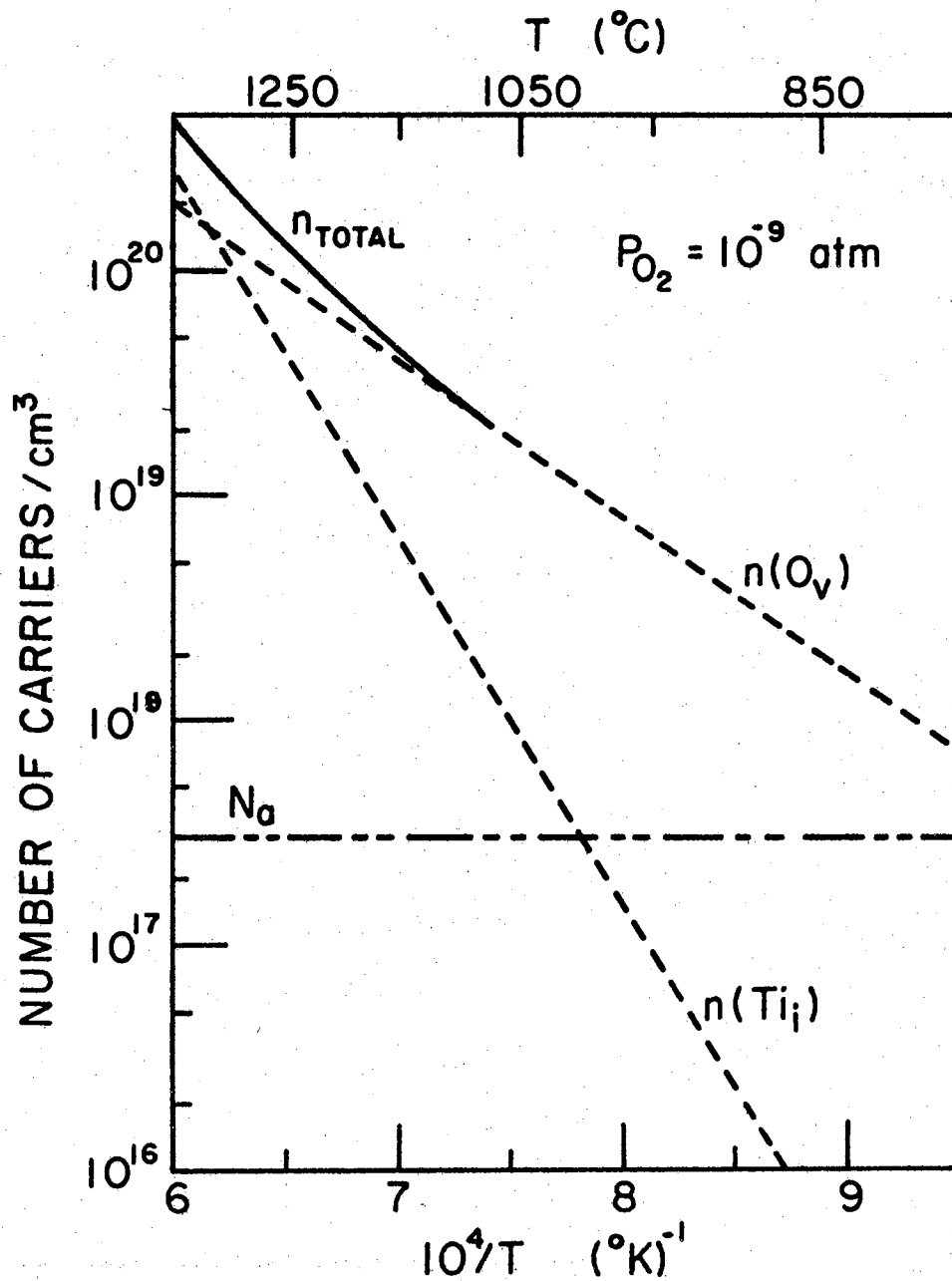
Figure 28. Carrier Concentrations Resulting from Oxygen Vacancy and Titanium Interstitial Defects as a Function of Reduction Temperature

$n(0_v)$ increases by less than one order of mganitude. It appears, then, that this two-defect model might give qualitative agreement with the observed low temperature resistivity and Hall measurements.

It is first necessary to point out several details. It should be understood that no great accuracy is claimed for the aforementioned rate constants. Secondly, as discussed in Chapter IV, the atomic defects generated in the reduction process are assumed to be "frozen" into the lattice. Hence, although the value of n in Figure 28 may change upon quenching the sample, the concentration of defects from which the electrons came is assumed to remain constant. Somewhat surprising, then, is the agreement between the equilibrium value of n as calculated from this model and the magnitude of n obtained from room temperature Hall data taken in this study. Considering a 1050 ^{o}C sample such as PA 3 for example, these values are 1.8×10^{19} cm^{-3} and 1×10^{19} cm^{-3}, respectively. These results would imply that the majority of donor defects are still ionized even at room temperatures and lend credibility to the proposed defect model.

Consider once again two donor levels lying near the conduction band, the upper level having donor concentration N_{d1} and ionization energy E_{d1}, and the lower level N_{d2} and E_{d2}. This is clearly similar to the divalent donor situation discussed earlier, with an important exception. The two donor levels are now independent, and thus, $N_{d1} \neq N_{d2}$. If E_{d1} and E_{d2} are not too close in energy, one would expect to see a behavior similar to that mentioned previously. It will become apparent from the following discussion that in this two-defect donor model, the titanium interstitial donor level must lie nearest the

conduction band.

The appropriate energy band scheme is shown in Figure 29A. As before, two completely different forms of behavior will exist depending on whether or not N_a is larger or smaller than N_{d1}. The two donor levels have each been tentatively associated with an atomic defect. If $N_a > N_{d1}$, the upper level will always be denuded of electrons even at $T = 0$ ^{o}K, and the Fermi level will reside at E_{d2}. As the specimen warms some electrons will be excited from the lower level into the conduction band and the Fermi level will ultimately drop below E_{d2}. At higher temperatures, when ionization of the lower level is complete, n reaches its limiting value of $N_{d1} + N_{d2} - N_a$. This is the type of behavior found in the samples reduced at 850 ^{o}C and a look at Figure 28 reveals $N_a > n$ (Ti_i) for these samples. This behavior is entirely equivalent to the situation presented for a divalent oxygen vacancy when $N_a > N_d$ (Figure 27B).

If, on the other hand, $N_a < N_{d1}$, (e.g. a sample reduced at 1050 ^{o}C), at absolute zero the lower donor level is filled and the upper level contains $N_{d1} - N_a$ electrons, and the Fermi level coincides with E_{d1}. As the temperature increases the upper level gives up its electrons to the conduction band until this supply is exhausted (n = $N_{d1} - N_a$). No further increases in n can occur until the Fermi level has dropped almost to the energy E_{d2} whence the lower set of donors begins to lose electrons. At high enough temperatures n again saturates at $N_{d1} + N_{d2} - N_a$ while E_f drops below E_{d2}. The behavior of n versus T
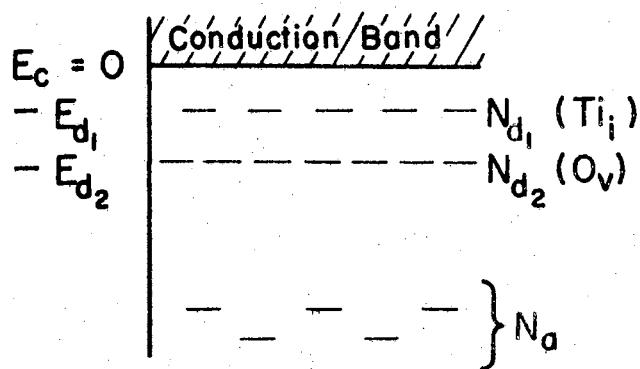
(A)
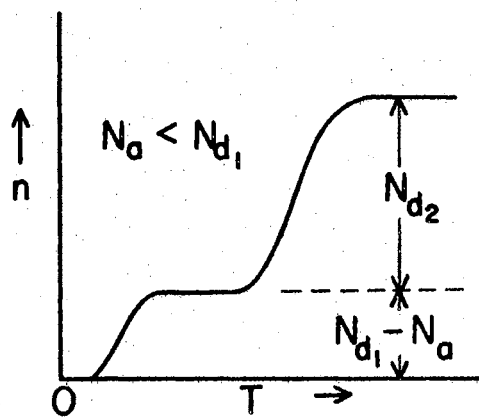
(B)

Figure 29. Energy Band Scheme and Carrier Density
as a Function of Temperature for a
Two Independent Donor Level Model

is shown schematically for the latter case in Figure 29B.

The preceding discussion can be expressed in a mathematical form if one assumes each of the independent donor levels is monovalent. Expressing densities as N_{dj} and energies as E_{dj} (with $j = 1,2$ in this example) Blakemore[45] gives for the densities of ionized levels

$$(Nd_j)_{ionized} = \frac{N_{dj}}{1 + B_j^{-1}[1 + F_j] \exp((E_f - E_{dj})/kT)}$$

where F_j is a quantity representing the influence of any excited states and B_j^{-1} represents the spin degeneracy of the impurity level. The conduction band electron density must equal the sum of all ionized donors minus all electrons in compensating acceptors:

$$(n + N_a) = N_a + N_c F_{\frac{1}{2}}(E_F/kT) = \sum_{j=1}^{2} \frac{N_{dj}}{1 + B_j^{-1}[1 + F_j] \exp(E_F - E_{dj})/kT}.$$

If the Fermi level is several kT below the conduction band (i.e. $E_f/kT < -2$), then $F_{\frac{1}{2}}(E_F/kT)$ can be replaced by $\exp(E_f/kT)$ as was done in Chapter II. The above expression then yields a cubic equation in $\exp(E_f/kT)$ or n.

Clearly this model is consistent with the general character of observed results and with the rate constants determined by Blumental, et. al.[13], and Kofstad[26]. It is still necessary, however, to consider the possible ionization energies of the suggested defects. To a first approximation, donor energies are often calculated from a Bohr ionization energy scheme which assumes that the donor is a hydrogen-like

center imbedded in a material of dielectric constant k with an electron
of effective mass m^*. This gives

$$E = \frac{13.6}{k^2} \frac{m^*}{m} \text{ (eV)}$$

where 13.6 eV is the ionization energy of hydrogen in a vacuum. If an
oxygen vacancy is considered to be a helium-like center (i.e. two elec-
trons), one must consider the first two ionization energies of He, 24.5
and 54 eV, respectively. The first four ionization energies of titan-
ium are 6.8, 13.6, 28.4, and 43.2 eV. Because k in rutile is aniso-
tropic, an average value must necessarily be used. Values of k used
in this type of calculation on rutile have varied from 25 (Reference
9) to 114 (Reference 3). Furthermore, one is uncertain how to make a
proper choice for m^*/m. Consequently, ionization energies found in
this manner are rather arbitrary, especially if the crystal has an
ionic character. Regardless of the values of k and m^*/m used, however,
the six vacuum ionization energies quoted probably reflect the ordering
of these energies in the crystal. That is, the energy necessary to
produce a Ti_i^{3+} is probably comparable to the energy required to singly
ionize an oxygen vacancy. On the other hand, more energy is necessary
to give an O_v^{2+} than a Ti_i^{4+}.

Kingsbury, et. al.[28], treat the potential at the interstitial site
as the sum of ionic and permanent-dipole potentials plus a lattice-po-
larization potential. They find that when these are considered, the
third and fourth electron energies of the titanium become +6.5 and
-0.59 eV respectively, that is, the electrons are very loosely bound.
The actual numbers seem somewhat meaningless, however, in that the

theory in this case necessitates tight binding, so the most that can be said is that the energies are probably very close to the conduction band. Their implication, then, is that Ti_i^o and Ti_i^{1+} are probably not credible entities. This would leave one or, at most, two electrons still bound to titanium interstitial donor states for excitation upon temperature increase.

Suppose for the purpose of illustration that the uppermost donor level is a Ti_i^{3+} which can be ionized to a Ti_i^{4+} and that oxygen vacancy levels (either one or two) lie lower in energy. This model gives the desired behavior, is consistent with the ESR results of Kingsbury, et. al.[28], and is also consistent with the piezoresistance results of Bir, et. al.[14]. The latter group suggested their results would be compatible with a multiple donor-level model.

It is still necessary, however, to consider two important unanswered questions. First, how might one explain the small changes in slope of ρ versus $1/T$ with increasing reduction state, and secondly, in "pure" rutile why does one not see a p-type character if there exists an excess of acceptor levels over donor levels?

Consider the former question first. As Table II shows (and see Figure 11) the magnitude of E_d changes from 0.114 eV for PA 7 to 0.086 eV for PA 8 to 0.053 eV for Pa 10 at liquid nitrogen temperatures. A possible explanation of this is that single isolated levels do not necessarily exist alone, but that additional levels may arise from association of defects. For example, one could have an oxygen vacancy, an oxygen vacancy associated with a trivalent impurity, an oxygen vacancy associated with a titanium ion on a normal lattice site, etc. A purely

qualitative argument could be made that changing the concentration of the parent defects changes the likelihood of creating associated defects, giving the different activation energies seen in measurements. Various types of associated defects have been postulated to explain experimental results (e.g., Dominik and MacCrone[39,40] or Breckenridge and Hosler[3]).

A somewhat more plausible explanation is that given to explain similar results in silicon[58], where the ionization energy of impurity centers was shown to decrease with increasing impurity concentration, N. In fact, the decrease in E_d is proportional to $N^{1/3}$, and these findings have been interpreted as being a result of the electrostatic attraction of other donors for an electron which has escaped its own donor. One might have a similar phenomenon in rutile, and in fact, this mechanism was invoked by Acket and Volger[59] to explain changes in slope observed by them in Hall measurements. Of course, the ionic character of rutile may also involve quite subtle effects.

Returning now to the question of compensation in "pure" rutile, it seems that in the unreduced state ($N_d = 0$) rutile should be a p-type semiconductor since it has an inherent acceptor concentration. This behavior has never been observed except for specimens highly doped with acceptor-type impurities. For example, Yahia[11] observed a p-type character in rutile doped with aluminum. Clearly then, there must be a donor concentration present even in unreduced rutile which is compensated by the impurity ion acceptors, thus resulting in a low conductivity in "pure" material. As mentioned in one of the earlier chapters, there is just such a donor concentration, resulting from the incorporation of hydrogen into the lattice during the Verneuil growth process.

The hydrogen becomes associated with an oxygen ion and can donate its electron to the conduction band (or be compensated by an acceptor). Hill's[27] work indicates that some of the hydrogen diffuses out of the sample if it is reduced in vacuum. In fact, the hydrogen appears to leave as water vapor, taking an oxygen with it. Thus reduction in vacuum at low temperatures (< 700 ^{o}C) essentially replaces two monovalent donor impurities with a divalent donor defect, and compensation still occurs. Shannon[20] supports the concept that hydrogen content can influence the creation of vacancies.

To recapitulate the bases of the suggested model, it supposes two types of major defects exist. Donor levels lying nearest to the conduction band result from partially ionized titanium interstitial defects, in particular Ti_i^{2+} and Ti_i^{3+} which can in turn be ionized to the 3+ and 4+ states, respectively. Lower lying are the donor levels resulting from the oxygen vacancy concentration. From the resistivity and Hall results found here, and also from those of Becker and Hosler, it appears that the interstitial donor levels lie at about 0.01 eV below the conduction band, and the oxygen vacancy level(s) lie lower, at about 0.05 to 0.1 eV. It is assumed that these energies are dependent upon the defect concentrations and that conduction takes place in the 3d-band of titanium. Oxygen vacancies are identified as the major defect resulting from low temperature (850 ^{o}C) vacuum reductions, with any interstitials being completely compensated by acceptors. At higher reduction temperatures, both types of defects are present and compensation becomes negligible. An example of a simple energy scheme, assuming no associated defects, is shown for representative samples PA 8 (lower two levels only) and PA 12 (all levels) in Figure 30. This
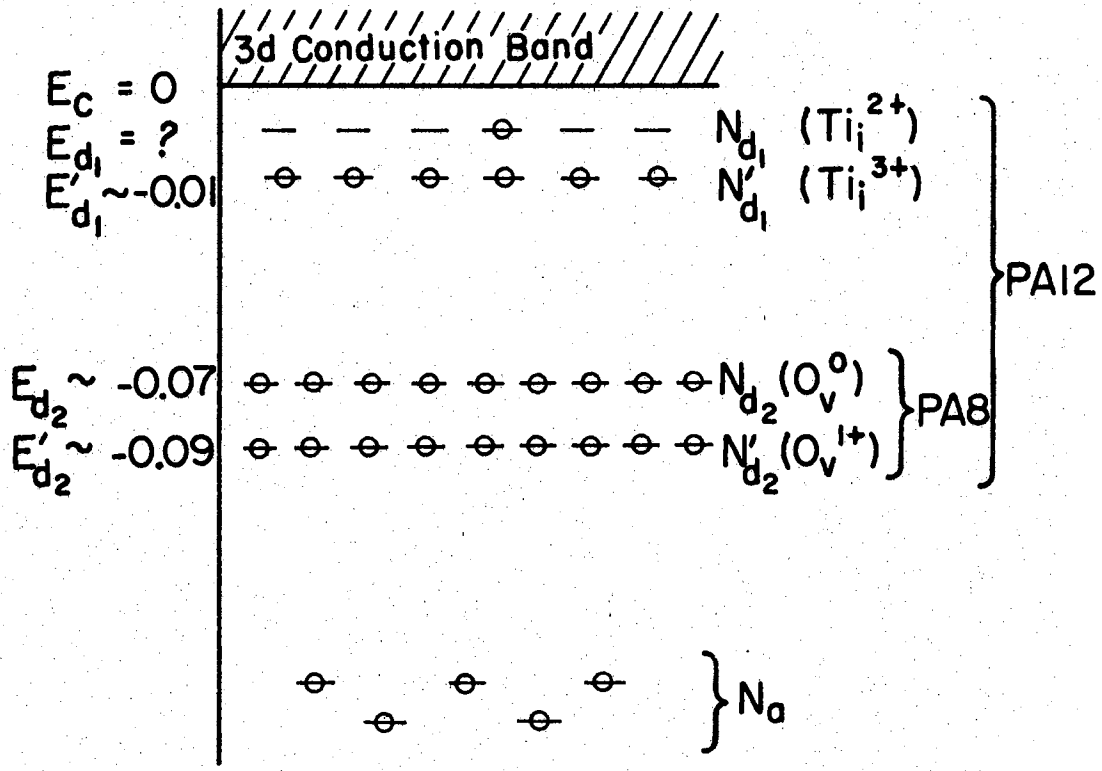
Figure 30. Possible Energy Band Scheme in Terms
of the Oxygen Vacancy and Titanium
Interstitial Donor Levels

scheme employs the conventional method of representing divalent donor centers (Reference 45, pg. 157). The ionization energies are expressed in eV. The energy required to ionize the Ti_i^{2+} donor level (to a Ti_i^{3+}) is uncertain and is accordingly labeled with a question mark. Hasiguti, et. al.[9], have reported an activation energy of about 0.005 eV at temperatures below 4 $^{\circ}K$ and this conceivably could be associated with the Ti_i^{2+} level. Their crystals, however, were reduced in hydrogen and may not be representative of the samples (and model) described here.

In Figure 30 the assignments for the valence states of the interstitial levels (Ti_i^{2+} and Ti_i^{3+}) are based solely on the conclusions of recent studies by other workers[28] which favor these levels, as opposed to the Ti_i^0 and Ti_i^{1+}. This scheme thus tacitly assumes that the Ti_i^0 and Ti_i^{1+} levels lie even closer to the conduction band and are compensated at all temperatures. It should be noted, however, that the model is equally valid if the choices of Ti_i^0 and Ti_i^{1+} are made in place of those levels shown on Figure 30. In this case, the 2+ and 3+ levels would lie even lower in energy, perhaps in the range of the oxygen vacancy levels or below. This would, in part, explain the large discrepancy between the energies found by Blumenthal, et. al.[13], and those implied by the results of the ESR groups[17,28] who all claim to see a Ti_i^{4+} level becoming a Ti_i^{3+} or vice versa. Of importance in explaining the experimental results, however, are upper levels arising only from the interstitial defect. Some of these are necessarily compensated by acceptors and the remaining electrons from these levels govern the low temperature electrical properties.

Thermoelectric Power

The results of the thermoelectric power data presented in the last chapter clearly indicate the importance of phonon effects. The electronic contribution, Q_{el} calculated from the expression given in Chapter II indicates that phonon effects are important even at temperatures higher than 100 ^{O}K. The basis of the calculation of Q_{el}, of course, depends upon the value chosen for ΔE_t. Although 2kT was used in this work (lattice scattering), it must be remembered that the value of Q_{el} was fitted to the experimental data at 200 ^{O}K. Consequently, changing ΔE_t from 2kT to 4kT (ionized impurity scattering) does not affect the calculation of Q_{el} but does have a considerable effect on m*/m, decreasing it from 28 to about 8 for sample PA 3.

The mobility results on this sample (Figure 14) are not compatible with simple lattice scattering, which predicts $\mu\alpha T^{-1.5}$. For sample PA 3, $\mu\alpha T^{-2.5}$. The mobilities of many semiconductors show a T^{-2} to T^{-3} dependence, and multiphonon processes (intervalley scattering) have been proposed to explain these results[60]. Intervalley scattering may be a possibility in rutile since Bir, et. al.[14], deduce from their piezoresistivity studies that the minimum in the conduction band is located on the k_z axis and that the band is not degenerate. For this type of scattering, the value of $\Delta E_t < 2kT$[36]. Lack of precise knowledge of the scattering mechanism, then, precludes an accurate evaluation of ΔE_t, and therefore of m*/m. Nevertheless, the values found for m*/m in this study (25 to 40) are in good agreement with those found by

Breckenridge and Hosler[3] and Frederikse[7]. The large magnitudes imply

that the band in question is narrow, and thus strengthen the argument

for the 3d-conduction band. It must also be remembered that the value

of $m*/m$ used in calculating Q_{el} was considered to be temperature inde-

pendent and from this standpoint the magnitude of Q_{el} can only be an

estimate. Consequently, Q_{ph} plots (Figure 21) must reflect any Q_{el}

uncertainty. Of major concern in Figure 21, however, are the slopes

and the _relative_ magnitudes of Q_{ph} for the samples in various states

of nonstoichiometry.

Since Herring's expressions[46] cannot be solved explicitly for Q_{ph}

magnitudes without more information about relaxation times, it is dif-

ficult to quantitatively interpret the above results in the light of

his theory. The salient feature, however, is the observed decreasing

magnitude of Q_{ph} with increasing reduction state. Since variables such

as sample dimensions, foreign impurity content, and orientations are

the same, the only variable which can account for this behavior is the

increasing defect concentration as one goes from PA 6 to PA 12. The

reason for the importance of this factor arises from Herring's point

that if the carrier density is large enough, the thermal conduction

current carried by the long wavelength phonons in a temperature gradi-

ent will be decreased due to interactions of the carriers with the pho-

nons. This, in turn, results in less phonon drag on the carriers than

they would experience if the carrier concentration were small.

Figure 19 or Table II also shows that the low temperature maximum

in the thermoelectric power shifts to higher temperatures with increas-

ed reduction. Comparisons of these temperatures with those at the maxima of the thermal conductivity curves show that the two nearly coincide. Assuming only boundary scattering, one would expect the maximum in the thermoelectric power to occur at a higher temperature than the maximum for the thermal conductivity since only long wavelength phonons are assumed to be important in the former case. This is consistent with sample PA 12 where κ_{max} occurs at about 12.5 ^{o}K and Q_{max} near 15 ^{o}K. Lightly-reduced samples such as PA 6, however, show the opposite tendency in that Q_{max} is at 10 ^{o}K and κ_{max} at 12.5 ^{o}K. Thurber and Mante's[36] vacuum-reduced sample is similar in behavior to PA 6 and its Q-curve also peaks at 10 ^{o}K.

At first glance, the shifting of the maximum might be thought to be a consequence of point defect scattering. However, the phonons which are considered to be important in the thermoelectric power--the phonon modes with small values of $\vec{q}$--are not expected to be strongly scattered by impurities since the relaxation time for this mechanism goes as ω^{-4}. As Griffin and Carruthers[61] have pointed out, scattering by bound donor electrons, on the other hand, would be expected to be an important mechanism for preferentially scattering low $\vec{q}$ phonons. If this were the case, one might expect the combined effects of boundary and bound donor electron scattering to shift the maxima of the Q-curves to higher and higher temperatures as the number of donors (or as the reduction state) increases. Unfortunately, even an estimate of the form of the phonon-bound donor electron relaxation time is difficult to ascertain for rutile without a more detailed knowledge of the band structure.

One also expects the _slope_ of Q_{ph} versus T above the maximum to decrease with increased carrier concentration and this is observed in Figure 21. As mentioned previously, Gashimzade, _et. al._[51] predict a value of $Q_{ph} \propto T^{-3.5} \ln T$ for a c-direction. In the temperature range 30 to 100 $^\circ$K, ln T goes nearly as $T^{0.3}$ so that the temperature dependence in the c-direction is about $T^{-3.2}$. From the changes in slope seen from Figure 21 (2.2 to 2.7) it is certainly conceivable that a "pure" sample might approach this value.

On the other hand, Herring's[46] semiquantitative treatment yields $Q_{ph} \propto \bar{\tau}/\mu T$, (for a cubic structure). Taking $\bar{\tau} \propto T^{-4}$ and $\mu \propto T^{-1.5}$, Herring obtained the result $Q_{ph} \propto T^{-3.5}$. The mobility shown in Figure 14, and discussed earlier, however, goes as $T^{-2.5}$ and not $T^{-1.5}$. If in fact, one uses the value $\mu \propto T^{-2.5}$ in Herring's expression, $Q_{ph} \propto T^{-2.5}$, in excellent agreement with the experimental slope for sample PA 3.

At very low temperatures, one expects the only scattering mechanism to be that of the sample boundaries. In this case the relaxation time is temperature independent and one only needs to know the temperature dependence of the mobility. This has not been obtained at low temperatures in the present work, but if one assumes the value $T^{-1.5}$, as did Herring, $Q_{ph} \propto T^{0.5}$. Values calculated for the various samples where Q-data below the maximum could be obtained are given in Table III. As mentioned in Chapter IV, the uncertainty in the measurements below 10 $^\circ$K is about $\pm$ 20% and this means a corresponding uncertainty in the slopes in Table III. The values at 9 $^\circ$K are in good agreement with a predicted value of $T^{0.5}$. However, the slopes at 7 $^\circ$K would im-

TABLE III

TEMPERATURE DEPENDENCE OF THE THERMOELECTRIC POWER

AND THERMAL CONDUCTIVITY BELOW 10 $^{\circ}$K

Sample	x in $Q_{ph} \propto T^x$		y in $\kappa \propto T^y$
	7 $^{\circ}$K	9 $^{\circ}$K	7 $^{\circ}$K
PA 13	0.77	0.56	----
PA 12	0.69	0.51	1.68
PE 12	----	0.50	----
PA 6	----	----	2.34
PA 10	----	----	2.45

ply that an additional mechanism must be introduced to explain the faster drop in Q_{ph} than that predicted by simple boundary scattering with μ taken proportional to $T^{-1.5}$.

In retrospect, while qualitative explanation of the experimental results is reasonably satisfactory, present concepts of the phonon-electron interactions involved in the phonon-drag effect are not well enough defined to provide estimates of magnitudes of this effect, nor predict conclusively the nature of the temperature dependences.

Thermal Conductivity

Table III also gives the temperature dependence of κ at low temperatures (7 $^{\circ}$K). These results are again not compatible with a simple boundary scattering mechanism which predicts $\kappa \propto T^3$. The decrease in

the slope of κ with increasing reduction state suggests an increasing importance of point defect or isotope scattering, since this mechanism is important for the high $\vec{q}$ phonons. More will be said on this point later.

Unlike present models of the phonon thermoelectric effect, thermal conductivities can be treated in a somewhat more quantitative fashion, using the expression given by Callaway which was discussed in Chapter II. Some of the thermal conductivity results shown in Figures 24 and 26 have been fitted using his expression by assuming a form for the relaxation time as

$$\tau_c^{-1} = v_c/L + A\omega^4 + B_o \exp(-\theta/\underline{a}T)\omega^2 T^3.$$

The origin of each term has already been briefly described, but it is still necessary to discuss the constants as they apply to reduced rutile.

The length parameter, L, can be calculated from the expression[53] $L = 1.12 \ (L_1 L_2)^{\frac{1}{2}}$, where $L_1 L_2$ is the cross-sectional area of the specimen. For sample PA 12 this yields L = 0.229 cm. Berman, et. al.[62], have pointed out that this parameter should depend not only on the cross-sectional area, but on the specimen length and the nature of the surface as well, e.g., whether the surface is polished or rough. All specimens used in this study had rough surfaces resulting from the cutting and lapping operations. Taking this fact and the distance between probes into account, the Berman correction reduces L by about 35%, to 0.150 cm. This is the value used in the boundary scattering term of the total relaxation time for samples PA 12 and PA 3. The low temperature data of sample PA 6 shown in Figure 26, however, were taken

after thie specimen had been cut lengthwise to determine specifically the effects of boundary scattering. For this reason the magnitude of L used in the κ-calculations for this specimen was 0.125 cm (the uncorrected value was 0.17 cm).

An average value of the sound velocity is required in the Callaway expression since longitudinal and transverse modes are not treated separately. For the c-direction in rutile this can be defined as $1/v_c = 1/3(2/v_t + 1/v_l)$. Lange[63] has recently measured the sound velocities for reduced and unreduced material, and found them to be independent of the reduction treatment. Using his values of $v_l = 10.66$ x 10^5 cm/sec and $v_t = 5.50$ x 10^5 cm/sec, the value of v_c is calculated to be 6.55 x 10^5 cm/sec.

According to Klemens[54], the constant A in the point defect scattering term of the total relaxation time, may be expressed as $A = (3V_o S^2/\pi v_c^3 G)$, where G^{-1} is the number of defects per unit cell, V_o the unit cell volume, and S^2 a scattering factor. Specifically, S^2 involves changes in the masses, nearest neighbor distances, and force constants within the unit cell, upon introduction of an isotope, impurity, or other defect. In a sample containing point defects (vacancies or interstitials), foreign impurities, and isotopes, one must calculate three separate values of A, and then sum these values to obtain the A used in the total relaxation time.

By measuring the thermal conductivity on their reduced sample and measuring it once more after reoxidation, Thurber and Mante[36] claim they were able to separate out the effects due to point defect scattering. This enabled them to estimate S^2 in reduced rutile as being of

the order unity. Using the values $V_o = 6.25 \times 10^{-23}$ cm^3, $v_c = 6.55 \times$

10^5 cm/sec, and $S^2 = 1$, and expressing the defect concentration, N_d, in

numbers per cm^3, one finds $A(\text{sec}^3) = 1.3 \times 10^{-62} N_d$. On the basis of

the carrier density curves calculated from the proposed defect model

(Figure 28) one may estimate a value for N_d if the specimen in question

has reached equilibrium during the reduction process. Thus for a 1050

^{o}C sample such as PA 12, $N_d \approx n(0_v^{2+})/2$, or $N_d \approx 8 \times 10^{18}$ cm^{-3}. This

gives an estimate of A as 10^{-43} sec^3. Comparing this value with that

found by Thurber and Mante for unreduced rutile (10^{-45} sec^3), one might

conclude that point defect scattering should completely overshadow iso-

tope and foreign impurity scattering in reduced material.

Consider, finally, the term of the total relaxation time which

pertains to phonon-phonon interactions. If umklapp processes were the

most important scattering mechanism, one might expect to see an expo-

nential behavior of K with temperature. This type of behavior was ob-

served by Thurber and Mante in "pure" rutile at temperatures higher

than 25 ^{o}K. Such a dependence was not noted in the results of the

present study, however, probably because of the high defect concentra-

tions, and for this reason the exponential factor was absorbed into

the proportionality constant. This in turn eliminated the somewhat

arbitrary choice of $\underline{a}$. The relaxation time for phonon-phonon inter-

actions thus becomes $\tau_{ph}^{-1} = B\omega^2 T^3$, which is the form used by Callaway

in describing umklapp processes in germanium. This is, of course, also

the form of the relaxation time commonly used to describe normal pho-

non-phonon processes. In this sense, B is the sum of the proportional-

ity constants for the two different phonon-phonon mechanisms and hence, cannot be considered solely representative of the strength of either one.

Using the values of L and A mentioned earlier for sample PA 12, and assuming a value for B, an IBM 360 computer was used to generate a curve by numerically integrating the Callaway expression. The value of the Debye temperature in the upper limit was taken to be 530 ^{o}K after Thurber and Mante. The value of B was varied to obtain a fit to the data at the higher temperatures (40 to 50 ^{o}K). It was necessary to decrease A about 20% from the estimated value in order to bring the computed curve into agreement with the data at the maximum. Once a value for B had been established in this manner, curves for samples PA 3 and PA 6 were generated using essentially this same value of B and varying only A.

To estimate the effect of the separate parameters upon κ, each was varied separately, and the behavior of κ noted. This revealed that for these samples, L is important only below the maximum as expected, B is important above 25 ^{o}K, and A is important over most of the temperature range, but is most prominent at the maximum. The results of the computed curves are shown for three samples in Figure 31, together with data points for comparison. The parameters L, A, and B used in the computations are listed in Table IV.

With reference back to the opening paragraph of this section, one notes on Figure 31 that the data, at the lowest temperatures, fall below the computed curve. The values of A and L could not be adjusted to fit the data at these temperatures, making it appear that an additional scattering mechanism--unaccounted for in the form of the total
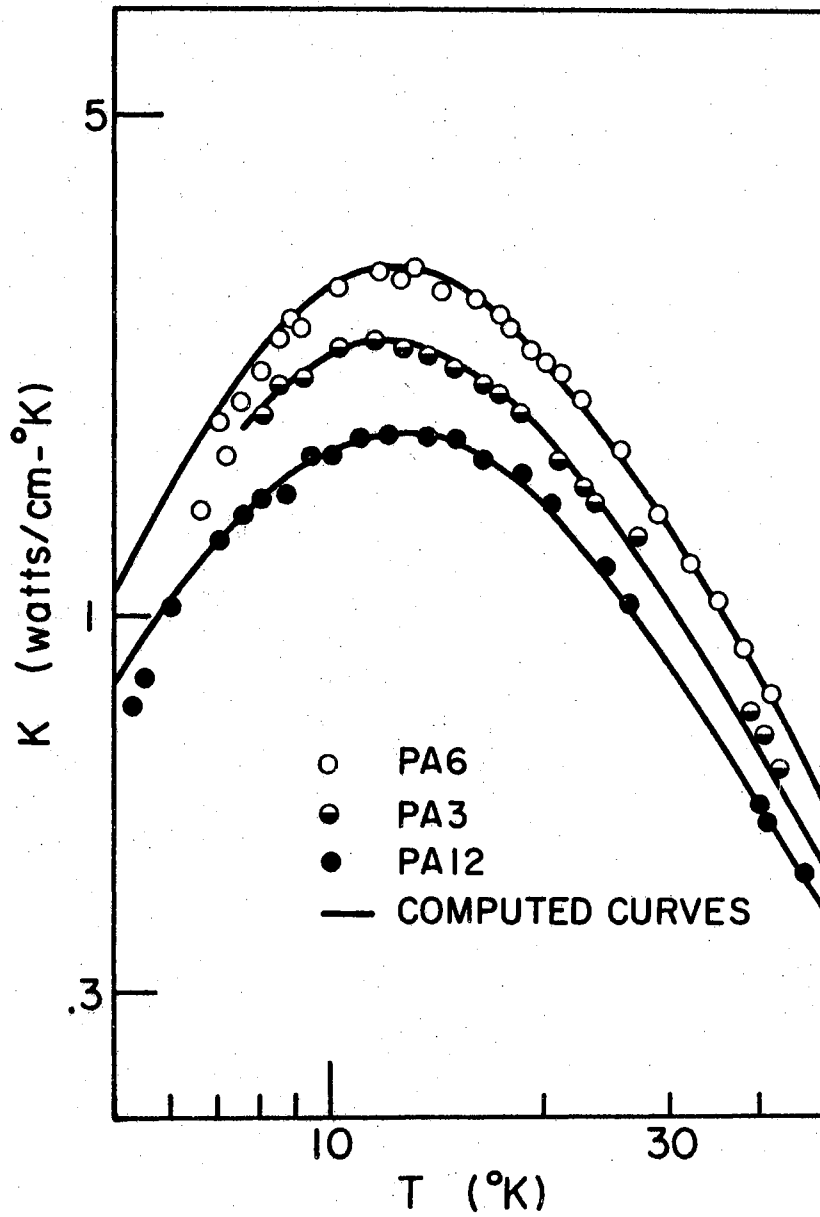
Figure 31. Thermal Conductivities as a Function
of Temperature as Computed from
the Calloway Expression and Com-
pared with the Actual Data

relaxation time used--is probably important below the maximum. This behavior is consistent with that observed in the thermoelectric power at low temperatures.

TABLE IV

PARAMETERS USED IN THE CALCULATIONS OF THERMAL CONDUCTIVITY

Sample	L(cm)	$A(sec^3)$	$B(^\circ K^{-3} sec)$	$N_d(cm^{-3})$	$N_d(est)$
PA 6	0.125	1.5×10^{-44}	3.0×10^{-22}	1.1×10^{18}	1.3×10^{18}
PA 3	0.15	3×10^{-44}	3.5×10^{-22}	2.2×10^{18}	3.3×10^{18}
PA 12	0.15	8×10^{-44}	3.5×10^{-22}	6×10^{18}	8×10^{18}

Since all crystals used in this investigation were cut from a single boule, and were essentially the same geometrical size, one would expect that only changes in the variable A would be required to explain the experimental decrease in the magnitude of κ with increased reduction state. That this is indeed the case--as deduced from the theoretical curves--can be seen from Table IV. One notes that B is essentially the same for all samples, while A varies from 8×10^{-44} sec^3 for PA 12 to 1.5×10^{-44} sec^3 for PA 6. The defect concentrations, N_d, as calculated from the expression $A = 1.3 \times 10^{-62} N_d$ are also included in Table IV, and estimates of N_d obtained by a completely different approach are presented in the last column ($N_d(est)$). This latter value for PA 12 was determined from Figure 28 as mentioned earlier. However, for samples PA 6 and PA 3 which were not reduced long enough for the

defect concentrations to reach the equilibrium values estimated on

Figure 28, an additional assumption was necessary. One observes from

this figure that the ratio $n(O_v)/n(Ti_i)$ is about 22 for an equilibrated

1050 $^{\circ}$C specimen. If this ratio is assumed to be independent of time,

at least for times long after the start of the treatment, one could de-

termine $n(O_v)$, and thus N_d ($\approx n(O_v)/2$), if the value of $n(Ti_i)$ were

known. According to the arguments given in the first part of this

chapter, one does know this value. It is the nearly constant portion

of the n versus $1/T$ curve (Figure 13 for sample PA 3). That is, in

this temperature range ($\sim 50 ^{\circ}$K), the energy-level model assumes that

all donor levels arising from oxygen vacancies are full and the conduc-

tion electrons arise from the ionized titanium interstitial donor

levels. Hence $n(Ti_i)$ is given by $3[Ti_i^{3+}] + 4[Ti_i^{4+}] - N_a$, or from

Figure 13, $n(Ti_i) \approx 3 \times 10^{17}$ cm^{-3} for sample PA 3. This leads to an

estimate of N_d as 3.3×10^{18} cm^{-3}, compared with 2.2×10^{18} cm^{-3} as de-

termined from the thermal conductivity results. Similar arguments for

specimen PA 6 give N_d(est) = 1.3×10^{18} cm^{-3} (versus 1.1×10^{18} cm^{-3}).

The agreement between the two values of N_d as calculated by completely

independent approaches argues strongly for the validity of the model

proposed earlier.

Anisotropy

The anisotropy ratio of κ_c/κ_a shown in Figure 25 is clearly in

agreement with that found for "pure" rutile by Thurber and Mante.

They attributed the decrease in the ratio near 25 $^{\circ}$K to the onset of

point defect and boundary scattering, and the constant value below 10
$^{\circ}$K to pure boundary scattering. If the first part of their interpreta-
tion is correct, it is indeed surprising to see a similar behavior in
strongly reduced material where point defect scattering is prominent
well above 25 $^{\circ}$K. The reader is referred to the work of these authors[36]
for their qualitative arguments concerning the behavior of κ_c/κ_a. In
general, the thermal conductivity (and thermoelectric power) anisotropy
in crystals is not well understood.

The nature of the anisotropy of the thermoelectric power is shown
in Figure 23. This curve actually plots the ratio of the total ther-
moelectric powers $(Q_{el} + Q_{ph})$ and thus one expects to see a large de-
viation at high temperatures (> 100 $^{\circ}$K) from the lnT dependence pre-
dicted by Gashimzade[51] since Q_{el} is prominent in this range. The elec-
tronic component is small at low temperatures, however, so in this
range the ratio is assumed representative of the phonon contributions
only. Hall measurements were not made on the a-direction sample (PE
12), and hence Q_{el} could not be evaluated for it directly. Using the
Hall anisotropy ratio R_c/R_a as a function of T given by Becker and
Hosler[12] (which they found to be independent of the reduction state),
an estimate of n versus 1/T was made for PE 12 and a rough value of
Q_{el} was obtained. Subtracting the electronic components from PA 12
and PE 12 shifts the ratio Q_c/Q_a in the temperature range 50 to 100 $^{\circ}$K
into good agreement with the lnT curve shown in Figure 23. No unam-
biguous explanation for the behavior observed below 25 $^{\circ}$K is available
at this time.

Summary of Conclusions

(1)   A model is presented which supposes that two types of de-
fects are created during the vacuum-reduction process and that these
defects are "frozen" into the specimens during a rapid quenching
period. The defects are oxygen vacancies and titanium interstitials.
Following low reduction temperatures (800 ^{o}C), the interstitial de-
fects are present in negligible amounts and have little effect on the
electrical properties of the material. As the reduction temperature
is increased, the interstitial defect concentration increases much
faster than the oxygen vacancy concentration. As a result, the titan-
ium interstitial defects play an ever-increasing role in the electri-
cal properties. At sufficiently high reduction temperatures (1000 ^{o}C),
when the donor level concentration arising from the interstitial de-
fects is greater than the acceptor level concentration arising from
foreign impurities, the electrons from these donor levels completely
dominate the low temperature electrical properties.

The important feature is that a titanium interstitial level,
which is not completely compensated, lies above the oxygen vacancy
levels. From measurements of the electrical properties, no assignment
as to the valence state of this level is possible. Recent ESR
studies[28], however, imply that Ti_i^o and Ti_i^{1+} levels cannot explain the
results of these investigations and hence Ti_i^{2+} and Ti_i^{3+} levels are
assumed to be the important ones. On this basis, the first two elec-
trons removed from the interstitial defect must be located on accep-
tors. The energy required to ionize the Ti_i^{2+} donor level is uncertain,

but is probably around 0.005 eV, and the activation energy of the Ti_i^{3+}

level is determined to be ~ 0.01 eV. The activation energy for re-

moval of the first electron from the oxygen vacancy is found experi-

mentally to be about 0.05 to 0.09 eV. Ionization of the second elec-

tron from the vacancy requires energies of about 0.07 to 0.11 eV, that

is, this level lies ~ 0.02 eV lower than the first level. All activa-

tion energies are assumed to be dependent upon the concentration of

defects.

This model is consistent with recent studies supporting the con-

cept of a titanium interstitial defect and qualitatively can explain

the behavior of the electrical properties determined in this study as

well as those observed by many others.

(2) A very large phonon contribution to the thermoelectric power

is observed. This effect increases with decreasing temperature,

eventually reaches a maximum in the temperature range 10 to 15 $^{\circ}K$, and

then decreases. The magnitude of this phonon contribution is clearly

dependent upon the number of point defects generated during the reduc-

tion process. This is a consequence of phonon scattering by carriers,

by bound donor electrons, or perhaps even by point defects. Unfortun-

ately, no present theory of this effect can predict magnitudes or tem-

perature dependences conclusively.

(3) The thermal conductivities of heavily reduced samples are

strongly influenced by point defect scattering in the temperature

range 10 to 50 $^{\circ}K$. At low temperatues, κ falls off more rapidly than

that predicted from a Callaway expression using point defect and

boundary scattering relaxation times only. This suggests that an addi-

tional scattering mechanism is present in highly reduced material.

(4) No appreciable size effect was noted in either the thermal conductivity or the thermoelectric power for sample PA 6. In addition, the maximum values in the Q-and κ-curves for each specimen occurred at approximately the same temperature. These two results would imply that nearly the same group of phonons are influential in both phenomena. Inspection of the computed curves for the thermal conductivity reveals that actually this is not a surprising conclusion in view of the strong effect of point defect scattering on this parameter. Since this scattering mechanism strongly scatters phonons of high $\vec{q}$, the low $\vec{q}$ phonon modes play a more prominent role in carrying the thermal current than would normally be expected.

BIBLIOGRAPHY

1. Earle, M. D., Phys. Rev. 61, 56 (1942).

2. Cronemeyer, D. C., Phys. Rev. 87, 876 (1952).

3. Breckenridge, R. G. and Hosler, W. R., Phys. Rev. 91, 793 (1953).

4. Frederikse, H. P. R. and Hosler, W. R., National Bureau of Stand-
        ards Report 6585 (1959).

5. Greener, E. H. and Whitmore, D. H., J. Appl. Phys. 32, 1320 (1961).

6. Frederikse, H. P. R., Hosler, W. R., and Becker, J. H., Proceedings
        of the International Conference on Semiconductor Physics,
        Prague, 1961, Publishing House of the Czechoslovak Academy
        of Sciences, Prague, 1961, paper R7.

7. Frederikse, H. P. R., J. Appl. Phys., 32, 2211 (1961).

8. Von Hippel, A., Kalnajs, J. and Westphal, W. B., J. Phys. Chem.
        Solids 23, 779 (1962).

9. Hasiguti, R. R., Minami, K., and Yomenitsu, H., J. Phys. Soc.
        Japan 16, 2223 (1961).

10. Bogomolov, V. N. and Shavkunov, P. M., Sov. Phys.-Solid State 5,
        1481 (1963).

11. Yahia, J., Phys. Rev. 130, 1711 (1963).

12. Becker, J. H. and Hosler, W. R., Phys. Rev. 137, A1872 (1965).

13. Blumenthal, R. N., Coburn, J., Baukus, J. and Hirthe, W. M., J.
        Phys. Chem. Solids 27, 643 (1966).

14. Bir, G. L., Bogomolov, V. N., Krivitskii, E. V. and Sulyatitskaya,
        T. E., Sov. Phys.-Solid State 7, 2414 (1966).

15. Hollander, L. E., Diesel, T. S. and Vick, G. L., Phys. Rev. 117,
        1469 (1960).

16. Hurlen, T., Acta. Chem. Scand. 13, 365 (1959).

17. Chester, P. F., J. Appl. Phys. 32, 2233 (1961).

18. Haul, R. and Dumbgen, G., J. Phys. Chem. Solids 26, 1 (1965).

19. Kevane, C. J., Phys. Rev. 133, A1431 (1964).

20. Shannon, R. D., J. Appl. Phys. 35, 3414 (1964).

21. Carnahan, R. D., and Brittain, J. O., J. Am. Cer. Soc. 48, 365 (1965).

22. Zijlstra, R. J. J., Leeuwerik, F. J. and Kleinpenning, Th. G. M., Phys. Letters 23, 185 (1966).

23. Iyengar, R. D., Codell, M., Karra, J. S. and Turkevich, J., J. Am. Cer. Soc. 88, 5055 (1966).

24. Wachtman, J. B., Spinner, S., Brower, W. S., Fredinger, T. and Dickson, R. W., Phys. Rev. 148, 811 (1966).

25. Kofstad, P., J. Phys. Chem. Solids 28, 1842 (1967).

26. Kofstad, P., J. Less-Common Metals 13, 635 (1967).

27. Hill, G. J., Brit. J. Applied Physics, Ser. 2, 1, 1151 (1968).

28. Kingsbury, P. I., Ohlsen, W. D. and Johnson, O. W., Phys. Rev. 175, 1091 (1968).

29. Kingsbury, P. I., Ohlsen, W. D. and Johnson, O. W., Phys. Rev. 175, 1099 (1968).

30. Johnson, O. W., Ohlsen, W. D. and Kingsbury, P. I., Phys. Rev. 175, 1102 (1968).

31. Grant, F. A., Rev. Mod. Phys. 31, 646 (1959).

32. Keesom, P. H. and Pearlman, N., Phys. Rev. 98, 1539A (1955).

33. Keesom, P. H. and Pearlman, N., Phys. Rev. 112, 800 (1958).

34. Keesom, P. H. and Sandin, T. R., Phys. Letters 26A, 167 (1968).

35. Sandin, T. R. and Keesom, P. H., Phys. Rev. 177 , 1370 (1969).

36. Thurber, W. R. and Mante, A. J. H., Phys. Rev. 139, A1655 (1965).

37. Baur, W. H., Acta. Cryst. 9, 513 (1956).

38. Kröger, F. A. and Vink, H. J., Solid State Physics, Vol. III, Ed. F. Seitz and D. Turnball, Academic Press, Inc., New York (1956).

39. Dominik, L. A. K. and MacCrone, R. K., Phys. Rev. 156, 910 (1967).

40. Dominik, L. A. K. and MacCrone, R. K., Phys. Rev. 163, 756 (1967).

41. Berman, R., Foster, E. L. and Ziman, J. M., Proc. Roy. Soc.

(London) A237, 344 (1956).

42. Kingery, W. D. and Charvat, F. R., J. Am. Ceram. Soc. 40, 306 (1957).

43. Yoshida, I., J. Phys. Soc. Japna 15, 2211 (1960).

44. Tauc, J., Photo and Thermoelectric Effects in Semiconductors, Pergamon Press, New York (1962).

45. Blakemore, J. S., Semiconductor Statistics, Pergamon Press, New York (1956).

46. Herring, C., Phys. Rev. 96, 1163 (1954).

47. Conwell, E. and Weisskopf, V. F., Phys. Rev. 77, 388 (1950).

48. Frederikse, H. P. R., Phys. Rev. 92, 248 (1953).

49. Drabble, J. R. and Goldsmid, H. J., Thermal Conduction in Semiconductors, Pergamon Press, New York (1961).

50. Casimir, H. B., Physica 5, 495 (1938).

51. Gashimzade, F. M., Sov. Phys.-Solid State 5, 650 (1963).

52. Callaway, J., Phys. Rev. 113, 1046 (1959).

53. Holland, M. G., Phys. Rev. 132, 2461 (1963).

54. Klemens, P. G., Proc. Phys. Soc. (London) A68, 1113 (1955).

55. Fischer, G., Greig, D. and Mooser, E., Rev. Sci. Inst. 32, 842 (1961).

56. Bogomolov, V. N. and Zhuze, V. P., Sov. Phys.-Solid State 5, 2404 (1963).

57. Champness, C. H., Proc. Phys. Soc. (London) B69, 1335 (1956).

58. Shockley, W., Electrons and Holes in Semiconductors, D. Van Nostrand, New York (1959).

59. Acket, G. A. and Volger, J., Phys. Letters 8, 244 (1964).

60. Heikes, R. R. and Ure, R. W., Thermoelectricity: Science and Engineering, Interscience Publishers, New York (1961).

61. Griffin, A. and Carruthers, P., Phys. Rev. 131, 1976 (1963).

62. Berman, R., Foster, E. L. and Ziman, J. M., Proc. Roy Soc. (London) A220, 171 (1953).

63. Lange, J., Phys. Rev. 176, 1030 (1968).

64. Van Gool, W., *Principles of the Defect Chemistry of Crystalline Solids*, Academic Press, New York (1966).

APPENDIX A

POINT DEFECTS

There are generally considered to be six primary types of defects which may occur in a crystalline solid: phonons, dislocations, foreign atoms, excitons, vacant lattice sites or interstitial atoms, and electronic disorder[38]. Only the last two types will be considered here. The effects of phonon interactions are discussed in Chapter II in relation to the thermal conductivity and thermoelectric power.

In treating crystals with vacancies and/or interstitials it is necessary to specify whether stoichiometry is preserved. For example, heating the hypothetical crystal MX to high temperatures may result in a concentration of M interstitials, $[M_i]$, together with an equal number of metal vacancies, $[V_m]$ (Frenkel defect). Another possibility might be vacant cation sites, $[V_m]$, together with an equal number of vacant anion sites, $[V_x]$ (Schottky-Wagner defect). Combinations of these can also occur, but in any event the important feature is that stoichiometry is maintained. One example of a process in which stoichiometry is not preserved might be heating MX in an ambient atmosphere of M vapor so that M ions enter the lattice in interstitial sites.

The previous examples represent cases of atomic disorder. There also exists the possibility of electronic disorder which may or may not depend on the atomic disorder. A semiconductor in its intrinsic region

presents an example of electronic disorder not involving atomic disorder. On the other hand, vacancies or interstitial atoms within a crystal can act as donors or acceptors and thus also give rise to electronic disorder.

The semi-quantitative treatment of the concentrations of atomic and electronic defects stems from the application of the law of mass action. In view of the importance of this law, a simple derivation similar to that given by Kröger and Vink[38] is presented below to introduce terminology and to clarify the relationships between parameters. Consider, for example, the reaction involving the creation of M interstitials and M vacancies in the crystal MX:

$$MX \rightleftharpoons M_{(1 - \delta)} (M_i)_\delta (V_m)_\delta X.$$
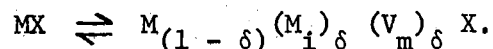
In this expression δ is the molar concentration of the defect and it is assumed that $\delta \ll 1$. Now, according to thermodynamics, at equilibrium the sum of the thermodynamic potentials, μ_i, of reaction partners i on the left side of the reaction equals that of the reaction partners on the right hand side. Treating those on the left as negative and ones on the right as positive,

$$\sum_i n_i \mu_i = 0.$$

Here n_i is the number of atoms i taking part in the reaction. Treating the atoms as statistically independent, and considering only small concentrations it can be shown (e.g. van Gool[64]) that the thermodynamic potential μ_i is a function of the concentration x_i of component i, that is

$$\mu_i = (\mu_i)_o + RT \ln x_i$$

where R is the universal gas constant, x_i is expressed in mole fractions, and $(\mu_i)_o$ is the thermodynamic potential of i under standard conditions (T = 25 ^oC, x_i = 1).

Combining these last two expressions

$$\sum_i n_i \ln x_i = - \sum_i n_i (\mu_i)_o / RT$$

or

$$\prod x_i^{n_i} = \exp \left(-\sum_i n_i (\mu_i)_o / RT \right).$$

The thermodynamic potential of i, however, can be expressed in terms of the partial enthalpy, h_i, and partial entropy, s_i, through the Gibbs function:

$$\mu_i = h_i - Ts_i.$$

This yields upon substitution

$$\prod x_i^{n_i} = \exp \left(\sum_i n_i (s_i)_o / R \right) \exp \left(-\sum_i n_i (h_i)_o / RT \right)$$

$$= C\exp(-\Delta H / RT)$$

$$= K.$$

This last expression is the law of mass action, with C a constant involving the entropy change in the reaction and ΔH the energy involved in the reaction. In terms of the example cited earlier, then, at any temperature T,

$$[M_i][V_m] = \text{constant.}$$

Because it is assumed that the density of imperfections is small ($\delta \ll 1$), the concentrations of the normal crystal components are assumed constant, and hence do not appear in the law of mass action. Concentrations may also be expressed in numbers per cm^3.

The applicability of this technique to a real crystal necessitates a knowledge of the type of defect as well as the ability to experimentally determine the constants C and ΔH, procedures which in practice are usually difficult.

APPENDIX B

POTENTIOMETER CIRCUITS

The circuit diagrams for the potentiometers used with the low temperature resistivity and Hall effect sample holder are shown in Figure 32, and the components are listed in Table V. These circuits are similar to those of Fischer, Greig and Mooser[55].

The potentiometers A and B were only used to supply a constant voltage and, therefore, did not require calibration. In the calibrated potentiometer, the current through the potential divider was drawn from either battery B_1 or B_2 and calibration was performed by adjusting R_{10} or R_{11} to obtain the desired current flowing through the ammeter, A. Depending on the position of the switch S_4, this current was either 10 ma or 0.10 ma, resulting in a potential drop across resistor R_1 of 1, 10^{-1}, 10^{-2} volts (10 ma) or 10^{-2}, 10^{-3}, 10^{-4} volts (0.10 ma). This potentiometer was calibrated against the Leeds and Northrup K-3 or the Keithley 149 and was found accurate to better than $\pm$ 1% on the higher ranges and about $\pm$ 5% on the 0.1 mv range.
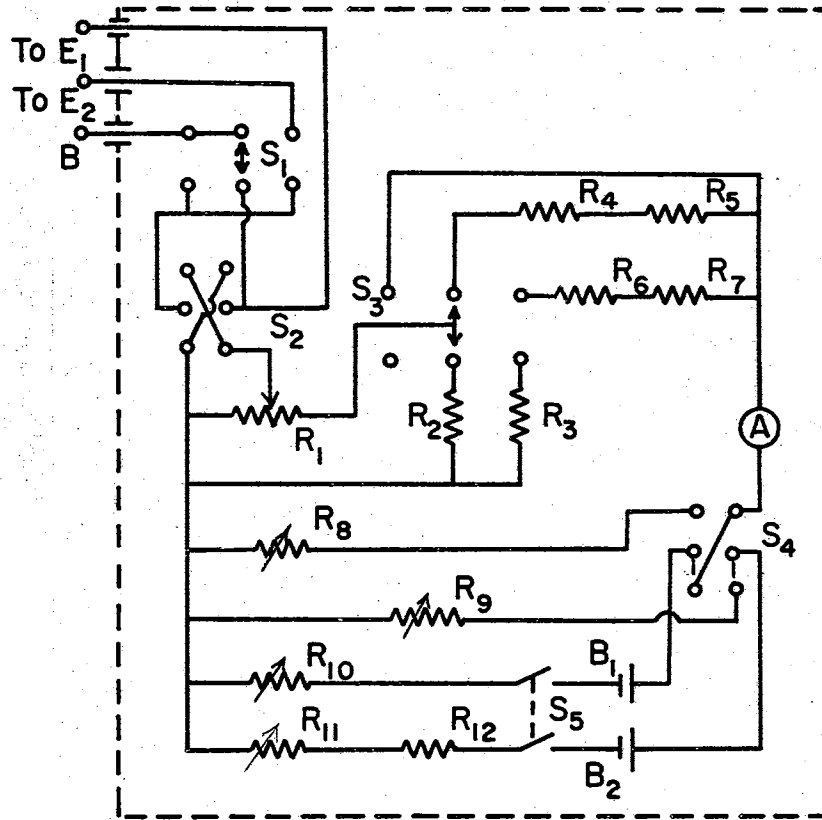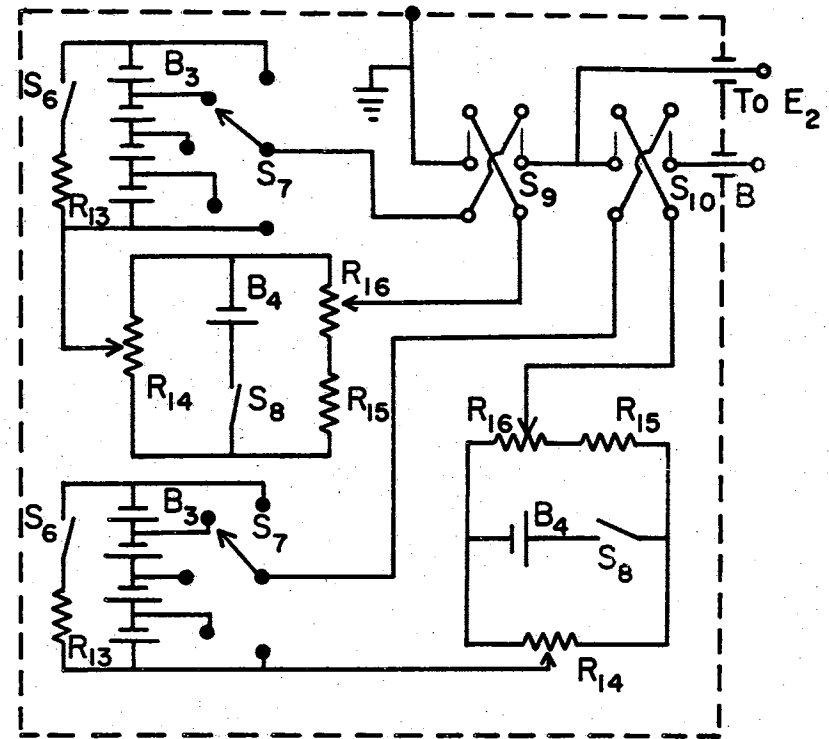
Figure 32. Circuit Diagrams of the Potentiometers Used in the Low Temperature Resistivity and Hall Effect Measurements

TABLE V

PARTS LIST FOR POTENTIOMETERS

Component	Value[a]	Manufacturer
A		Weston Model 81
R_1	100	Borg 205
R_2	20	Baurnes 3053
R_3	1	IRC WW4J
R_4, R_7	50	Baurnes 3053
R_5, R_6	50	IRC WW4J
R_8	500	Ohmite Cu 5011
R_9	5×10^3	Ohmite Cu 5011
R_{10}	100	Baurnes 3400
R_{11}	10^4	Baurnes 3400
R_{12}	10^4	IRC WW4J
R_{13}	2.5×10^5	IRC WW4J
R_{14}	10^3	General Radio 510D
R_{15}	200	IRC WW4J
R_{16}	25	Borg 2251B
B_1, B_2, B_4	1.456	Mallory RM 12
B_3	28.0 (4)	Mallory RM 413
S_{1-4}, S_9, S_{10}		Shallcross 2J56A6-1
S_5, S_6, S_8		Cutter-Hammer 8376K1
S_7		Shallcross 1J54A6-1

[a]Resistances in ohms, battery voltages in volts.

VITA 3

Gary Allen Baum

Candidate for the Degree of

Doctor of Philosophy

Thesis: ELECTRICAL AND THERMAL PROPERTIES OF NONSTOICHIOMETRIC RUTILE
         AT LOW TEMPERATURES

Major Field: Physics

Biographical:

   Personal Data: Born at New Richmond, Wisconsin, October 2, 1939,
       the son of Margaret and Herbert F. Baum.

   Education: Graduated from New Richmond High School, New Richmond,
       Wisconsin, in 1957; received the Bachelor of Science degree
       from Wisconsin State College, River Falls, Wisconsin, with
       majors in Physics and Mathematics, in May, 1961; received the
       Master of Science degree from Oklahoma State University,
       Stillwater, Oklahoma, with a major in Physics, in May, 1964;
       completed requirements for the Doctor of Philosophy degree
       in August, 1969.

   Professional Experience: Employed as a Research Engineer with the
       Douglas Aircraft Company, Santa Monica, California, from 1963
       to 1964; employed as a Senior Physicist with the Dow Chemical
       Company, Golden, Colorado, from 1964 to 1966.